INVESTIGATION INTO THE USE OF PHENYL AZIDES FOR THE PHOTOIMMOBILISATION OF DNA

BY

TRACEY ANN PRICE

A thesis submitted to the department of Pure and Applied Chemistry, University of Strathclyde, in accordance with the requirements for the degree of Doctor of Philosophy.

June 2010

Abstract

This thesis details the research into the use of phenyl azides for the photoimmobilisation of DNA, with particular focus on characterising their photochemistry and the design of a library of novel phenyl azides for the functionalisation of a variety of substrates.

Three phenyl azides containing a para carboxylic acid have been prepared with their photochemical activation rates characterised. Upon illumination at 365 nm with and without the presence of a primary amine first order rate kinetic were observed. As a result from an investigation into further modification of the three synthesised phenyl azides, 2-(4-azidophenyl)acetic acid [3] was selected for the core structure for future applications. The photochemistry of the chosen phenyl azide was verified by 1H NMR, by illumination at 365 nm in the presence of a primary amine.

The photoimmobilisation of DNA was successfully achieved on quartz, epoxide polymer and gold via the functionalisation with the chosen phenyl azide 2-(4-azidophenyl)acetic acid [3]. Characteristic fluorescence and surface enhanced resonance Raman spectroscopy (SERRS) spectra observed of the dye labelled DNA upon the quartz substrate and resonance Raman spectroscopy (RRS) and SERRS StreamLine™ maps prepared depicting the site of photoimmobilisations on the epoxide polymer and gold substrate respectively.

Two novel photoactive dip-pen nanolithography (DPN) inks were also prepared containing the chosen phenyl azide 2-(4-azidophenyl)acetic acid [3] with diffusion coefficients obtained. The diffusion coefficient for the thioctic acid based ink for the gold substrate was 10 times larger than that of the silane based ink for the silicon dioxide substrate. The novel inks were prepared with the intention to photoimmobilise DNA in a similar manner to that previously described.

Declaration

Acknowledgements

First and foremost I would like to thank my PhD supervisor, Prof Duncan Graham for all his help, support and advice with my research.

A special thank you goes to Dr Karen Faulds, Dr Dave Robson, Dr Robert Stokes, Dr Karen McCarney and Dr Carl Hall for all their fresh ideas, technical advice and support that have contributed to the writing of this thesis.

I would also like to thank Dr Allan Mackintosh and Dr Alexander Kuehne for synthesising the epoxide polymer, Mark McGrady for running the contact angle analysis and Dr Alan Kennedy for obtaining beautiful X-ray crystals structures from not necessarily perfect crystals.

Last but not least I would like to thank Jason, as he gave me the strength and motivation to keep on going when times were really difficult.

Contents Page

Abbreviations

A	Adenine
AFM	Atomic force microscopy
APTES	3-Aminopropyltriethoxysilane
BASED	Bis-(β-(4-azido salicylamido)ethyl)disulfide
BHQ	Black hole quencher
br	Broad
Boc	*tert*-Butyloxycarbonyl
C	Cytosine
$CDCl_3$	Deuterated chloroform
CDI	1,1'-Carbonyldiimidazole
CI-MS	Chemical ionisation mass spectroscopy
CPG	Controlled pore glass
CT	*Chlamydia trachomatis*
d	Doublet
Δ	Heat
DCA	Dichloroacetic acid
DCC	*N*,*N*'-Dicyclohexylcarbodiimide
DTT	Dithiothreitol
DEPC	Diethylpyrocarbonate
DIPEA	*N*,*N*'-Diisopropylethylamine
DMD	Digital micromirror device
DMF	Dimethylformamide
DMSO-d_6	Deuterated dimethylsulfoxide
DMTr	Dimethoxytrityl

DMTr-Cl	Dimethoxytrityl chloride
DNA	2'-Deoxyribonucleic acid
DPN	Dip-pen nanolithography
EI-MS	Electron ionisation mass spectroscopy
ESI-MS	Electrospray ionisation mass spectroscopy
eq	Equivalents
FAB-MS	Fast atom bombardment mass spectroscopy
FESEM	Field emission scanning electron microscopy
Fmoc	9*H*-Fluorenylmethyloxycarbonyl
G	Guanine
HMDS	Hexamethyldisilazane
HPLC	High performance liquid chromatography
hr	Hour
ISC	Intersystem crossing
LFM	Lateral force microscopy
m	Multiplet
med	Medium
MeNPOC	Methylnitropiperonyloxycarbonyl
MHz	Mega Hertz
mp	Melting point
m/z	Mass/charge ratio
ns	Nano second
NMR	Nuclear magnetic resonance
PBS	Phosphate buffered saline
PCR	Polymerase chain reaction

PGA	Photogenerated acid
p-NP	p-Nitrophenol
q	Quartet
RRS	Resonance Raman spectroscopy
s	Singlet
SAMs	Self-assembled monolayers
SEC	Size exclusion chromatography
SEM	Scanning electron microscopy
SERS	Surface enhanced Raman spectroscopy
SERRS	Surface enhanced resonance Raman spectroscopy
sh	Sharp
st	Strong
t	Triplet
T	Thymine
TFA	Trifluoroacetic acid
TLC	Thin layer chromatography
Tm	Melting temperature
Tr-Cl	Trityl chloride
UV	Ultraviolet
UV-vis	Ultraviolet-visible
wk	Weak
w/v	Weight/volume
v/v	Volume/volume

CHAPTER 1

INTRODUCTION

1. Introduction

1.1. DNA

DNA is the hereditary material contained in every living organism that provides coded genetic information required for the functions of life.

1.1.1. Primary Structure of DNA

DNA is a large linear biopolymer composed of a series of deoxyribonucleotide units (deoxyribonucleoside 5'-monophosphates). A single stranded piece of DNA is frequently referred to as an oligonucleotide when less than 100 bases long (Figure 1.1).

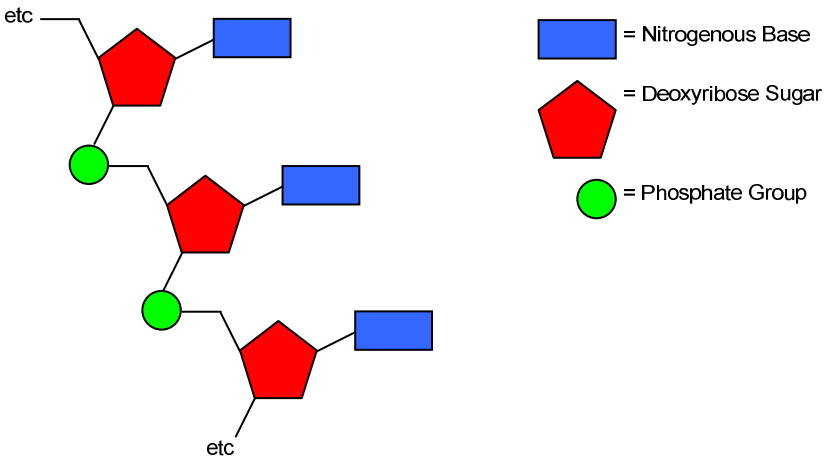

Figure 1.1: Schematic structure of an oligonucleotide

All nucleotides have the basic generic structure (Figure 1.2), consisting of the following three components:

1. deoxyribose sugar – a pentose sugar unit (ribose) lacking an oxygen atom at the 2' position,
2. nitrogenous base – attached at the 1' position on the deoxyribose sugar,
3. phosphate group – attached at the 5' position on the deoxyribose sugar.

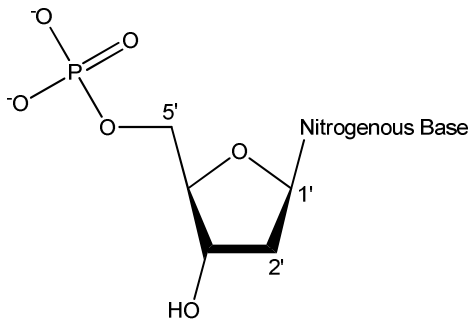

Figure 1.2: Generic structure of a nucleotide

The nitrogenous bases are derivatives of two parent compounds; purine and pyrimidine (Figure 1.3).

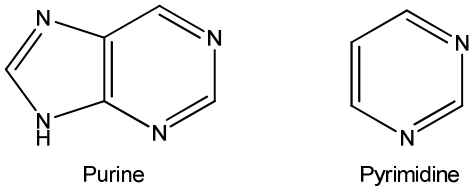

Figure 1.3: Structures of purine and pyrimidine

In DNA there are two purine nitrogenous bases; adenine (A) and guanine (G) and two pyrimidine nitrogenous bases; cytosine (C) and thymine (T). The bases are attached to the sugar via a *N*-β-glycosol linkage. The purine nitrogenous bases are attached at the *N*-9 whilst the pyrimidine nitrogenous bases are attached at the *N*-1 (Figure 1.4).

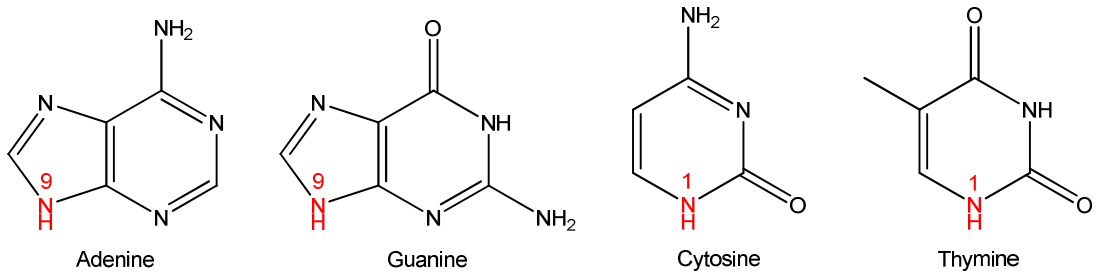

Figure 1.4: Four DNA nitrogenous bases

The phosphate group is phosphoric acid attached to the 5' hydroxyl of the deoxyribose sugar. When in DNA the phosphate group is also attached to the 3' hydroxyl of the sugar via a phosphodiester linkage (Figure 1.5). Along with the deoxyribose sugar, the phosphate group forms the backbone structure of DNA and is uniform throughout the whole structure.

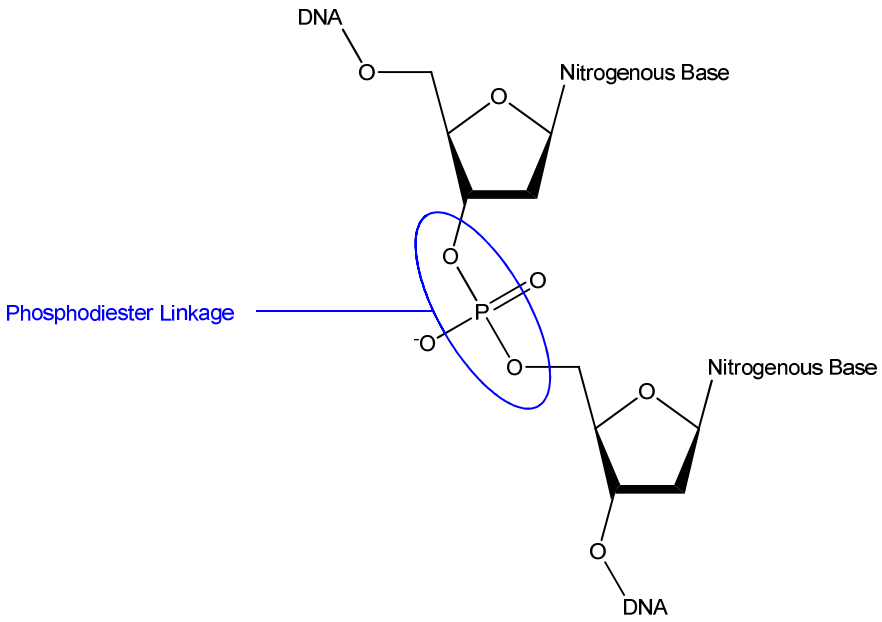

Figure 1.5: Single stranded DNA showing the phosphodiester linkage

1.1.2. Secondary Structure of DNA

The DNA double helix (Figure 1.6) was discovered by Watson and Crick in 1953, which led them to winning the Nobel Prize for Physiology and Medicine 9 years later in 1962 with Wilkins.[1-3]

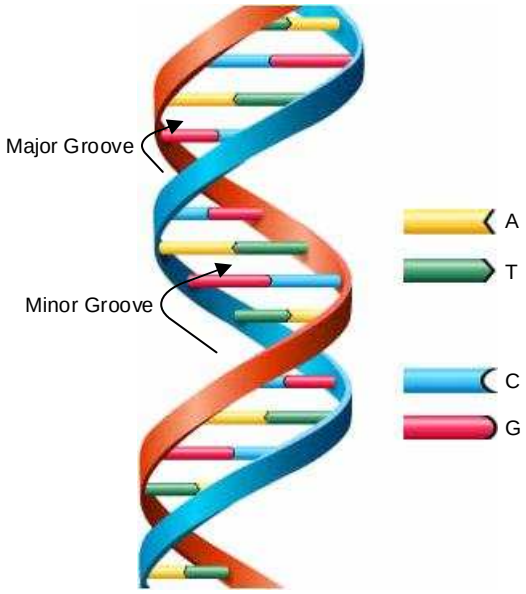

Figure 1.6: DNA helix showing the major and minor grooves[4]

By using results published previously by Chargaff and Franklin, Watson and Crick were able to elucidate the secondary structure of DNA.

In 1950 Chargaff published his work on nitrogenous bases.[5] He proposed that the ratios of A:T and C:G were equal and that the number of purine nitrogenous bases to pyrimidine nitrogenous bases was also equal. From this Watson and Crick were able to suggest the structures of the nitrogenous base pairs (Figure 1.7).

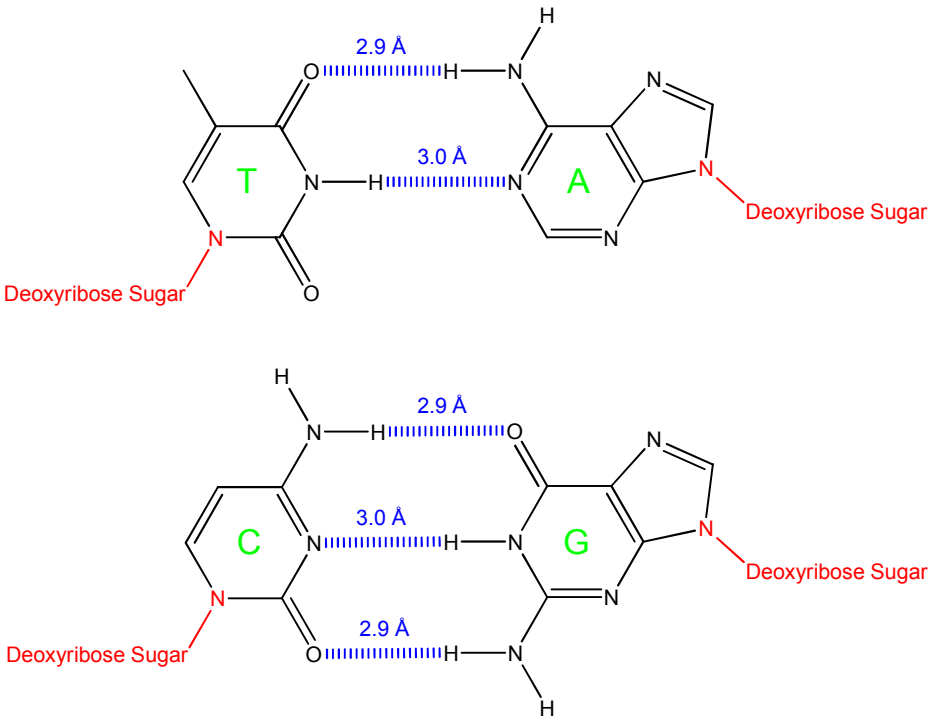

Figure 1.7: Watson and Crick nitrogenous base pairs showing hydrogen bond lengths

In 1953 Franklin published X-ray diffraction photographs of DNA (Figure 1.8).[6] Watson and Crick were able to extract information from these photographs to elucidate the secondary structure of DNA:

- cross pattern characteristic of a helix → ✕
- diamond shapes indicate long/extended molecules → ◇
- missing smears indicate interference from second helix → 0

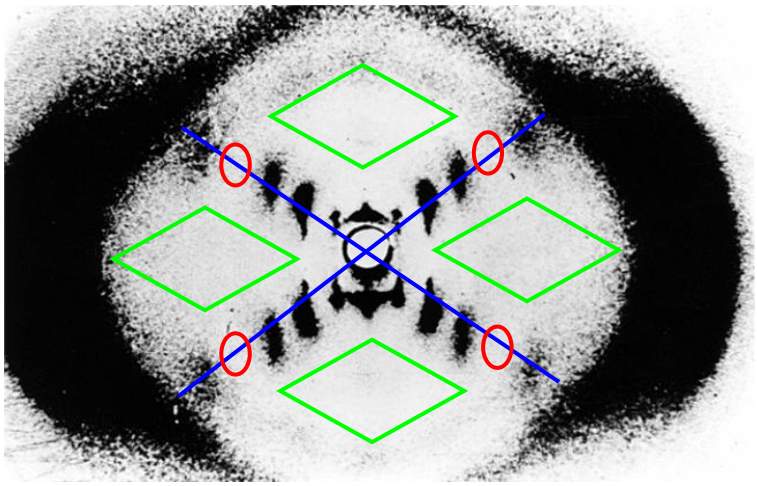

Figure 1.8: X-ray diffraction pattern of DNA

This information lead Watson and Crick to suggest that the secondary structure of DNA occurs as a double helix (duplex). DNA predominately exists as a right handed double helix with complementary anti-parallel strands held together by the hydrogen bonding of the nitrogenous base pairs and stabilised by the π-π interaction of the nitrogenous bases.

1.1.3. Synthesis of DNA

DNA occurs naturally within the body, however synthetic DNA can be made for diagnostics and as therapeutic agents. The advantage of synthesising DNA is that the sequence of nitrogenous bases can be controlled and quantities approaching kilograms can be produced if necessary.

At present the most common way of producing synthetic DNA is via phosphoramidite chemistry developed by Caruthers *et al.*[7-10] In combination with solid phase techniques, DNA sequences can be produced in high yields and purity.

Orthogonal Protection Groups

The amino groups on the nitrogenous bases and the 5' hydroxyl group on the deoxyribose sugar have to be protected to avoid any unwanted side reactions during synthesis. The amino protecting groups must stay intact throughout the whole DNA synthesis however the 5' hydroxyl protecting group must be removed with each phosphoramidite monomer addition. In order for this to happen an orthogonal protecting group strategy is employed, so that when the 5' hydroxyl protecting group is removed the amino protecting groups remain intact.

The amino groups of the nitrogenous bases are protected by imine formation following treatment with dimethylformamide (DMF) or by amide formation following treatment with benzoyl chloride, acetic chloride or isobutyric anhydride and are all cleaved with base (Figure 1.9).

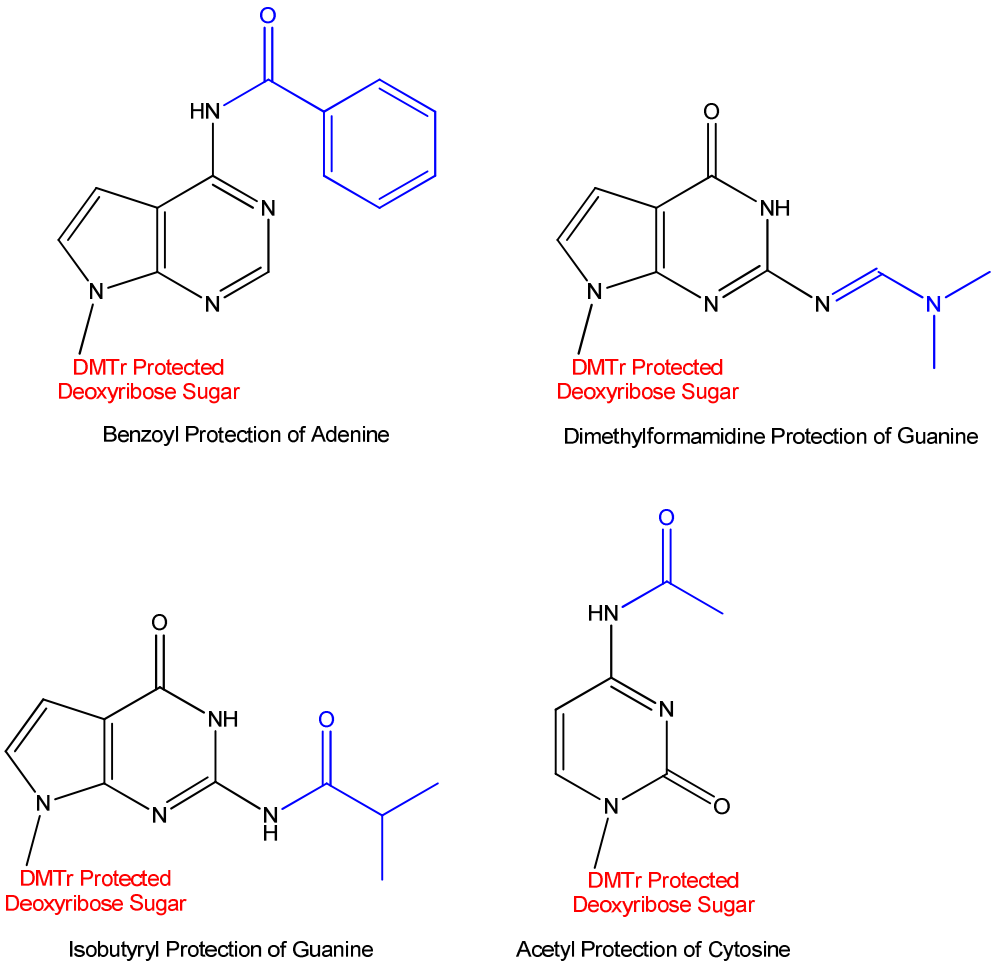

Figure 1.9: Protecting groups of amino groups on nitrogenous bases

The 5' hydroxyl of the deoxyribose sugar is protected by ether formation with dimethoxytrityl chloride (DMTr-Cl) and is cleaved with acid (Figure 1.10).

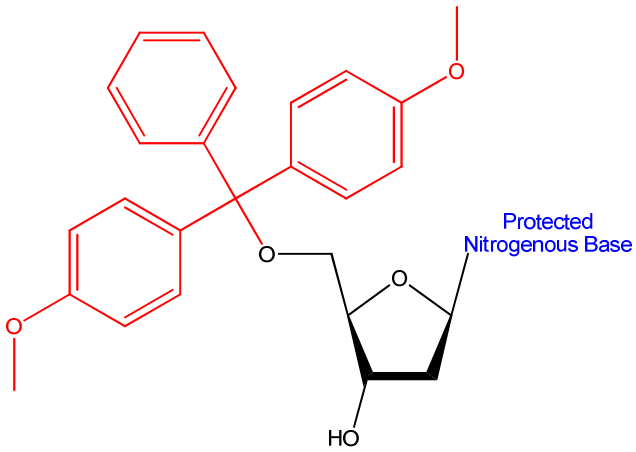

Figure 1.10: DMTr protection of 5' hydroxyl group

Solid Support

The synthetic DNA strands are immobilised onto a solid support and are produced in a 3' to 5' direction, this enables all the reagents to be added successively in excess, with any unreacted material removed by a simple washing step. The most common solid support is controlled pore glass (CPG), composed of beads of borosilicate glass. The CPG are packed inside a column which provides a chemically stable platform which enables DNA synthesis to take place on. These are commercially available, enabling typical synthetic scales of 40 nM to 10 μM. All columns with CPG beads for DNA synthesis typically have the first nucleoside already attached. These are known as standard CPG, whereas universal CPG has no nucleoside attached. By having the first nucleoside already attached to the CPG beads it reduces the amount of synthetic steps, in turn increasing the yield.

Attachment of the first nucleoside to the universal CPG can be also achieved by a two step reaction. First the reaction between a succinimyl linker in pyridine with the first dimethoxytrityl protected nucleoside to form the free carboxylic acid (Scheme 1.1).

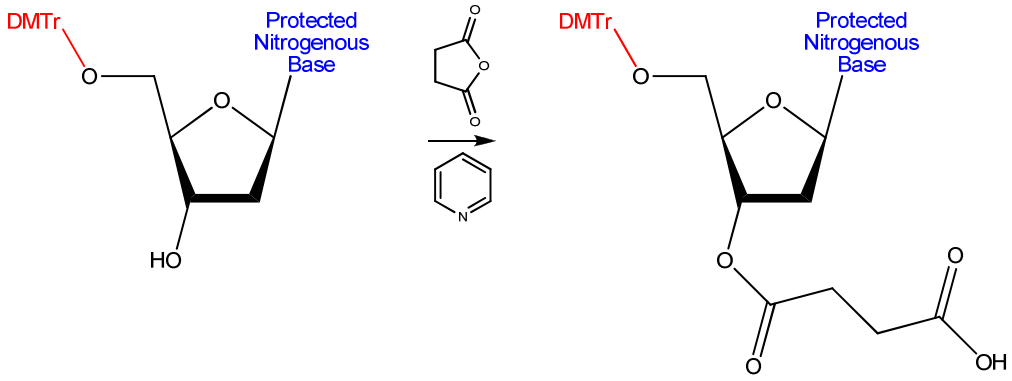

Scheme 1.1: Addition of the succinimyl linker to the first nucleoside

The second reaction is an amide forming reaction between the free carboxylic acid and the free amine on the CPG in the presence of *N*,*N*'-dicyclohexylcarbodiimide (DCC) and p-nitrophenol (p-NP) and thus immobilises the first nucleoside on the CPG (Scheme 1.2).

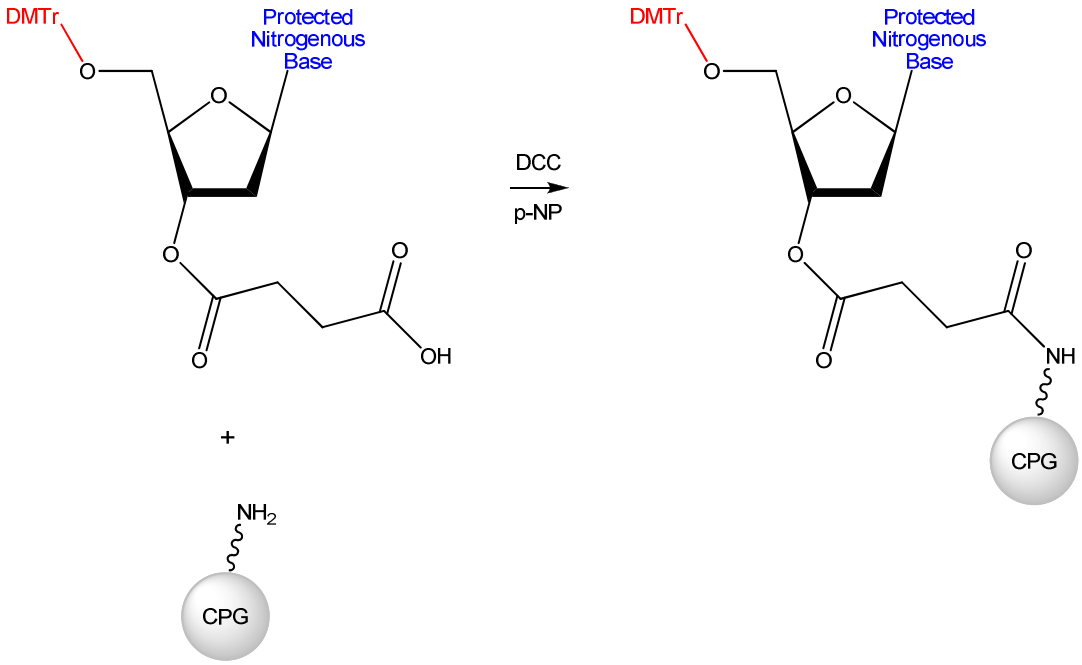

Scheme 1.2: Addition of the first nucleoside to the CPG bead

Deblocking

For the coupling reaction to occur the dimethoxytrityl group protecting the 5' hydroxyl of the deoxyribose sugar must be removed. This is achieved by washing with a 3 % v/v solution of dichloroacetic acid (DCA) in DCM (Scheme 1.3).

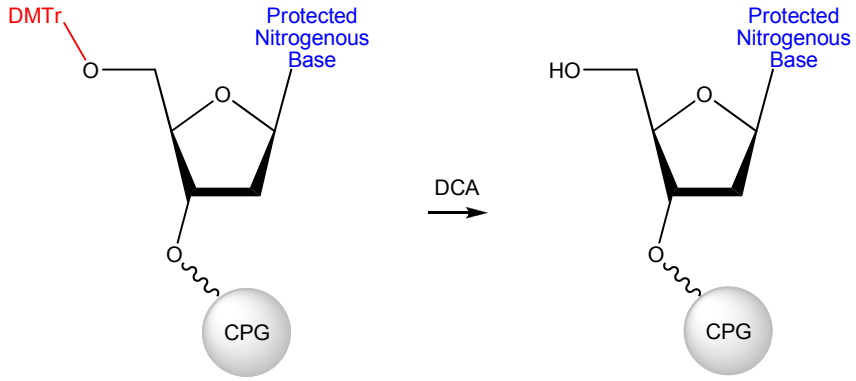

Scheme 1.3: Removal of the DMTr protecting group with acid

Coupling

The formation of the phosphite linkage between the nucleoside attached to the CPG bead and the new phosphoramidite nucleoside is referred to as the coupling step. All nucleosides for DNA synthesis are usually supplied as the 3'-cyanoethyl phosphoramidites. This again reduces the amount of synthetic steps.

Nucleoside phosphoramidites can also be produced by a phosphitylation reaction between the fully protected nucleoside and the chlorinated phosphitylating reagent in the presence of the hindered amine, *N*,*N*'-diisopropylethylamine (DIPEA) (Scheme 1.4).

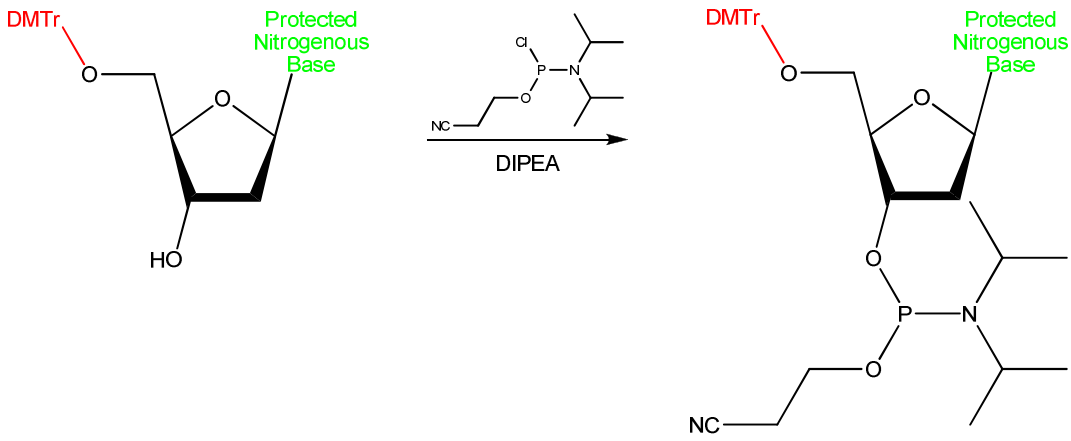

Scheme 1.4: Formation of the 3'-cyanoethyl phosphoramidite

The addition of tetrazole as a catalyst with the phosphoramidite nucleoside forms the phosphite triester linkage (Scheme 1.5).

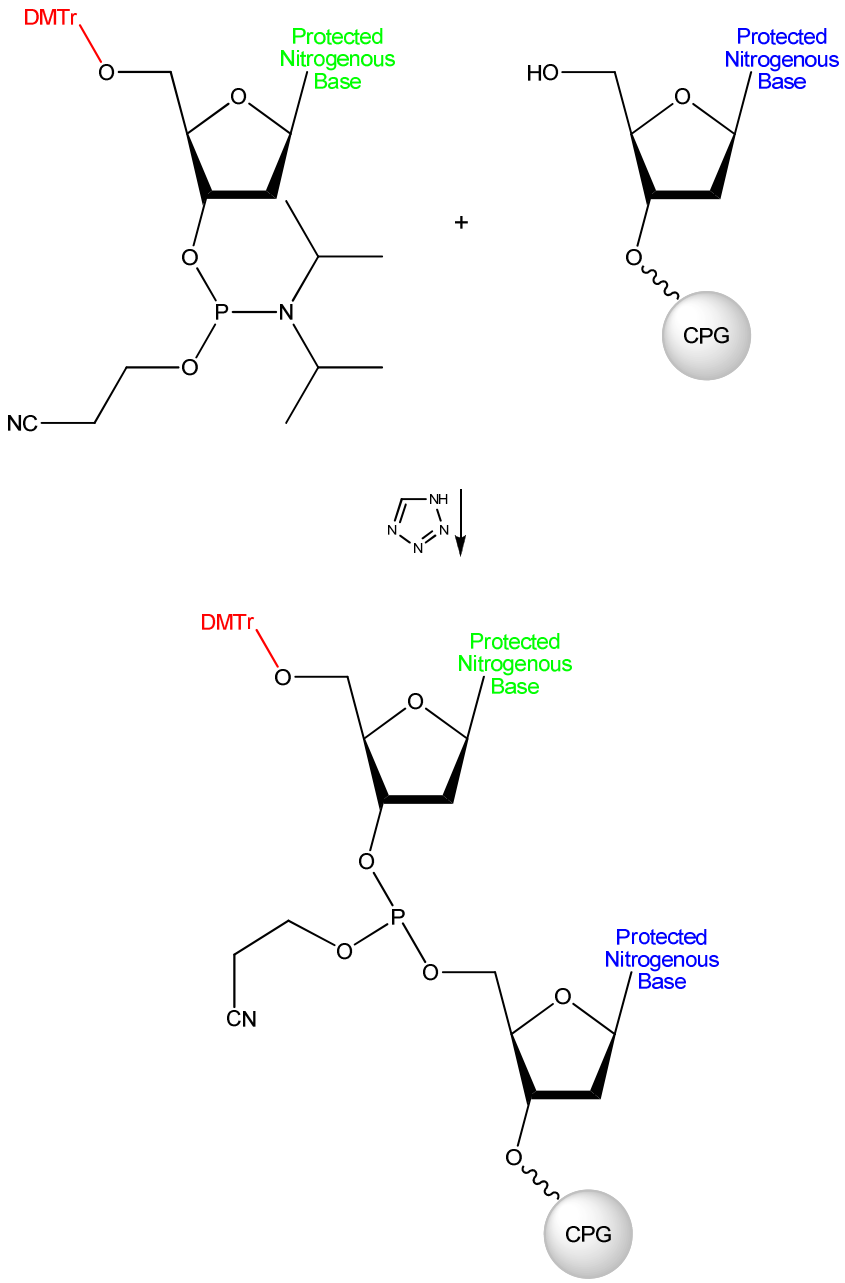

Scheme 1.5: Formation of the dinucleotide

Capping

Although the addition of a single phosphoramidite monomer to the growing synthetic DNA chains is highly efficient (>98 %), there will be some free 5' hydroxyls left unreacted on the deoxyribose sugar. This can be a problem if they then go on to react further with a different phosphoramidite monomer because the wrong DNA sequence will be made.

To prevent this from happening, a capping step is introduced to prevent the failed DNA chain from growing any further. This is achieved by acylating the hydroxyls with acetic anhydride with *N*-methylimidazole acting as a catalyst (Scheme 1.6).

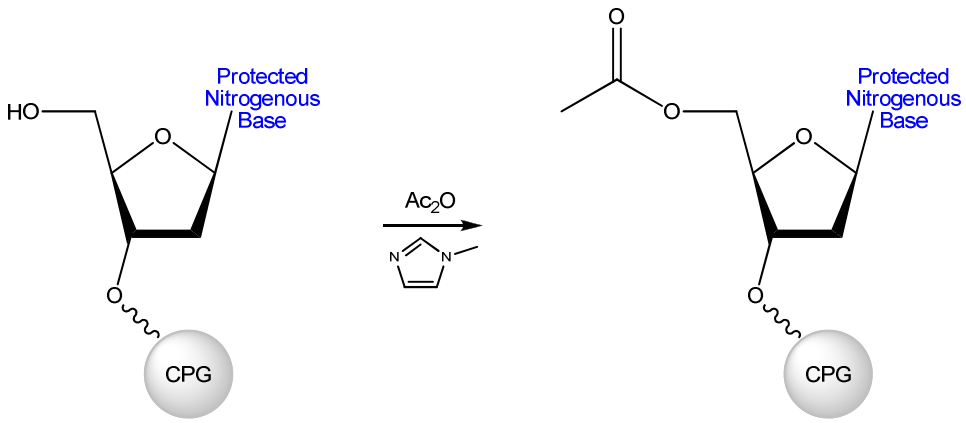

Scheme 1.6: Capping of the unreacted 5' hydroxyl group

Oxidation

The phosphite triester linkage between the two nucleosides is unstable to both acid and base. To prevent this linkage from breaking apart in acidic or basic conditions it is oxidised from the P(III) phosphite triester to the more stable P(V) phosphotriester. This is achieved by reaction with iodine and pyridine in water (Scheme 1.7).

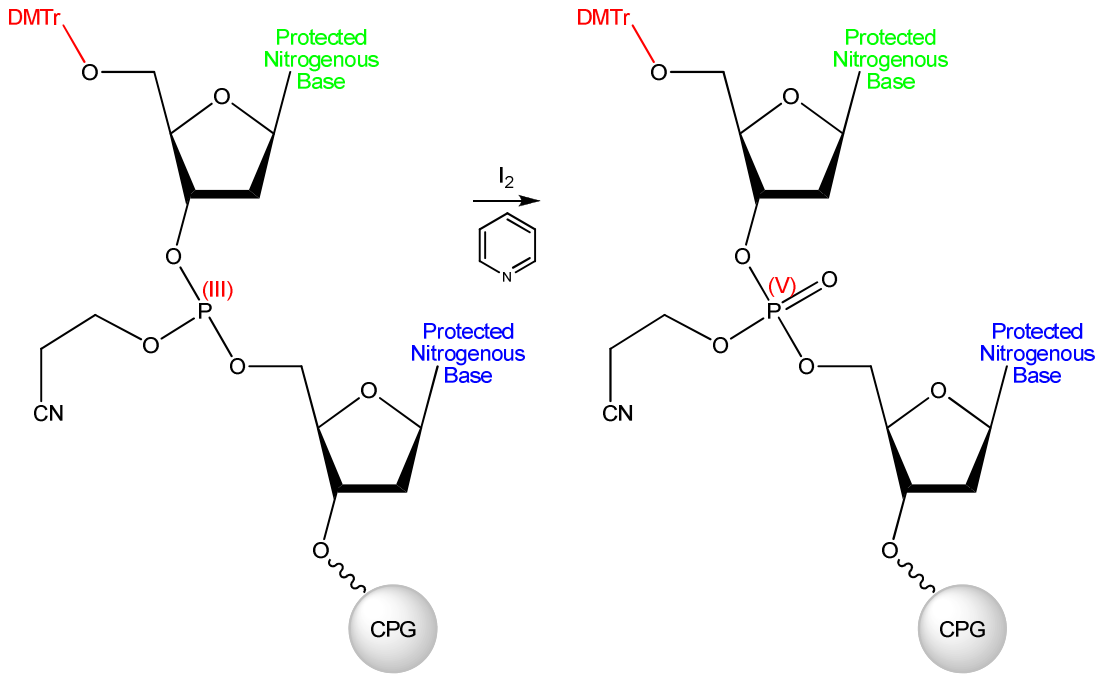

Scheme 1.7: Oxidation of the dinucleotide from P(III) to P(V)

Synthetic Cycle

To obtain the desired stand of synthetic DNA, the following steps are repeated with the corresponding phosphoramidite monomers:

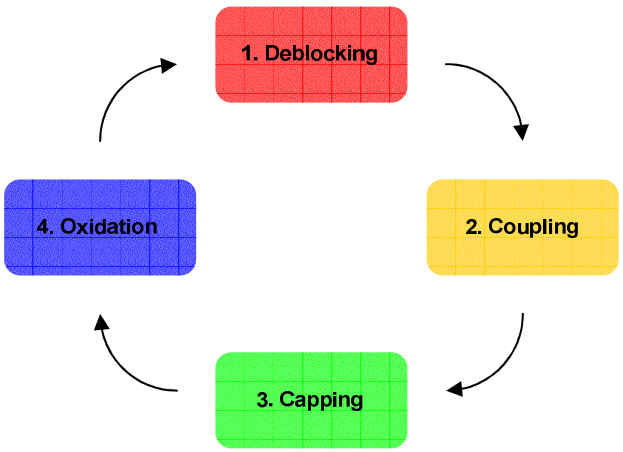

Figure 1.11: Synthetic cycle

Cleavage and Deprotection

The final steps in solid phase synthesis are to cleave the DNA sequences from the CPG beads, deprotect the amino groups on the nitrogenous bases and to remove the cyanoethyl group of the phosphate triester. All these steps are achieved by the addition of a concentrated aqueous solution of ammonium hydroxide. Cleavage from the CPG beads happens very quickly at room temperature. However deprotection of the amino groups and the removal of the cyanoethyl groups take longer and must be performed at an elevated temperature, typically 5 hours at 55 °C or 3 hours at 65 °C.

Purification

The purification of the desired synthetic DNA is required to remove any failed sequences which have been capped and any other impurities. This is done by HPLC, either by ion exchange or reverse phase. After purification, the DNA has a high salt content. Size exclusion chromatography (SEC) is used to remove the salt and freeze drying will remove any volatile counter ions.

1.1.4. Light Directed Synthesis of DNA

To date there has been two distinct methods reported on light directed synthesis of DNA, however both target the deblocking step of DNA synthesis. The first uses a photogenerated acid (PGA) to remove the dimethoxytrityl (DMTr) protection of the 5' hydroxyl, whereas the other uses an entirely novel protection group on the 5' hydroxyl which is cleaved by UV light.

Photogenerated Acid [11, 12]

Research by Dr Xiaolian Gao demonstrated a method of light directed synthesis of DNA on to a glass substrate in a 3' to 5' manner utilising a PGA. The standard 5' OH protecting group of DMTr is used but use a specific PGA upon illumination with UV light to remove the DMTr group (Scheme 1.8).

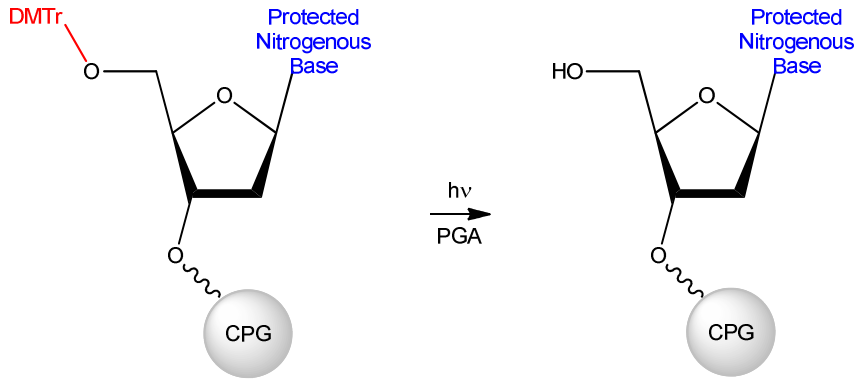

Scheme 1.8: Removal of the DMTr protecting group with a PGA

The PGA used was triarylsulfonium hexafluorostibate (Secant Chemicals Inc.) and when illuminated with UV light the following reaction occurs, generating the desired acid plus a variety of photoproducts (Scheme 1.9).

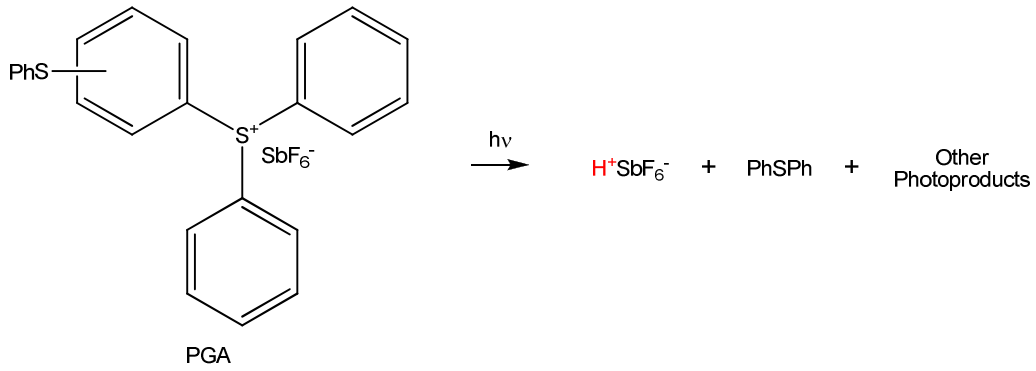

Scheme 1.9: Generation of the photoacid from the reaction of triarylsulfonium hexafluorostibate with UV light

This work was in collaboration with Xeotron Co. (Houston, Texas USA), where Gao is a co-founder and chief science officer. In 2004 Xeotron was acquired by Invitrogen in 2004, where they continue to sell Xeotron's XeoChip™ microarray. XeoChip™ microarrays are built up by software in a computer projecting UV light onto a digital micromirror device (DMD) in the desired positions to synthesise the required DNA strands. This eliminates the requirement for thousands of different physical photolithographic masks.

MeNPOC Protection [13, 14]

In the alternative method, a team lead by Dr Stephen P. A. Fodor developed a method for the light directed synthesis of DNA again on to a glass substrate in a 3' to 5' manner utilising a novel photo removable protection group. The novel group is methylnitro piperonyloxycarbonyl (MeNPOC) (Figure 1.12) and acts in the same way as the conventional DMTr as a 5' OH protecting group.

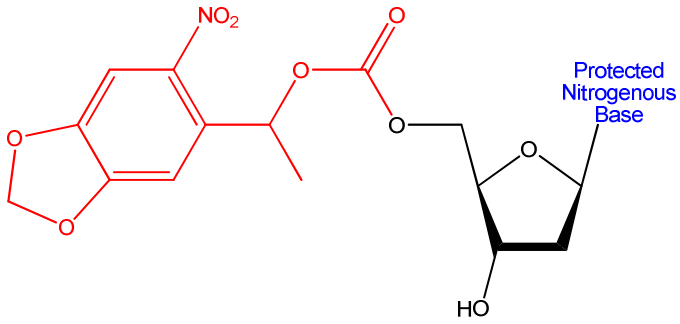

Figure 1.12: MeNPOC protection of 5' hydroxyl group

However this group is removed using UV light instead of a dilute acid solution (Scheme 1.10).

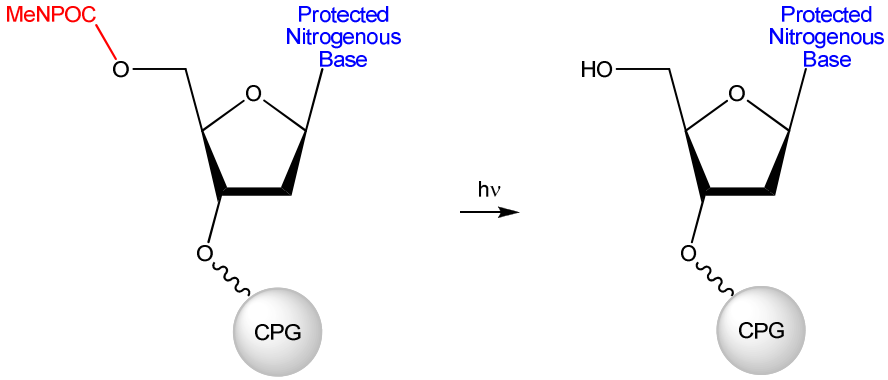

Scheme 1.10: Removal of the MeNPOC protecting group with UV light

This technology has now been commercialised by Affymetrix Inc. (Santa Clara, USA) in their GeneChip® microarray, where Fodor is a cofounder. Affymetrix now produce GeneChip® microarrays capable of analysing thousands of DNA sequences at once, this is achieved by building up the arrays using a variety of steel photolithographic masks to establish an illumination pattern and therefore the desired sequences onto the glass substrate.

1.2. Photoactive Groups

Photoactive chemicals are widespread thought the natural world and frequently used in chemistry to provide clean and efficient reactions compared to that of their equivalent chemical solution based reactions. For example, the UV conversion of pre-vitamin D to form the essential vitamin D, or the use of photoacid generators in polymeric materials.[15, 16] However there are two main classes of photoactive groups of great interest at present; ones that are removed by UV light and ones that are activated by UV light.

1.2.1. Groups Removed by UV Light

The UV labile compounds can also be classified as UV "bond breaking" as upon illumination with UV light they break existing covalent bonds to leave a specific functionality. There are two main examples of these types of compounds; o-nitrobenzyls and phenacyl esters.

o-Nitrobenzyls

o-Nitrobenzyls are a versatile group of molecules as they have the ability to protect a variety of functional groups. The chemical bond formed during the protection step will determine what functionality is revealed upon photodeprotection.

If a carbamate linkage is made between the two reactants, photodeprotection will reveal an amine with the liberation of carbon dioxide gas (CO_2) (Scheme 1.11).[17]

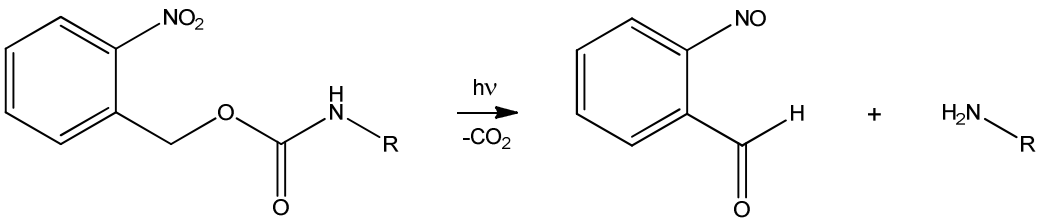

Scheme 1.11: Photodeprotection of an o-nitrobenzyl carbamate

A carbonate linkage will reveal an alcohol upon photodeprotection, also with the liberation of CO_2 gas (Scheme 1.12).[18]

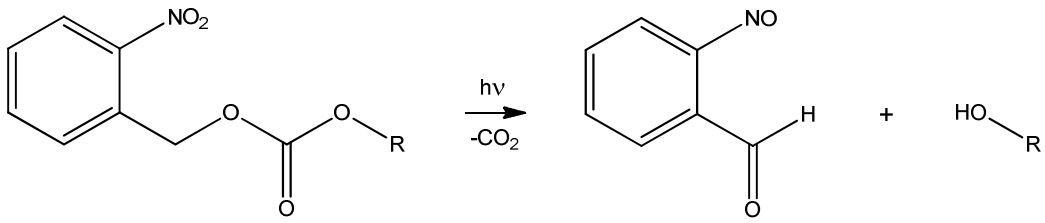

Scheme 1.12: Photodeprotection of an o-nitrobenzyl carbonate

However an ester linkage is slightly different as photodeprotection will reveal a carboxylic acid with no liberation of CO_2 gas (Scheme 1.13).[18]

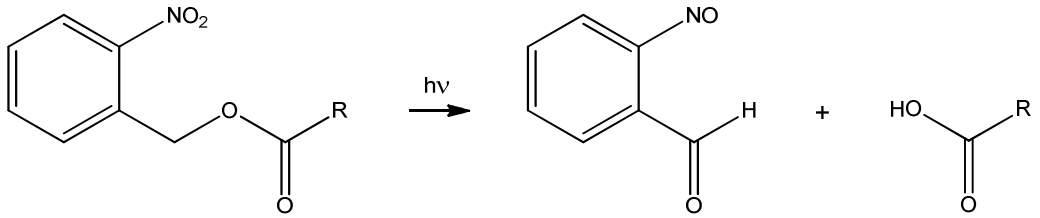

Scheme 1.13: Photodeprotection of an o-nitrobenzyl ester

Phenacyl Esters

Phenacyl esters are a specific group of molecules as upon deprotection by illumination with UV light they leave a carboxylic acid which is then available for further reactions. In general, the photodeprotection of the phenacyl esters liberates an acetophenone based side product along with the desired carboxylic acid (Scheme 1.14).[19]

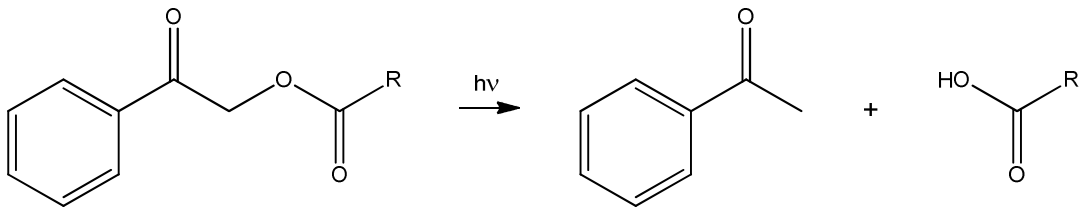

Scheme 1.14: Generic photodeprotection of phenacyl esters

However if the benzene ring has a 2,5-dimethyl substitution the system undergoes a internal cyclisation to liberate a dihydroindenone based side product along with the desired carboxylic acid (Scheme 1.15).[20]

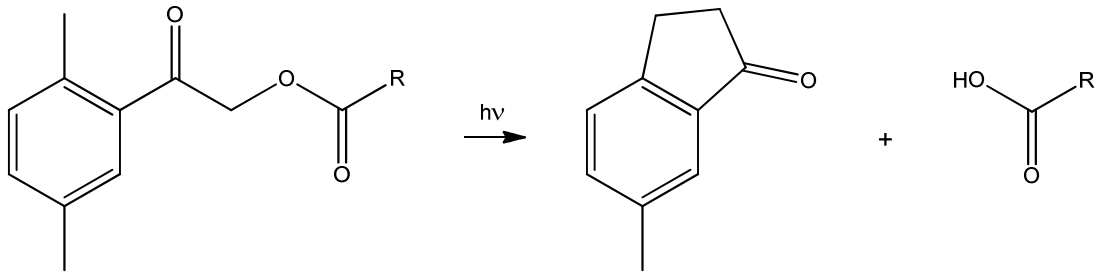

Scheme 1.15: Photodeprotection of a 2,5-dimethylphenacyl ester

1.2.2. Groups Activated by UV Light

However the UV activated compounds can also be classified as UV "bond forming" as upon illumination with UV light they form new covalent bonds with specific molecules in solution. There are two main examples of these types of compounds; benzophenones and phenyl azides.

Benzophenones

Benzophenones are a particularly useful group of molecules as the triplet state formed when irradiated with UV light can react with a reactive hydrogen containing compound to insert a carbon hydrogen bond (Scheme 1.16).[21] In addition to this, when the triplet state is deactivated, not via covalent bond formation, it can be readily reactivated. This unique feature of multiple-activation allows for greater efficiency of photocrosslinking as the benzophenone has more than one chance to react with its intended target.[22]

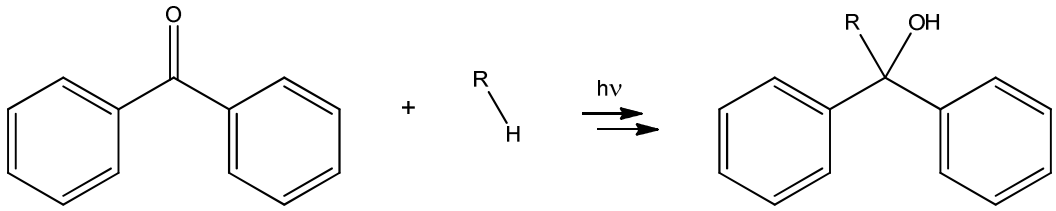

Scheme 1.16: Photoactivation of benzophenone with a reactive hydrogen containing compound

Phenyl Azides

Phenyl azides are a unique set of photoactive groups as they exclusively react with amines (except tertiary) when irradiated with UV light (Scheme 1.17).[23] Even though this reaction is a multi-step process it has been the focus of many research groups, in particular that of Prof. Matthew S. Platz, Ohio State University; Prof. Nina P. Gritsan, Novosibirsk State University and Prof. Gary B. Schuster, University of Illinois. As a result there have been many books and literally hundreds of research articles published about the photochemistry of phenyl azides.

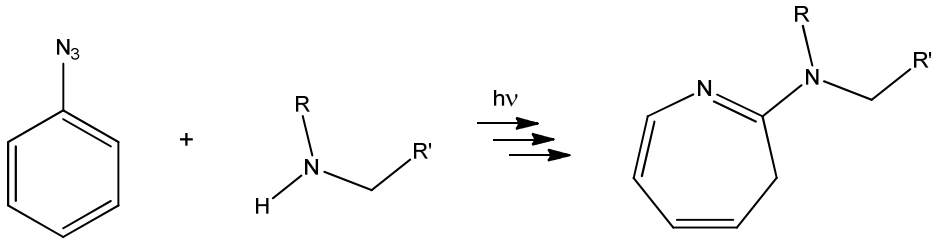

Scheme 1.17: Photoactivation of phenyl azide with a primary amine

1.3. Primary Aim of Research

The main aim of this research was to design a unique set of photoactive compounds that can be utilised for the photoimmobilisation of DNA on specific substrates. Both the photochemistry and chemistry of these compounds will be fully investigated with regards to their rates of reaction in UV light and their suitability for the functionalisation of the substrates.

CHAPTER 2

UV ACTIVATION OF PHENYL AZIDES

2. UV Activation of Phenyl Azides

2.1. Introduction

Phenyl azides were chosen as the photoactive group of choice for the basis of the research in this thesis, primarily as their photochemistry has been well established. Also the starting materials required for their synthesis are readily available and can easily be modified around the benzene ring for further functionalisation. The unique reaction between phenyl azides and amines can be then utilised for future applications of photoimmobilising DNA, as DNA can be readily functionalised to contain a primary amine.

2.1.1. Chemistry of Phenyl Azides

The first recorded synthesis of phenyl azide was by Griess in 1864 from the reaction between benzenediazonium perbromide and ammonia (Scheme 2.1).[24]

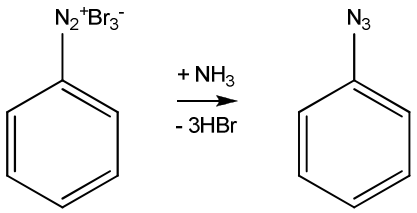

Scheme 2.1: Greiss synthesis of the first phenyl azide

Nowadays phenyl azides are more commonly synthesised by one of two routes:

1. nucleophilic substitution of an aromatic halogen (Scheme 2.2),

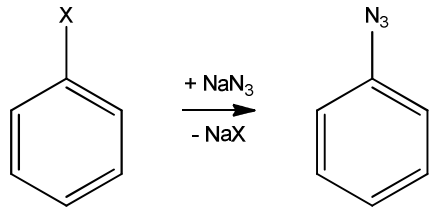

Scheme 2.2: Phenyl azide synthesis via nucleophilic substitution

2. diazotisation of an aromatic primary amine followed by subsequent aromatic nucleophilic substitution (Scheme 2.3).

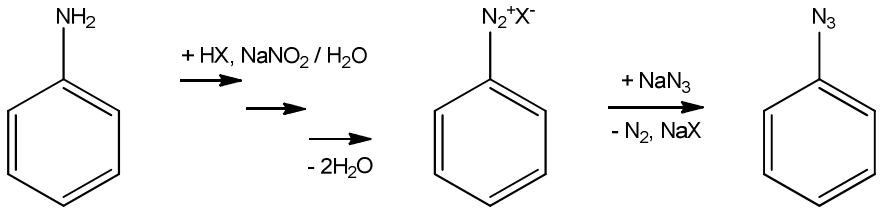

Scheme 2.3: Phenyl azide synthesis via diazotisation and nucleophilic substitution

Several key reviews have been published about the photochemistry of phenyl azides summarising the history and key research developments to date. From these comprehensive reviews, the modern mechanism and intermediates of the reaction between phenyl azide and a primary amine was determined (Scheme 2.4).[25-28]

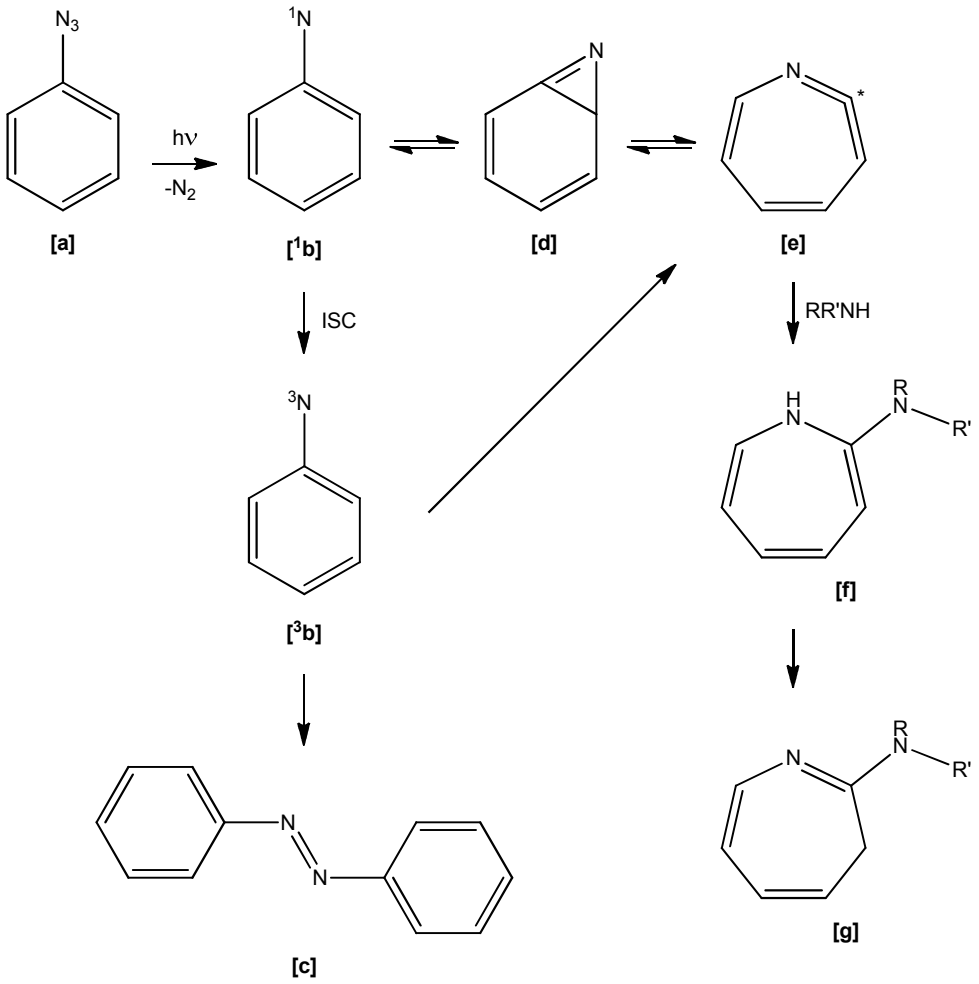

Scheme 2.4: Modern mechanism of phenyl azide photochemistry

When phenyl azide [a] is activated by UV light, singlet phenyl nitrene [^{1}b] is irreversibly formed through the loss of molecular nitrogen. Singlet phenyl nitrene can rearrange to the lower energy triplet phenyl nitrene [^{3}b] via intersystem crossing (ISC) and can either dimerise to form diphenyldiazene [c] or cyclise to form cyclic ketenimine [e]. Cyclic ketenimine is also formed from singlet state phenyl nitrene via a 1*H*-benzazirine intermediate [d]. When cyclic ketenimine is in the presence of an amine the reactive alpha carbon (*) reacts with the amine to form a 1*H*-azepine amine [f] which rearranges to form the desired more stable 3*H*-azepine amine [g].

Phenyl nitrenes are typically short lived reactive intermediates and are not trappable. However cyclic ketenimine has been found to be the major trappable reactive intermediate that is present in solution upon photolysis of phenyl azide at ambient temperatures (298 K). It is known that the rate of decay of singlet phenyl nitrene is equal to the rate of formation of the cyclic ketenimine, as a first order process.[29] This occurs in a two step process, first with a rate limiting cyclisation to benzazirine, followed by an electrocyclic ring opening to the cyclic ketenimine.[30] The proposed benzazirine intermediate from the photolysis of the parent phenyl azide has never been directly observed, however analogous benzazirines from 1- and 2-naphthyl azides have been characterised by IR.[31] The subsequent reaction between the cyclic ketenimine and a secondary amine to form a 1*H*-azepine amine has also been found to be a first order process.[32]

2.2. Results and Discussion

The aims of this chapter were to synthesise a suitable phenyl azide to be used as the core structure for future applications and to systematically investigate its chemical properties, with respect to its ability for further functionalisation and UV activation with and without the presence of a primary amine at a selection of wavelengths.

2.2.1. Synthesis of Phenyl Azides [1], [2] and [3]

The selection of suitable phenyl azides for this study was dependent on future applications as this would be the core component and would require further modifications.

To achieve this, the two requirements for the desired phenyl azide were set out:

1. carboxylic acid – for the provision of further functionalisation via an amide or ester reaction,
2. para azide – to avoid steric hindrance when the phenyl azide undergoes photolysis in the presence of a primary amine.

4-Azido-2-hydroxybenzoic acid [1] was chosen as a suitable substrate as it meets the required specifications and the starting material required is readily available in large quantities at a fraction of the cost of the desired product. It has also been used as component in a homobifunctional photocrosslinking reagent supplied by Thermo Scientific (Figure 2.1).[33, 34]

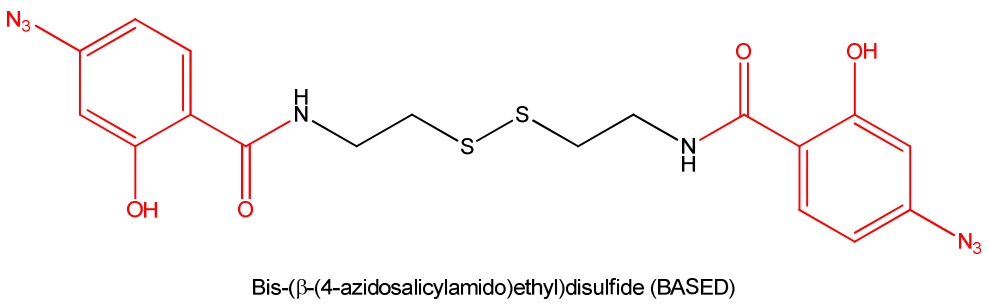

Bis-(β-(4-azidosalicylamido)ethyl)disulfide (BASED)

Figure 2.1: Example of a homobifunctional photocrosslinking reagent from Thermo Scientific

4-Azido-2-hydroxybenzoic acid [1] was synthesised via a modified Gano *et al.* method from 4-amino-2-hydroxybenzoic acid, by first diazotisation of the aromatic primary amine with sulfuric acid (H_2SO_4) and sodium nitrite ($NaNO_2$), followed by aromatic nucleophilic substitution with sodium azide (NaN_3) (Scheme 2.5).[35]

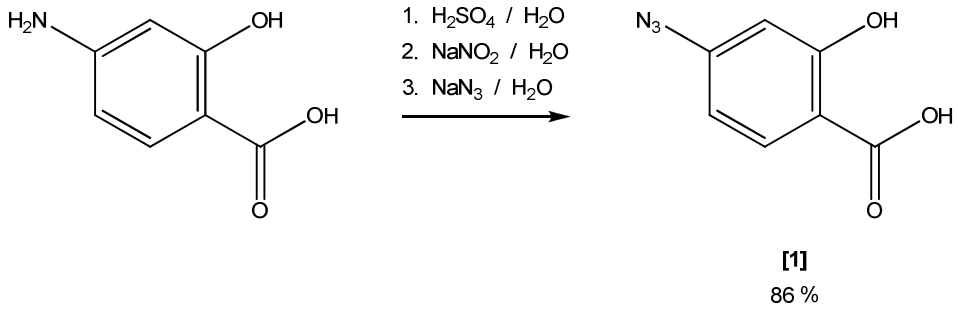

Scheme 2.5: Synthesis of 4-azido-2-hydroxybenzoic acid [1]

Attempts to purify this via flash column chromatography were problematic as the desired product had the tendency to remain on the silica gel even with a variety of polarities and solvent systems. This was almost certainly down to the phenolic hydroxyl interacting or reacting with the silica gel. Purification was achieved via subsequent washing with copious amounts of 1 % v/v HCl and distilled water to remove any unreacted starting material. After 5 wash cycles a yield of 86 % was achieved and a sample was recrystallised from ethyl acetate (EtOAc) to obtain a crystal for analysis via X-ray diffraction. The resulting ellipsoidal crystal structure is shown in Figure 2.2 as an entirely planar structure.

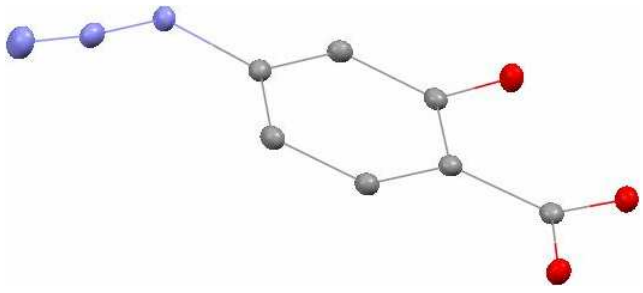

Figure 2.2: Ellipsoidal crystal structure of 4-azido-2-hydroxybenzoic acid [1]

Due to the tricky work up required for 4-azido-2-hydroxybenzoic acid [1] which did not result in an overly pure product, a new phenyl azide was required, as it was believed that any further modifications of this phenyl azide would again result in an impure product due to the phenolic hydroxyl.

An obvious choice for the new phenyl azide was to remove the phenolic group resulting in 4-azidobenzoic acid [2]. Again this was synthesised following the modified Gano *et al.* method from 4-aminobenzoic acid (Scheme 2.6), but purified this time via flash column chromatography.

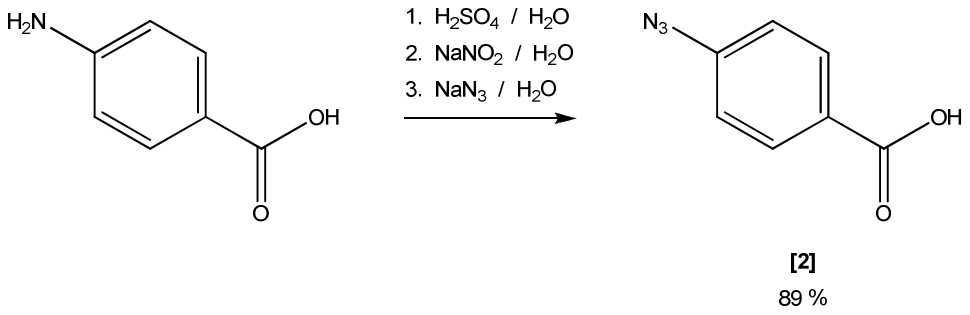

Scheme 2.6: Synthesis of 4-azidobenzoic acid [2]

After purification a yield of 89 % was achieved and a sample was recrystallised from EtOAc to obtain a crystal for analysis via X-ray diffraction. The resulting unit cell matched that given by Sasaki *et al.*[36]

A simple crude 10 mmol reaction with 2-aminoethanol with 1,1'-carbonyldiimidazole (CDI) over 24 hrs was performed to check the suitability for future modification, unfortunately a crude yield of the resultant product was found to be 21 %, and even after a 48 hr reaction only a 24 % crude yield was achieved. The only possible explanation for this poor yield could possibly be due to the proximity of the carboxylic acid to the aromatic ring.

To resolve this likely problem, a new phenyl azide was designed to have a spacer CH_2 group between the benzene ring and the carboxylic acid, this lead to 2-(4-azidophenyl)acetic acid [3]. This was also synthesised following the modified Gano *et al.* method from 2-(4-aminophenyl)acetic acid (Scheme 2.7), and purified via flash column chromatography.

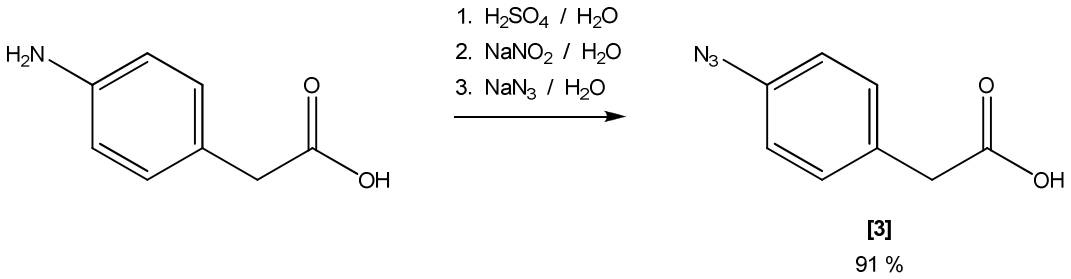

Scheme 2.7: Synthesis of 2-(4-azidophenyl)acetic acid [3]

After purification a yield of 91 % was achieved and a sample was recrystallised from EtOAc to obtain a crystal for analysis via X-ray diffraction. The resulting ellipsoidal crystal structure is shown in Figure 2.3 where the extra CH_2 group causes a kink in the expected planar structure.

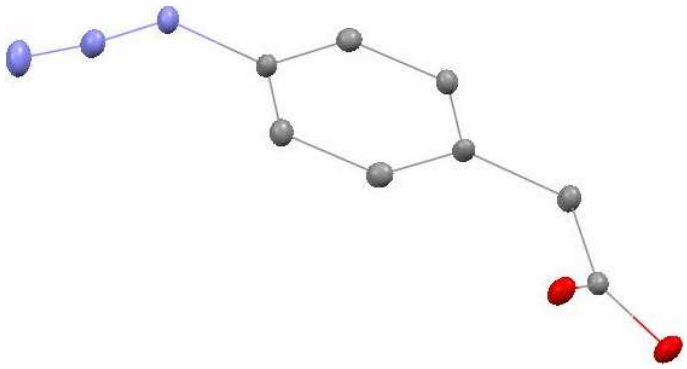

Figure 2.3: Ellipsoidal crystal structure of 2-(4-azidophenyl)acetic acid [3]

Again a simple crude 10 mmol reaction with 2-aminoethanol with CDI over 24 hrs was performed to check the suitability for future modification, and a crude yield of the resultant product was found to be 84 %. Therefore this phenyl azide would be used as the core structure for future applications.

2.2.2. UV Activation of Phenyl Azides [1], [2] and [3]

Rate of Reaction Study

The investigation into first order rate of reaction of all the three synthesised phenyl azides with and without the presence of a primary amine, was conducted at different wavelengths.

1-Hexylamine (Figure 2.4) was selected as the primary amine for two reasons:

1. long alkyl chain – liquid at room temperature, which makes for easy weighing out,
2. non-aromatic – ensuring there is no interference and confusion with the phenyl azide UV-vis spectra.

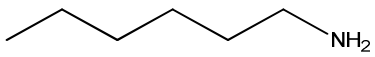

Figure 2.4: 1-Hexylamine

Within the electromagnetic spectrum the wavelength range for UV light is 400 nm to 100 nm. This range is subdivided into three divisions; UV-A, UV-B and UV-C.[37]

1. UV-A – 400 nm to 315 nm (black light),
2. UV-B – 315 nm to 280 nm (erythemal UV),
3. UV-C – 280 nm to 100 nm (germicidal UV).

Two wavelengths were chosen for this study, one in the UV-A range and the other in the UV-B range, as any wavelength in the UV-C range will mutate DNA, which will not be appropriate use in future applications. The wavelengths used were 302 nm (UV-B) and 365 nm (UV-A) from UV lamps enclosed in a transilluminator. These lamps have broad outputs centred on their respective wavelengths (Figure 2.5).[38]

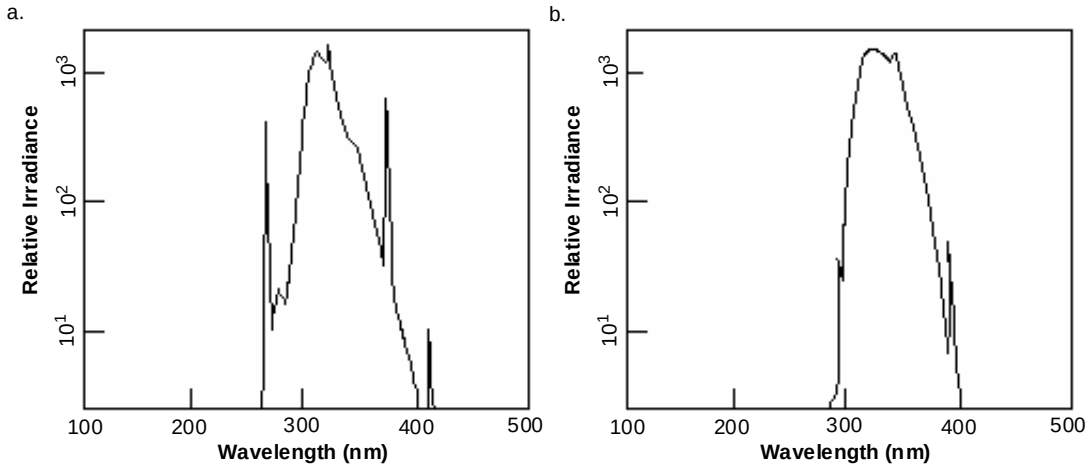

Figure 2.5: UV spectral output chart; a. 302 nm, b. 365 nm

Six stock solutions at 5×10^{-5} M in MeOH were prepared for the UV activation study in the combinations outlined in Table 2.1.

Stock Solution Code	Phenyl Azide [1]	Phenyl Azide [2]	Phenyl Azide [3]	1-Hexylamine
[a]	✓			
[b]	✓			✓
[c]		✓		
[d]		✓		✓
[e]			✓	
[f]			✓	✓

Table 2.1: Stock solutions prepared in MeOH for the UV activation study

To six separate quartz cuvettes, 2 mL of each stock solution were added, sealed and a UV-vis absorption spectrum was taken before illumination. The cuvettes were then placed flat down in the transilluminator with the transparent side against the UV lamp. The lamp was then switched on at the desired UV emission wavelength (302 nm or 365 nm) and the solutions inside the cuvettes were illuminated.

A UV-vis absorption spectrum was then taken again after the following time durations 5, 10, 15, 20, 25, 30, 45, 60, 75, 90, 105, 120, 150, 180, 210, 240, 300, 360, 420, 480, 540, 600, 720, 840, 960, 1080 and 1200 seconds.

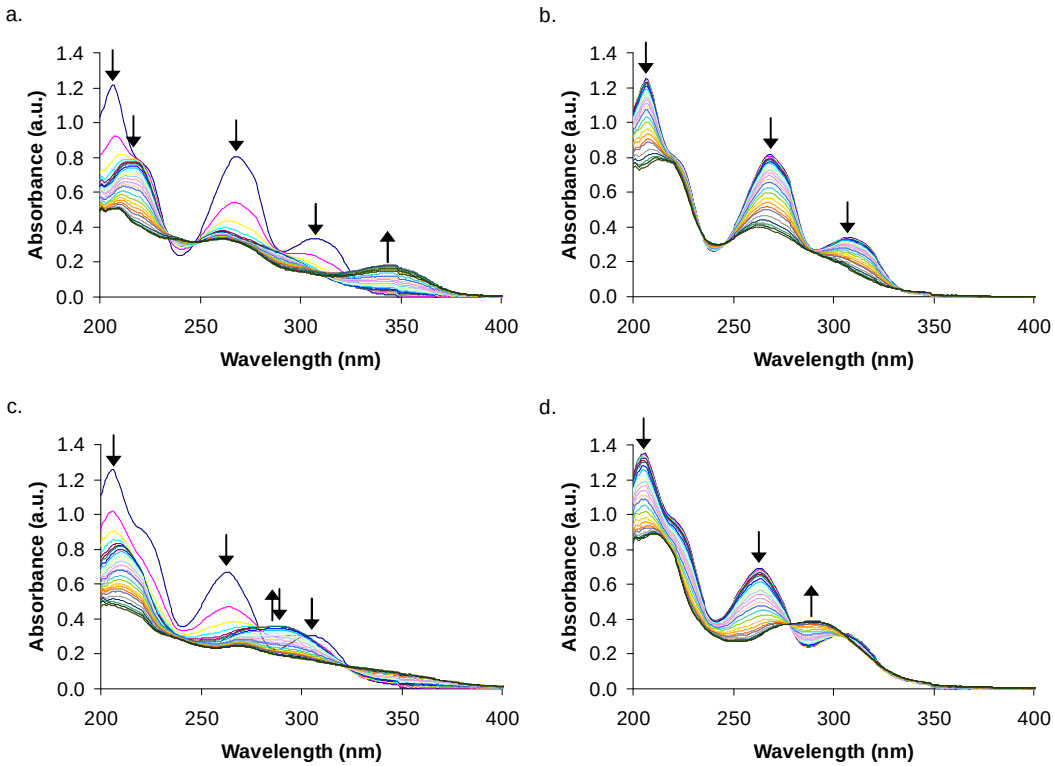

Figure 2.6: UV-vis spectra of: a. [a] at 302 nm; b. [a] at 365 nm; c. [b] at 302 nm; d. [b] at 365 nm

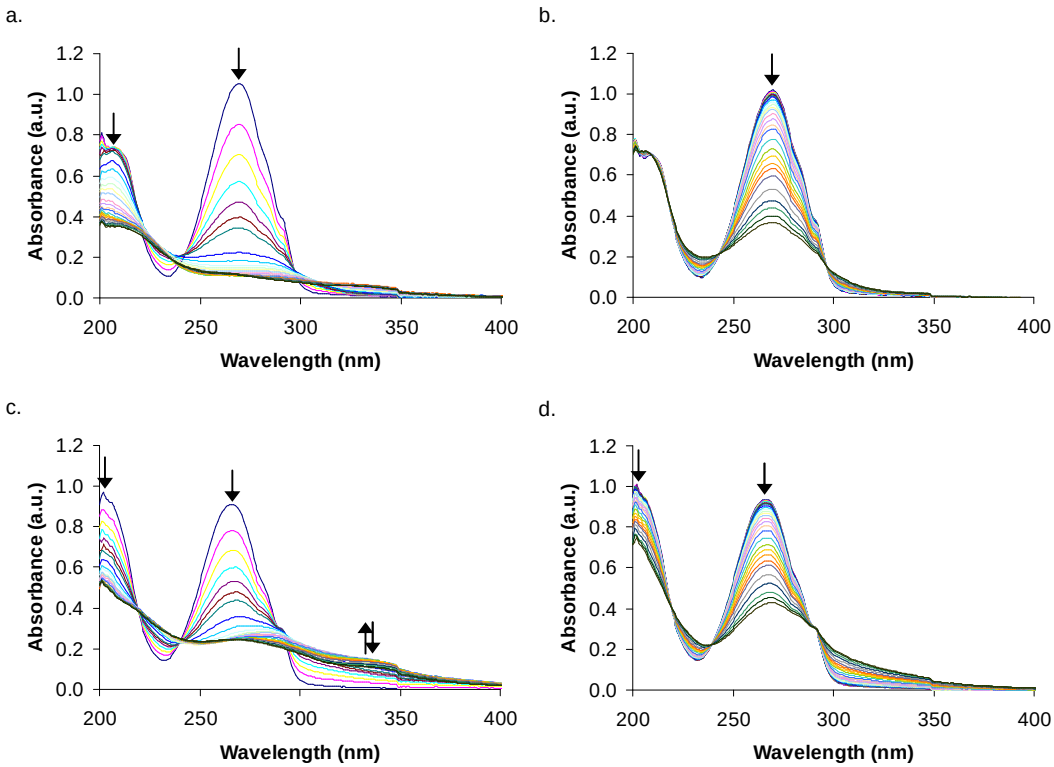

Figure 2.7: UV-vis spectra of: a. [c] at 302 nm; b. [c] at 365 nm; c. [d] at 302 nm; d. [d] at 365 nm

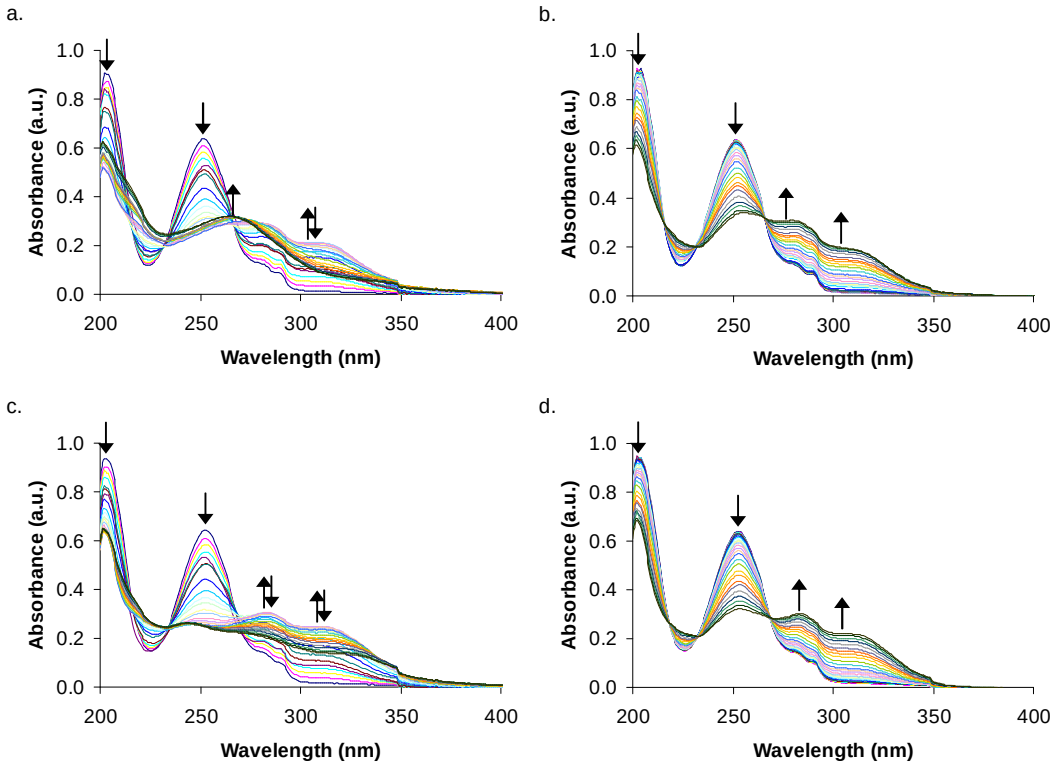

Figure 2.8: UV-vis spectra of: a. [e] at 302 nm; b. [e] at 365 nm; c. [f] at 302 nm; d. [f] at 365 nm

Equation 2.1 describes the first order raw law for the disappearance of the starting material [A]:

$$-\frac{d[A]}{dt} = k[A]$$

Equation 2.1: First order rate law [39, 40]

This can be integrated directly, where initially the concentration of [A] is $[A]_0$, and at a later time t it is $[A]_t$ (Equation 2.2):

$$\ln[A]_t = -kt + \ln[A]_0$$

Equation 2.2: Integrated rate law [39, 40]

Since absorption and concentration of an analyte are linked by the Beer-Lambert law (Equation 2.3), they are directly proportional to each other via their molar extinction coefficient and in this case they can be used interchangeably.

$$A = \varepsilon \cdot c \cdot l$$

Equation 2.3: Beer-Lambert law

Although stock solutions were prepared using the serial dilution technique to a concentration of 5×10^{-5} M, it is not guaranteed that all of the solutions are at the same concentration. Therefore by rearranging the integrated rate law, it is possible to counteract this; in essence you are expressing the concentration at time t as a percentage of the concentration at time 0 (Equation 2.4).

$$\ln[A]_t/[A]_0 = -kt$$

Equation 2.4: Rearranged integrated rate law [39, 40]

First order graphs of $\ln([A]_t/[A]_0)$ versus time (s) were then plotted for each solution at both wavelengths of illumination, where [A] is the λ_{max} E_2-band (π - π^* transition) and is typically around 204 nm as this is the λ_{max} for benzene (Table 2.2).[41] By monitoring the disappearance of this peak it was possible to measure the rate of formation of the cyclic ketenimine, as it is equal to the rate of decay of singlet phenyl nitrene, which is obtained from the gradient of the slope (–k).

Phenyl Azide	E_2-Band (nm)
[1]	**206**
[2]	**201**
[3]	**203**

Table 2.2: E_2-bands of phenyl azide [1], [2] and [3]

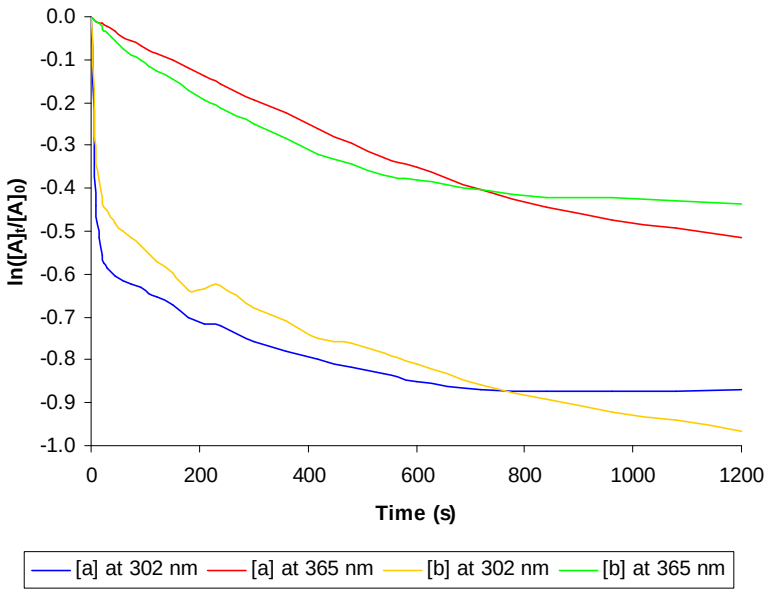

Figure 2.9: First order plots of UV activation of phenyl azides [1] with and without 1-hexylamine at 302 nm and 635 nm

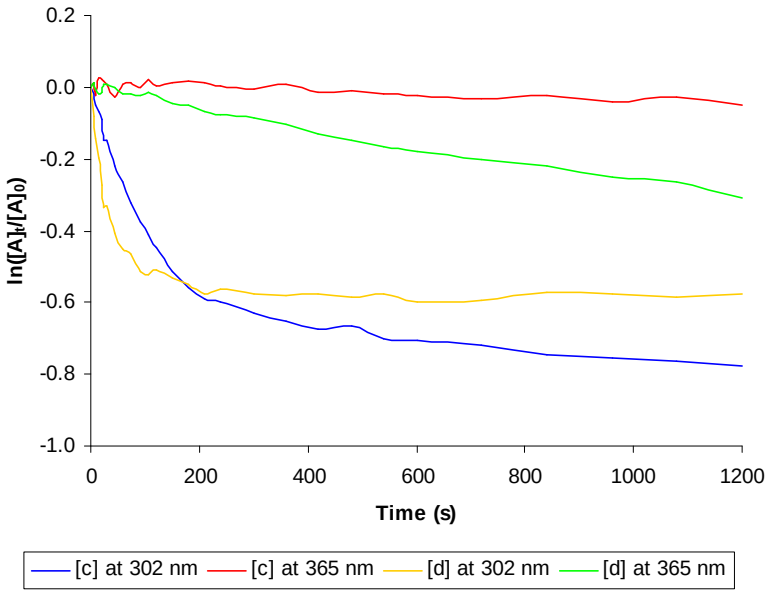

Figure 2.10: First order plots of UV activation of phenyl azides [2] with and without 1-hexylamine at 302 nm and 635 nm

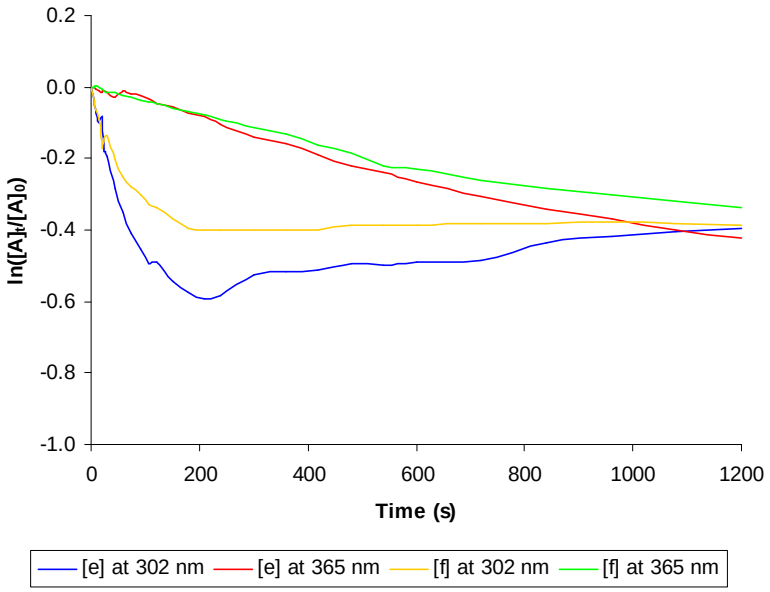

Figure 2.11: First order plots of UV activation of phenyl azides [3] with and without 1-hexylamine at 302 nm and 635 nm

From the first order graphs shown in Figure 2.9, Figure 2.10 and Figure 2.11 the UV activation of phenyl azides [1], [2] and [3] with and without the presence of 1-hexylamine using the 302 nm source did not follow a typical first order reaction plot. In this case the rate of reaction was occurring much faster than that at 365 nm, this is because the shorter wavelength photon has a higher energy than the longer wavelength. The rate constants for the UV activation of phenyl azides [1], [2] and [3] with and without the presence of 1-hexylamine using the 365 nm source were then calculated from the gradient of the slopes from the graphs in Figure 2.9 and expressed in Table 2.3.

Solution at 365 nm	Rate Constant (s^{-1})	R^2
[a]	4.71×10^{-4}	0.972
[b]	4.11×10^{-4}	0.872
[c]	4.60×10^{-5}	0.615
[d]	2.66×10^{-4}	0.984
[e]	3.85×10^{-4}	0.985
[f]	3.13×10^{-4}	0.973

Table 2.3: Rate constants and goodness of fit (R^2) values

With the exception of 4-azidobenzoic acid [2], the rate constants were larger for illumination on their own than in the presence 1-hexylamine and followed a better goodness of fit. These small discrepancies are more than likely due the subsequent reaction between the cyclic ketenimine and 1-hexylamine forming the 3*H*-azepine product. The small rate constant observed for the 4-azidobenzoic acid without 1-hexylamine appeared to be coming from the lack of conversion of the singlet phenyl nitrene to the 1*H*-benzazirine, as the E_2-band absorption remained relatively constant.

NMR Study

The reaction between the chosen phenyl azide, 2-(4-azidophenyl)acetic acid [3], and 1-hexylamine when exposed to UV light was investigated by NMR. The reaction was monitored using 1H NMR as it would provide spectroscopic verification of the product being formed. Scheme 2.8 shows the expected product formed between the reaction of 2-(4-azidophenyl)acetic acid [3] and 1-hexylamine with UV light.

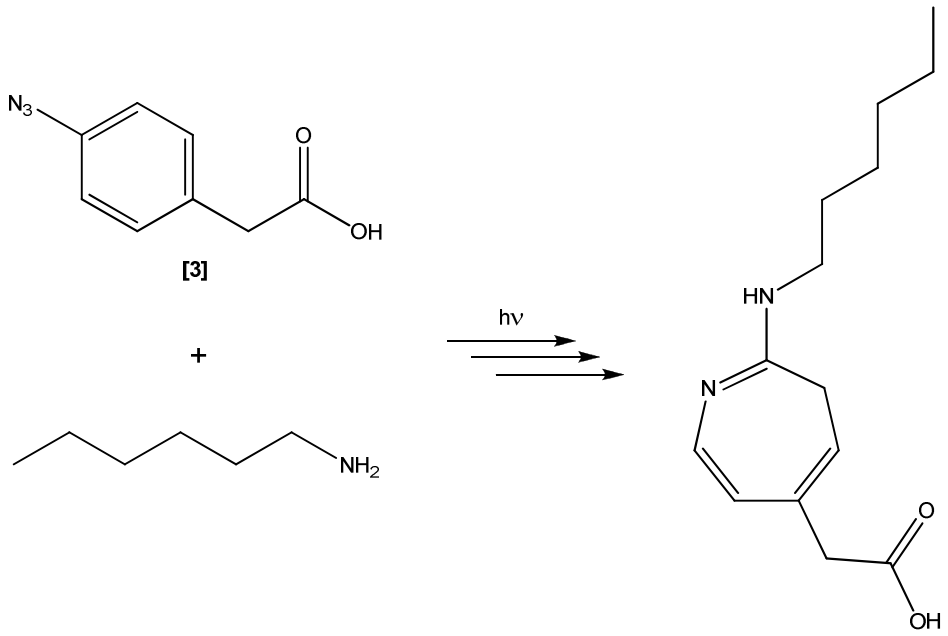

Scheme 2.8: Reaction between 2-(4-azidophenyl)acetic acid [3] and 1-hexylamine under UV light

The UV emission source used for this study was a blacklight blue lamp with an output of 365 nm with fractions of visible light.

To a quartz NMR tube, 1 mL of a 1:1 0.1 M solution of 2-(4-azidophenyl) acetic acid [3] and 1-hexanamine in DMSO-d_6 was added, sealed and a 1H NMR taken before illumination. The NMR tube was then clamped 5 cm away from the UV lamp and illuminated for 5 minutes followed by a 1H NMR. This process of illuminating for 5 minutes and taking a 1H NMR was repeated up to 30 minutes.

Upon illumination gas bubbles were observed within the solution, this can be identified with confidence as nitrogen gas, from the irreversible conversion of the phenyl azide to its respective singlet phenyl nitrene. This was not observed during the rate of reaction study, but this is more than likely due to the low concentration of the phenyl azide used, rather than no reaction occurring.

Figure 2.12 is a stacked 1H NMR spectrum shows the gradual appearance of the product peaks over time.

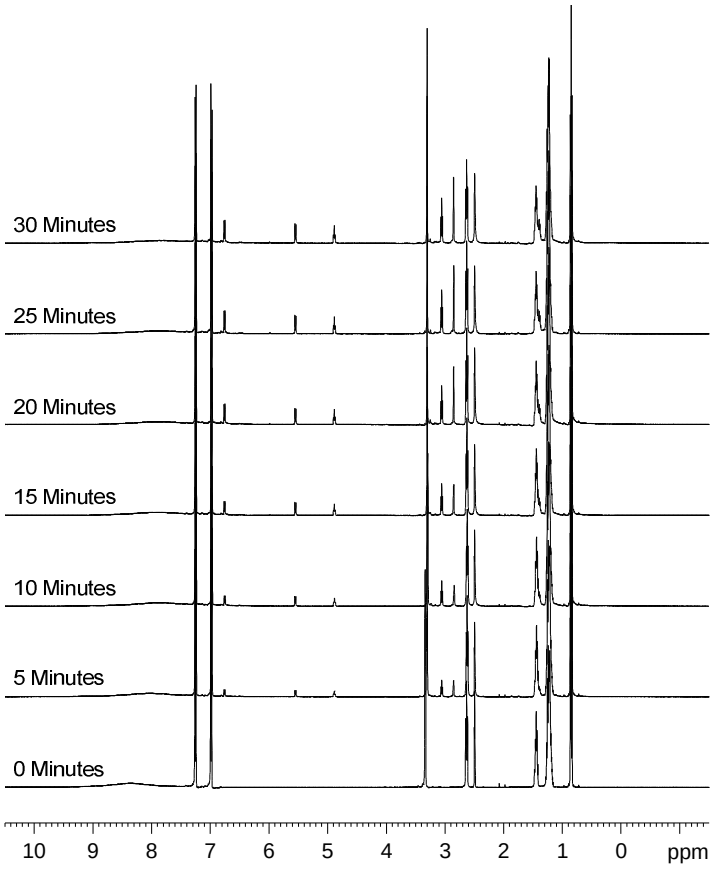

Figure 2.12: Stacked 1H NMR spectrum

By subtracting the 1H NMR spectrum at 30 minutes from that at 0 minutes a difference spectrum is generated (Figure 2.13), and can be used to monitor the disappearance of the starting materials (below the baseline) and the appearance of the product (above the baseline).

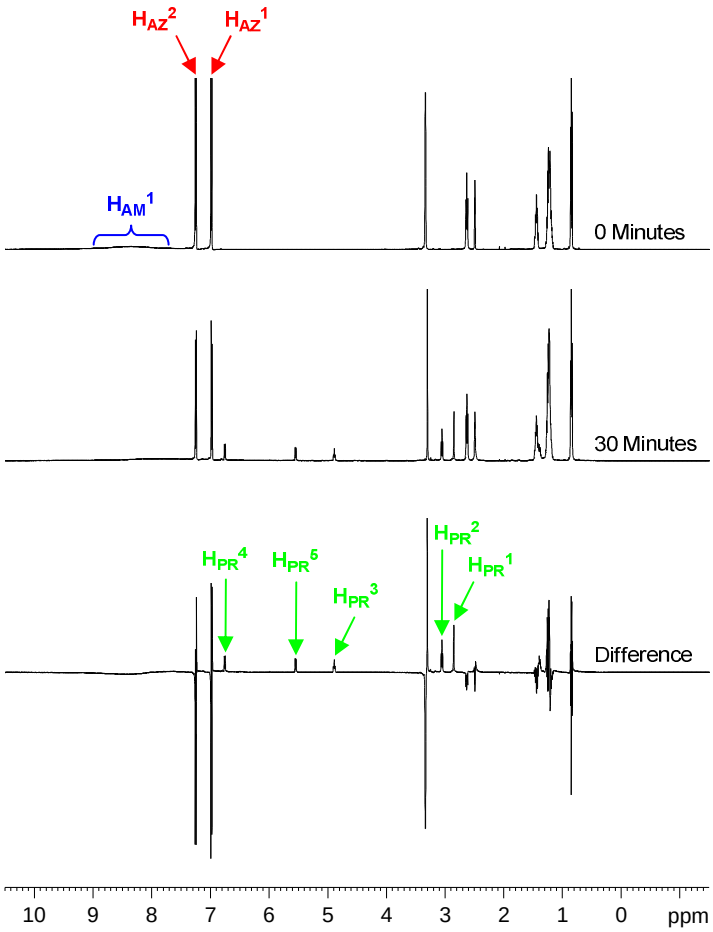

Figure 2.13: 1H NMR spectra at 0 minutes, 30 minutes and the difference; showing the positions of key protons in the starting materials and products

Highlighted on the 0 minutes spectrum and difference spectrum are the protons of interest which have been subsequently been assigned to the starting materials and product outlined in Scheme 2.9.

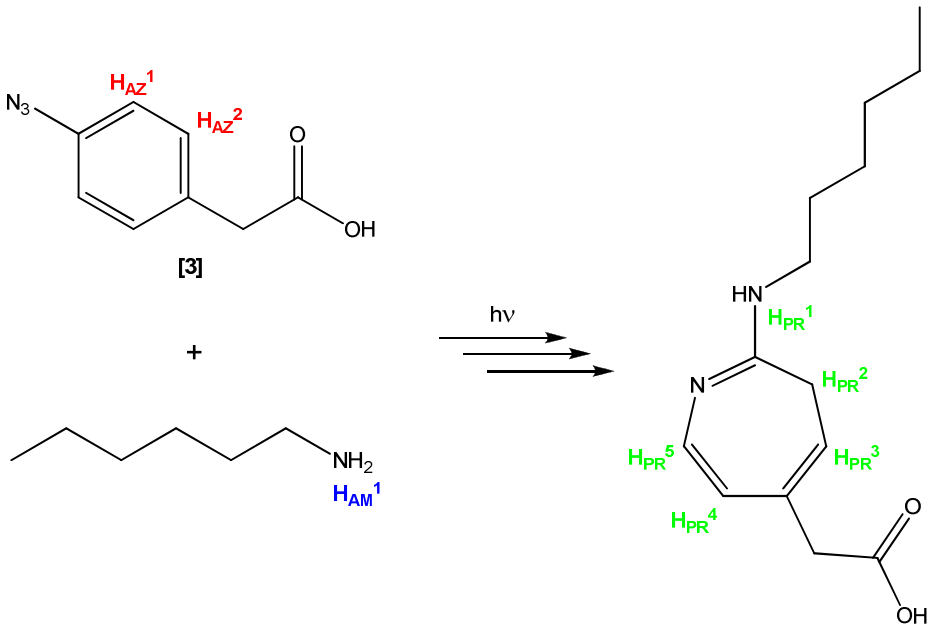

Scheme 2.9: Reaction between 2-(4-azidophenyl)acetic acid [3] and 1-hexylamine under UV light, highlighting key protons

Table 2.4 summaries the chemical shifts, integrations and multiplicities of the starting materials and product. The crucial protons, to prove the phenyl azide photochemistry, were the amino protons of 1-hexylamine at 8.5 ppm, which were shown to gradually disappear over time. This coincided with the appearance of a singlet at 2.8 ppm which was attributed to the single amine proton of the product.

Proton	Chemical Shift (ppm)	Integration	Multiplicity
H_{AZ}^{1}	7.1	2	Multiplet (AA'BB' splitting)
H_{AZ}^{2}	7.2	2	Multiplet (AA'BB' splitting)
H_{AM}^{1}	8.5	2	Broad Singlet
H_{PR}^{1}	2.8	1	Singlet
H_{PR}^{2}	3.1	2	Triplet
H_{PR}^{3}	4.9	1	Triplet
H_{PR}^{4}	6.8	1	Doublet
H_{PR}^{5}	5.6	1	Doublet

Table 2.4: Chemical shifts, integrations and multiplicities of starting materials and product

2.3. Experimental

2.3.1. Solvents and Reagents

All solvents and reagents used for experimental work were of laboratory grade and were purchased from commercial sources (Aldrich, Sigma, Fluka and Alfa Aesar).

2.3.2. Chromatography

Flash column chromatography was carried out using silica gel 60 (Merck), where specific solvent systems are expressed in Table 2.5.

TLC was carried out using aluminium sheets coated with silica gel 60 0.2 mm F254 (Merck), where specific solvent systems are expressed in Table 2.5.

Code	Solvents	Ratios
[A]	EtOAc:Pet Ether 60-80	50:50
[B]	EtOAc:MeOH	95:5
[C]	Pet Ether 60-80:EtOAc	50-0:50-100

Table 2.5: Chromatography solvent systems

TLC Plate Detection Tests

Products were visualised on TLC plates with the following techniques:

- UV absorption at 264 nm where appropriate,
- Ninhydrin (0.2 g ninhydrin in 500 mL EtOH) and heat to 110 ºC,
    - Amines → dark blue/purple.
- Bromocresol green (0.1 g bromocresol green in 500 mL EtOH and 5 mL 0.1 M NaOH),
    - Acids → yellow / Amines → dark blue.

2.3.3. Chemical Analysis, Spectroscopy and Instrumentation

Prior to analysis, all samples were dried over P_2O_5 under vacuum in a desiccator overnight.

1H and 13C NMR spectra for characterisation were recorded on a Brüker DPX400 spectrometer with the solvent peak as a reference and with *J* values quoted in Hertz.

High resolution mass spectral analyses were performed as an outside service by the EPSRC mass spectrometry service centre, University of Swansea.

Elemental analyses were performed on a Perkin-Elmer 240 elemental analyser as a University of Strathclyde service.

Single crystal X-ray diffractions were performed on a Brüker Nonius Apex II CCD diffractometer at 120 K using Mo K α radiation (0.71073Å) as a University of Strathclyde service, where crystallographic details and refinement parameters are outlined in Appendix 7.2.

Mercury (Version 1.4.2, Build 2) was used to generate ellipsoidal crystal structure figures.[42-46]

UV illumination source for the rates of reaction study was a UVP 2UV transilluminator, using sealed quartz cuvettes as the reaction container.

UV-vis absorption spectra were recorded using a Varian Cary 300 Bio UV-vis spectrophotometer with quartz cuvettes of a path length of 10 mm.

UV illumination source for the 1H NMR study was a 2 × 8 W blacklight blue (BLB) UVA tubes (Philips F8/T5/BLB) in a Vilber-Lourmat model number VL-208 irradiation unit, using a sealed quartz NMR tube (Aldrich) as the reaction container.

1H NMR spectra for the UV light activation study were recorded on a Brüker DRX500 spectrometer with the solvent peak as a reference.

2.3.4. Synthetic Procedures

4-Azido-2-hydroxybenzoic acid [1]

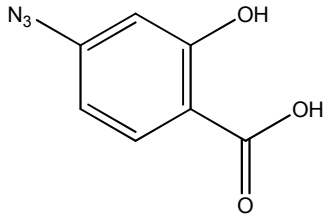

[1]

4-Amino-2-hydroxybenzoic acid (5.00 g, 33 mmol, 1 eq) was dissolved in H_2SO_4 (25 mL) and distilled water (130 mL) and cooled to 0 ºC. When dissolved, a cold solution of $NaNO_2$ (2.80 g, 41 mmol, 1.21 eq) in distilled water (25 mL) was added and stirred at 0 ºC for 1 hr. A cold solution of NaN_3 (3.60 g, 55 mmol, 1.70 eq) in distilled water (20 mL) was then added dropwise over 1 hr. This was stirred at 0 ºC for a further 1 hr and subsequently left to stir overnight at ambient temperature. The reaction mixture was washed with EtOAc (150 mL × 2) and then with saturated NaCl solution (150 mL × 2). Purification was achieved by repeated alternate washing with copious amounts of 1 % v/v HCl and distilled water. The organic phase was then dried with Na_2SO_4 and concentrated *in vacuo* to afford title compound [1] (5.02 g, 86 %) as a light brown solid (Found: C, 47.4; H, 2.8; N, 22.75 % $C_7H_5N_3O_3$ requires C, 46.9; H, 2.8; N, 23.5 %); δ_H(400 MHz; DMSO-d_6) 6.63-6.68 (2H, m, ArH), 7.79-7.81 (1H, d, *J*8.8 , ArH), 12.66 (1H, br s, CO_2H); δ_C(100 MHz; DMSO-d_6) 106.8, 109.9, 110.4, 132.1, 146.4, 162.4, 171.3; m/z (MS-ESI) 178.0257 ($[M–H]^-$ $C_7H_4N_3O_3^-$ requires 178.0258); ν_{max} (NaCl/nujol)/cm^{-1} 3441 wk, br (–OH, phenol H-bonded), 2124 st, sh (–N_3), 1657 st, sh (C=O, CO_2H); mp 192-193 ºC (dec).

4-Azidobenzoic acid [2]

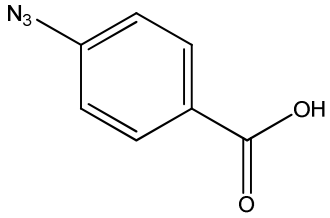

[2]

Preparation was as for compound [1] but 4-aminobenzoic acid (4.48 g, 32.6 mmol) was used instead of 4-amino-2-hydroxybenzoic acid (5.00 g, 32.6 mmol). Purification was achieved by flash column chromatography [A] to afford title compound [2] (4.73 g, 89 %, R_f = 0.65 [B]) as a cream solid (Found: C, 51.8; H, 3.0; N, 25.25 % $C_7H_5N_3O_2$ requires C, 51.6; H, 3.1; N, 25.8 %); δ_H(400 MHz; DMSO-d_6) 7.20-7.23 (2H, m, AA'BB' splitting, ArH), 7.94-7.98 (2H, m, AA'BB' splitting, ArH), 12.94 (1H, s, CO_2H); δ_C(100 MHz; DMSO-d_6) 119.2, 127.3, 131.2, 131.2, 143.9, 166.5; m/z (MS-ESI) 162.0307 ([M–H]$^-$ $C_7H_4N_3O_2^-$ requires 162.0309); ν_{max} (NaCl/nujol)/cm^{-1} 2108 st, sh (–N_3), 1683 st, sh (C=O, CO_2H); mp 184-186 ºC (dec).

2-(4-Azidophenyl) acetic acid [3]

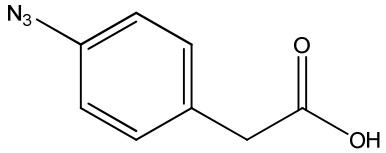

[3]

Preparation was as for compound [1] but 2-(4-aminophenyl)acetic acid (4.94 g, 32.6 mmol) was used instead of 4-amino-2-hydroxybenzoic acid (5.00 g, 32.6 mmol). Purification was achieved by flash column chromatography [C] to afford title compound [3] (5.26 g, 91 %, R_f = 0.49 [B]) as a light brown solid (Found: C, 54.35; H, 4.2; N, 23.5 % $C_8H_7N_3O_2$ requires C, 54.2; H, 4.0; N, 23.7 %); δ_H(400 MHz; DMSO-d_6) 3.57 (1H, s, CH_2), 7.04-7.08 (2H, m, AA'BB' splitting, ArH), 7.28-7.32 (2H, m, AA'BB' splitting, ArH), 12.32 (1H, s, CO_2H); δ_C(100 MHz; DMSO-d_6) 39.9, 118.9, 131.0, 132.0, 137.7, 172.5; m/z (MS-CI) 178.0611 ([M+H]$^+$ $C_8H_8N_3O_2^+$ requires 178.0611); ν_{max} (NaCl/nujol)/cm^{-1} 2122 st, sh (–N_3), 1695 st, sh (C=O, CO_2H); mp 89-90 ºC.

CHAPTER 3

PHOTOIMMOBILISATION OF DNA

3. Photoimmobilisation of DNA

3.1. Introduction

3.1.1. Immobilisation of DNA

The most popular way method of immobilising DNA to a solid support is via the functionalisation of glass using trialkoxysilanes (Scheme 3.1).

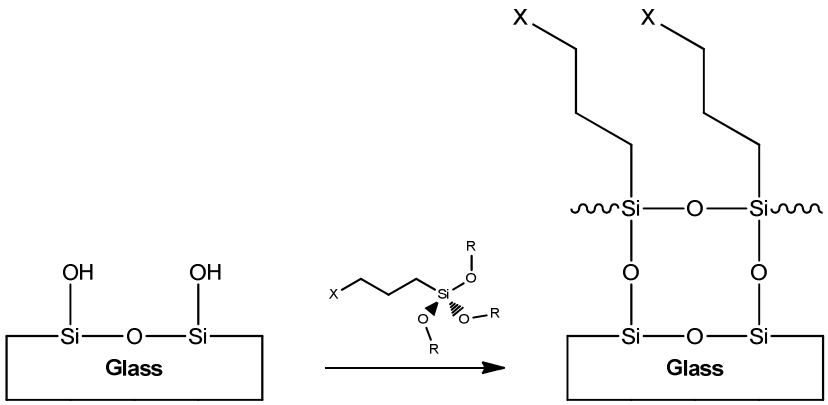

Scheme 3.1: Reaction of trialkoxysilanes with glass where X represents the functional group

There are a wide variety of trialkoxysilanes commercially available, ones of particular interest are mercapto-, amino-, carboxy- and glycidoxy- trialkoxysilanes, which contain the functional groups –SH, $–NH_2$, $–CO_2H$ and epoxide respectively. Since DNA can be readily functionalised to contain a useful functional group, such as mercapto and amino, established standard chemical methods can be used to immobilise DNA onto the glass. For example Rogers *et al.* utilised 3-mercaptopropyltrimethoxysilane for the attachment of 5'-disulfide-modified oligonucleotides via disulfide bonds.[47] Also in a method described by Carré *et al.*, 3-aminopropyltriethoxysilane was utilised for the immobilisation of DNA via ionic interactions by exploiting the electrostatic interactions developed between the positively charged amine functions and the negatively-charged phosphate groups of DNA.[48]

An alternative way of immobilising DNA has been achieved via the use of sulfur based ligands onto gold nanoparticles. Thiol, thioctic acid and dithiocarbamate modified DNA have all been shown to successfully attach to the gold nanoparticles through the sulfur ligand (Figure 3.1).[49-51]

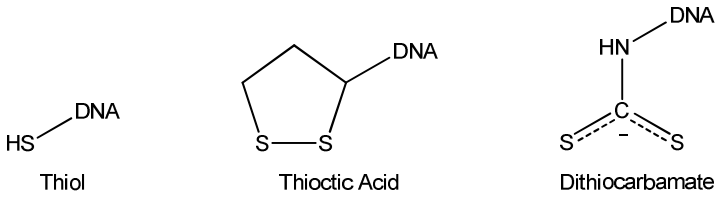

Figure 3.1: Structures of sulfur based ligands used for the immobilisation of DNA onto gold nanoparticles

Both the thioctic acid and dithiocarbamate ligands showed a significant increase in stability of the gold nanoparticles towards dithiothreitol (DTT) displacement to that of the thiol ligand. This increase in stability has great potential for the use in self-assembled monolayers (SAMs) on flat gold substrates, where the use of other substrates such as glass are unsuitable.

3.1.2. Detection of DNA

Fluorescence Spectroscopy

The intrinsic fluorescence of natural DNA is extremely weak, and realistically can not be used in the detection of DNA in biological applications.[52] However if DNA is covalently modified with a strong fluorophore it provides a sensitive method of detection via fluorescence spectroscopy.

Fluorescence is the result of a three stage process illustrated by the Jablonski diagram below (Figure 3.2).

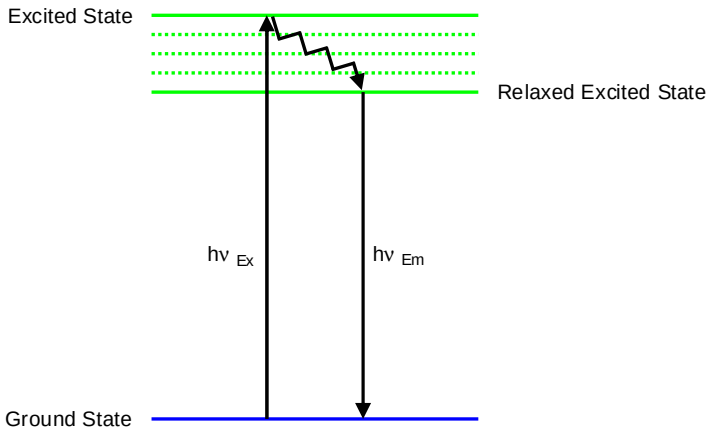

Figure 3.2: Jablonski diagram illustrating the fluorescence process

The fluorescence process starts by the absorption of a photon of energy ($h\nu_{Ex}$) from an external source by the fluorophore to an excited state. This excited state only exists for a very short period of time (1-10 ns). During this time the fluorophore partially dissipates some energy yielding a relaxed excited state from which fluorescence emission originates. A photon of energy ($h\nu_{Ex}$) is then emitted, resulting in the fluorophore relaxing to its ground state. Due to the energy loss during the excited state lifetime, the energy of this photon is of lower energy, and therefore of longer wavelength than the excitation photon.

This difference in energy ($h\nu_{Ex} - h\nu_{Em}$) is known as the Stokes shift and makes florescence a very sensitive technique, as emission photons can be detected against a low background.

Fluorescence spectroscopy still remains at present the most common method for the detection of DNA with recent advances in sensitivity having lead to the detection of DNA at sub-femtomolar concentrations.[53]

SERRS

When a photon of light interacts with a molecule it can either be absorbed or scattered. Scattering occurs when light collides with the electron cloud surrounding the nuclei of the molecules and can occur in two ways; elastic and inelastic. In elastic scattering there is no change in energy between the scattered and incident photons, this is Rayleigh scattering. However one in every 10^6-10^8 photons that are scattered will undergo inelastic scattering, where the scattered photons have a different energy to that of the incident photons, this is Raman scattering.[54] There are two types of Raman scattering; Stokes and anti-Stokes. Stokes scattering is when the scattered light is of lower energy than that of the incident, anti-Stokes when the scattered light is of higher energy than that of the incident. For anti-Stokes to occur the molecule already has to be in a slight excited state to occur, which is why Stokes scattering is more abundant than anti-Stokes. These scattering processes are outlined in Figure 3.3.

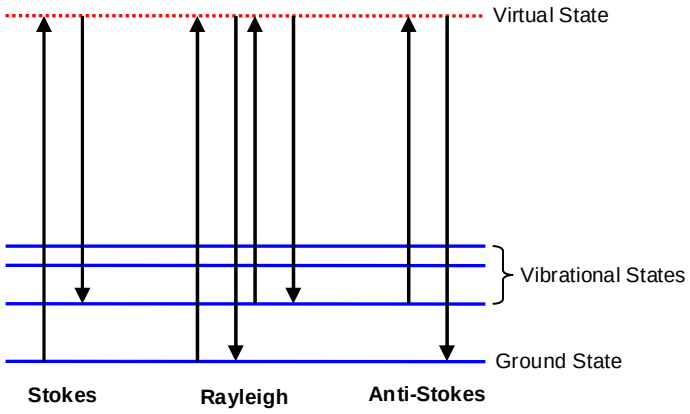

Figure 3.3: Jablonski diagram illustrating the Raman and Rayleigh scattering processes

The sensitivity of Raman scattering can be greatly improved by tuning the excitation laser frequency to be close, or in resonance with a wavelength at which the molecule absorbs strongly. The molecule in question will typically be a chromophore. The incident photon will promote the molecule to an excited electronic state as opposed to a virtual state in normal Raman scattering (Figure 3.4). This is known as resonance Raman scattering and can lead to enhancements of up to 10^4 in the intensity of the Raman signal. The spectra obtained from resonance Raman are simpler as the chromophore vibrations are only enhanced, but the competing fluorescence process can often swamp the Raman signals.

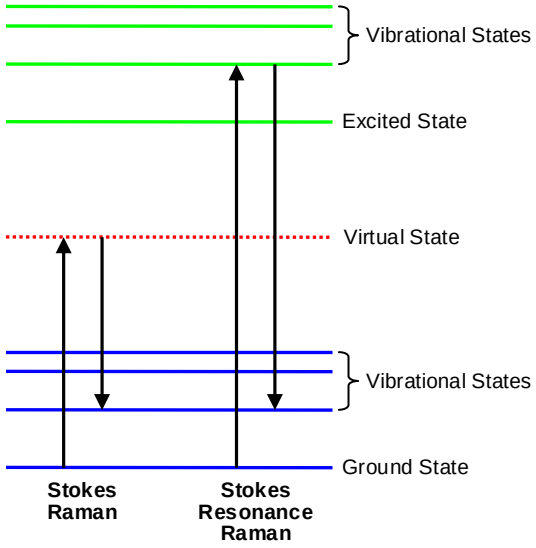

Figure 3.4: Jablonski diagram illustrating the Raman and Resonance Raman scattering processes

When the molecule is adsorbed onto a roughened metal surface, enhancement of the Raman process occurs. This was first observed by Fleichmann *et al.*, when pyridine was adsorbed onto a roughened silver electrode to give enhancements of up to 10^6 in the intensity of the Raman signal.[55] Further work confirmed this to be surface enhanced Raman scattering (SERS). This enhancement in intensity arises from two different mechanisms, an electromagnetic enhancement and a chemical enhancement.[56-60] Various metal surfaces have been examined, silver, gold and copper are the most effective, with silver being the best enhancer overall. Typical surfaces used in SERS include: evaporated films, roughened electrodes, and aggregated colloids.[61-63]

The combination of resonance Raman and surface enhanced Raman scattering, has lead to a very sensitive technique called surface enhanced resonance Raman scattering (SERRS). This was first observed by Stacy and van Duyne by the adsorption of a Ruthenium (II) complex on to a roughened silver electrode.[64] By adsorption of a chromophore onto a roughened metal surface in combination with tuning the excitation laser frequency to be in resonance with a wavelength at which molecule absorbs strongly, enhancements of up to 10^{10} in the intensity of the Raman signal can be achieved. The added benefit of SERRS is that any fluorescence is quenched by the roughened metal surface.

In 2004 Faulds *et al.* reported that SERRS was a more sensitive technique for the detection of labelled oligonucleotides compared to fluorescence. The detection limits calculated for the commercially available fluorescent dye labels (HEX, TAMRA, Cy3, ROX, Cy5, R6G, FAM and TET) were typically at least three orders of magnitude lower for SERRS than those obtained for fluorescence.[65, 66] Another advantage of SERRS has over fluorescence is its multiplexing ability, as fluorescence suffers from broad overlapping spectra, where as SERRS produces fingerprint spectra which makes it easy to identify the components of a mixture without the need for separation procedures.[67] In 2008 Stokes *et al.* reported the unique SERRS multiplexing capability of squaraine dyes (Figure 3.5), as a distinctive peak at 1740 cm^{-1} which is not present in SERRS spectra of a wide variety of commercial available fluorescent dye labels.[68]

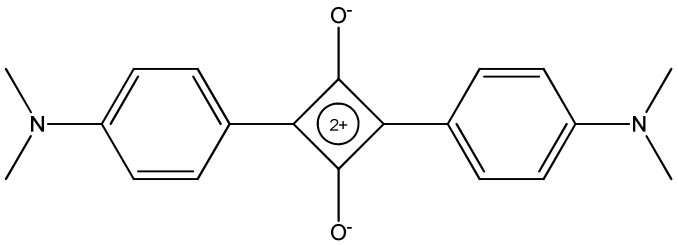

Figure 3.5: Bis(4-alkylaminophenyl)squaraine

3.1.3. Hybridisation of DNA

It has been shown that by modifying DNA with a chromophore it is possible to detect it using fluorescence and SERRS with great sensitivity. However the desire to detect natural DNA is of significant importance in the disease states testing, but the inherent weak fluorescence, the lack of a chromophore and highly negative phosphate backbone of DNA makes it difficult to analyse it by fluorescence spectroscopy and SERRS. A way of over coming this is to modify a complementary strand of DNA with a chromophore and hybridise this to the target DNA sequence. This provides a method of detecting natural DNA without the need for further modification.

Successful hybridisation of an oligonucleotide to its complement is dependent on several factors:

- length of oligonucleotide,
- concentration of oligonucleotide,
- nitrogenous base composition of oligonucleotide,
- salt concentration,
- temperature of hybridisation,
- length of time of hybridisation,
- degree of mismatching of nitrogenous bases in the hybrid,
- pH of hybridisation buffer.

These factors are specific for a given oligonucleotide and its complement, a successful set of hybridisation conditions for one sequence might not necessarily work for another.[69]

It is possible to monitor the degree of hybridisation via UV-vis absorption spectroscopy by carrying out a UV melting experiment. The UV absorbance at 260 nm for single stranded DNA is larger than that of the duplex formed. This is due to hypochromicity and occurs from the coupling of transition dipoles between neighbouring stacked nitrogenous bases. Measuring the UV absorbance as temperature increases produces a characteristic UV-vis absorption spectrum (Figure 3.6).

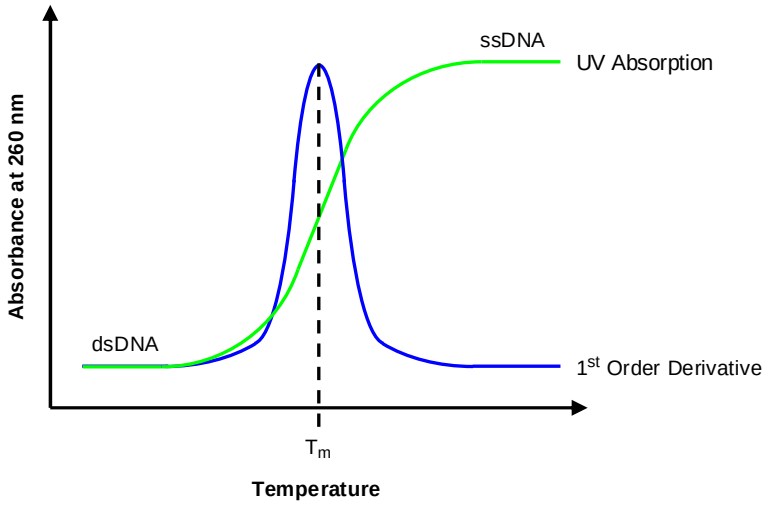

Figure 3.6: Schematic representation of the change in UV absorbance of DNA during hybridisation and the first order derivative

By calculating the first order derivative of the UV-vis absorption spectrum it is possible to calculate the melting temperature (T_m). The T_m characterises the stability of the DNA hybrid formed between an oligonucleotide and its complement and at this temperature 50% of a given oligonucleotide is hybridised to its complementary strand. It is also possible to calculate the T_m of a given oligonucleotide by its strand length and nitrogenous base composition (Equation 3.1 and Equation 3.2).[70]

$$T_m\,[°C] = 2(n_A + n_T) + 4(n_C + n_G)$$

Equation 3.1: T_m for a given DNA sequence of 15 nitrogenous bases or less

$$T_m\,[°C] = 69.3 + 41\frac{(n_C + n_G)}{L} - \frac{650}{L}$$

Equation 3.2: T_m for a given DNA sequence of more than 15 nitrogenous bases

There are three hybridisation methods that are widely used in the detection of natural DNA, each with their own advantages and disadvantages.

Standard Hybridisation

The standard hybridisation technique is the most simplest of hybridisation technique as the complement is modified with a chromophore which provides the detection element (Scheme 3.2).

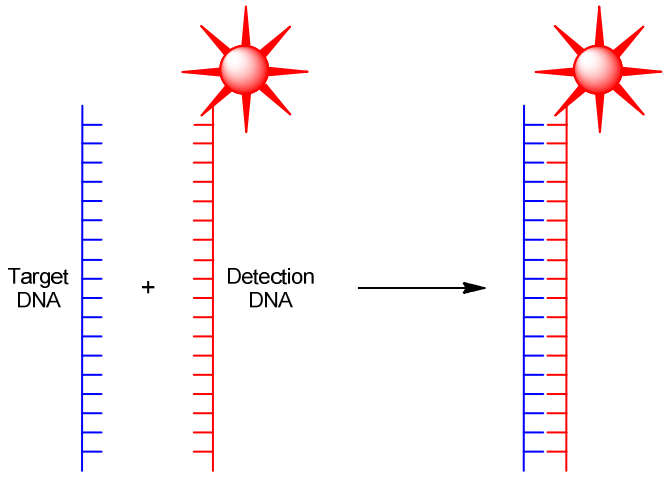

Scheme 3.2: Standard hybridisation

The main disadvantage of this technique is that you have to distinguish between the hybridised DNA and that of the detection DNA.

Molecular Beacon Hybridisation [71, 72]

In molecular beacon hybridisations, the detection DNA ('molecular beacon') has a characteristic hair-pin structure. Within the loop the target DNA is complementary and the stem is formed by annealing 'arms' located either side of the detection DNA sequence. On one of the arms contains a fluorophore and on the other contains a black hole quencher (BHQ). When the molecular beacon is in its closed/unhybridised form the BHQ quenches the fluorescence, but when hybridised it opens out and fluoresces (Scheme 3.3).

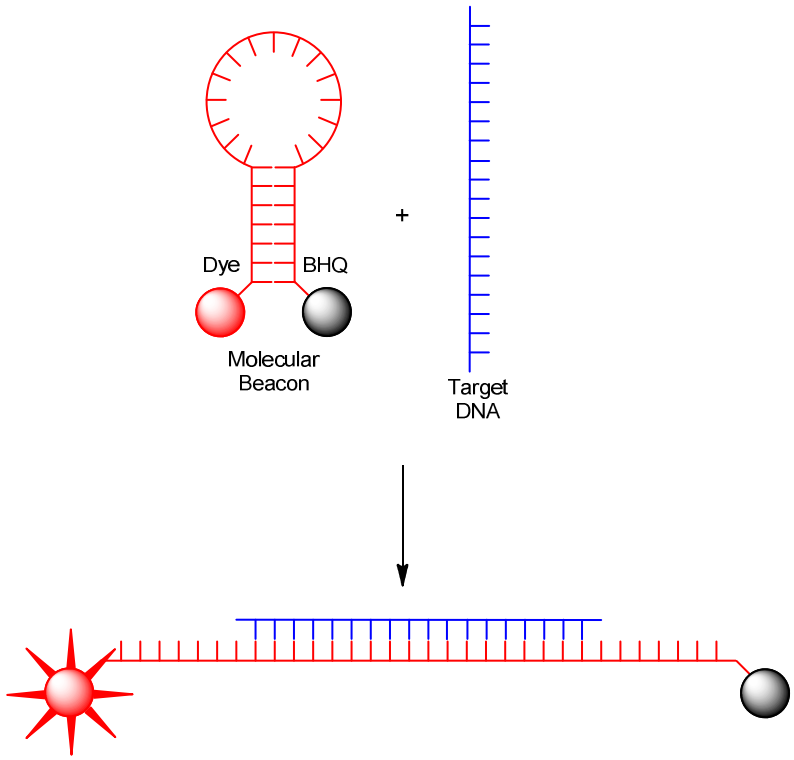

Scheme 3.3: Molecular beacon hybridisation

This has a significant advantage over standard hybridisation as only the hybridised DNA will fluoresce. However molecular beacons are expensive to synthesise and are not suitable for detection using SERRS as the hybridised DNA and molecular beacon will both give signals.

Split Assay Hybridisation [73]

Split assay (sometimes referred to as sandwich assay) hybridisations are similar in fashion to the standard hybridisation but the detection DNA strand containing the chromophore is split into two pieces. This split enables the immobilisation of the DNA to a suitable substrate by modifying the capture DNA, which provides a recognition site for when the target DNA and detection DNA are hybridised (Scheme 3.4).

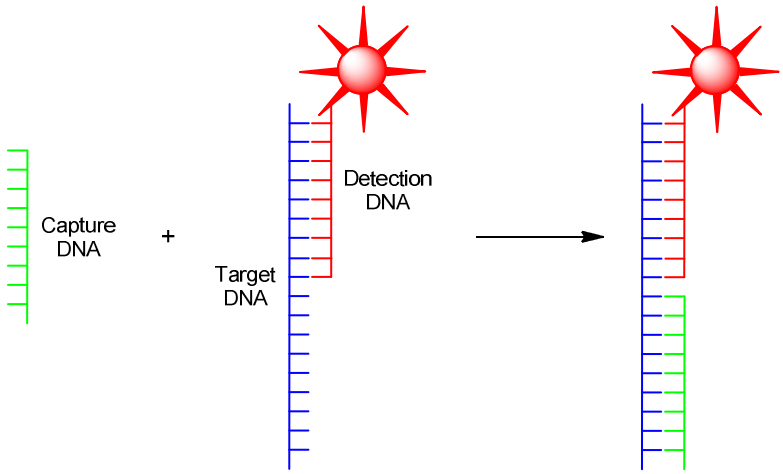

Scheme 3.4: Split assay hybridisation

The advantage of this technique is the hybrid is immobilised to a substrate and any excess unhybridised DNA can be simply washed away.

3.2. Results and Discussion

The aims of this chapter were to use or modify the chosen phenyl azide from chapter 2 to functionalise a variety of substrates (quartz, epoxide polymer and gold) and to subsequently attempt to photoimmobilise DNA on these.

3.2.1. Photoimmobilisation of DNA onto Quartz

Quartz was chosen as a substrate of choice for photoimmobilisation for two main reasons:

1. fully UV transparent,
2. readily functionalised with a trialkoxysilanes.

Even though both standard glass and quartz are made from silicon dioxide, it is the additives put in to change the properties of standard glass, such as sodium carbonate for lowering the melting point, calcium oxide for chemical durability, boron for thermal resistance, that affect its ability to transmit UV light.

Preparation of Phenyl Azide Functionalised Quartz

The functionalisation of quartz with phenyl azide is prepared via a multi-step process, so that at each step could be examined by measuring its water contact angle. This is to monitor any changes in hydrophobicity, as each organic layer is added.

A quartz coverslip was immersed into a boiling hot piranha solution (3:1 H_2SO_4:H_2O_2) for 30 minutes. It was then rinsed in copious amounts of distilled water and dried over nitrogen resulting in the surface being free from any organic residues and fully hydroxylated (Scheme 3.5), providing a clean and hydrophilic surface for the subsequent silanation step.[74]

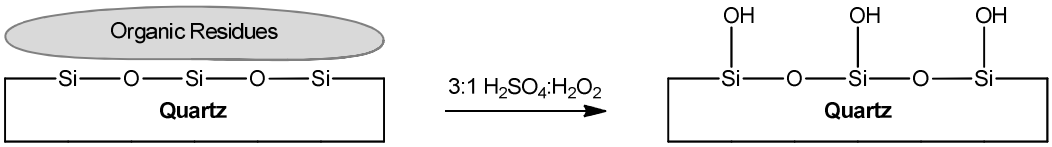

Scheme 3.5: Piranha treatment of quartz

The freshly cleaned quartz coverslip was then immersed into a 5 % v/v solution of 3-aminopropyltriethoxysilane (APTES) in MeOH for 1 hour at room temperature. After that the coverslip was sonicated twice in MeOH for 5 minutes, dried over nitrogen and placed in a vacuum oven at 120 °C overnight. After this period the surface of the coverslip was functionalised entirely with primary amines (Scheme 3.6).

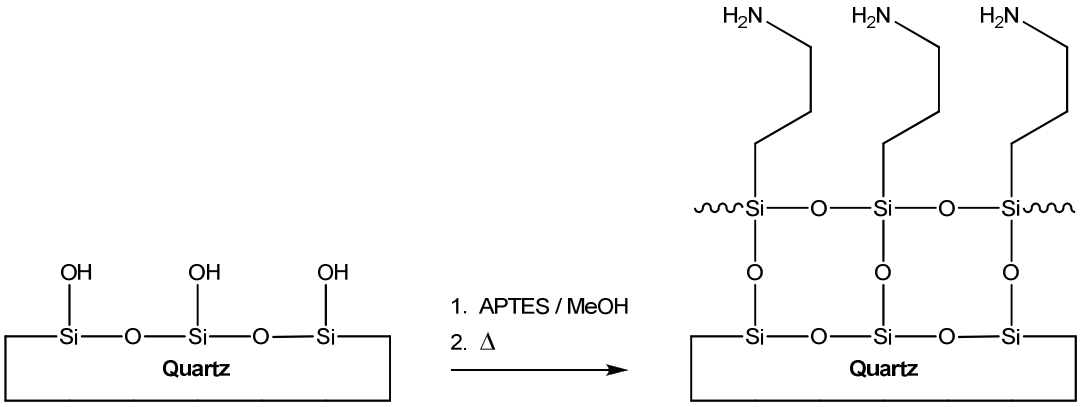

Scheme 3.6: APTES functionalisation of quartz

A 1:1.2 solution of 2-(4-azidophenyl) acetic acid [3] and CDI in DCM was prepared, on a 1 mM scale, and stirred for 30 minutes. The amino functionalised quartz coverslip was immersed into the prepared solution and agitated for 1 hour. The coverslip was sonicated again twice in MeOH for 5 minutes and then dried over nitrogen. This final step results in a coverslip functionalised with the desired phenyl azide (Scheme 3.7).

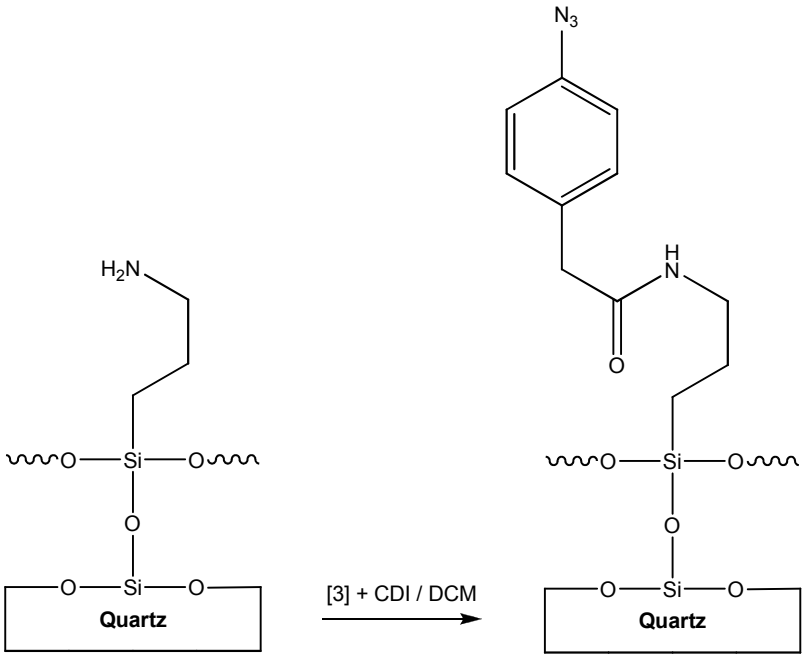

Scheme 3.7: Phenyl azide functionalisation of quartz

Water contact angles were then measured of the untreated quartz, piranha treated quartz, APTES functionalised quartz and phenyl azide functionalised quartz. This was carried out to confirm whether that well established solution chemistry is compatible for functionalising quartz. This was achieved by the vertical deposition of a 1 μL water droplet onto the substrate via a 100 μL syringe coupled to a 27 gauge needle with a 90 ° bevel tip. Figure 3.7 shows illustrative CCTV profiles of the water droplet on each substrate.

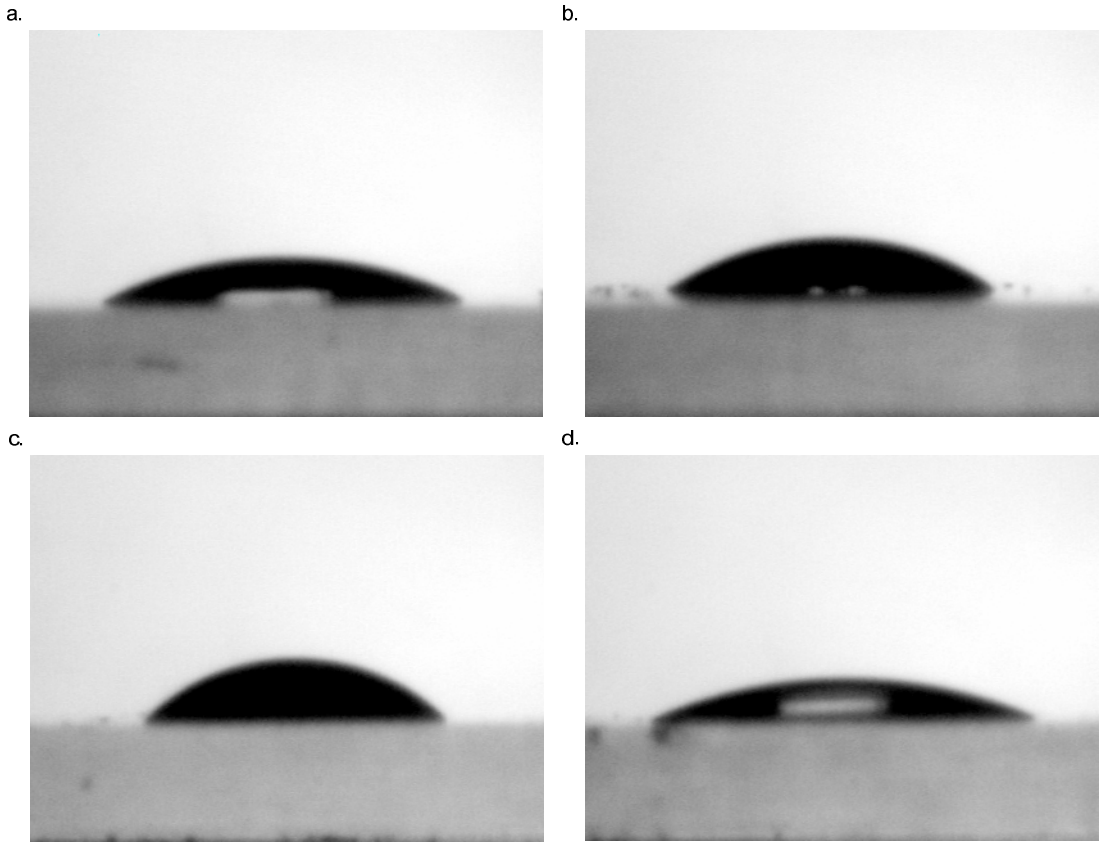

Figure 3.7: Illustrative CCTV water droplet profiles a. untreated quartz; b. piranha treated quartz; c. APTES functionalised quartz; d. phenyl azide functionalised quartz

From the average water contact data (Figure 3.8) it is clear that there were some unexpected irregularities. It was expected that the contact angle for the piranha treated quartz to be smaller than that of untreated quartz as the organic residues have been stripped away and the quartz has been fully hydroxylated. However the converse was found as the contact angle for the untreated quartz was 27 ° to that of 37 ° for the piranha treated quartz. An expected increase in contact angle to 42 ° was observed when the APTES was reacted with the piranha treated quartz, it is more hydrophobic since the quartz has an organic monolayer covalently bound to it. The other unexpected result came from the reaction of 2-(4-azidophenyl) acetic acid [3] with the APTES functionalised quartz resulting in the contact angle dropping to 24 ° from 42 °.

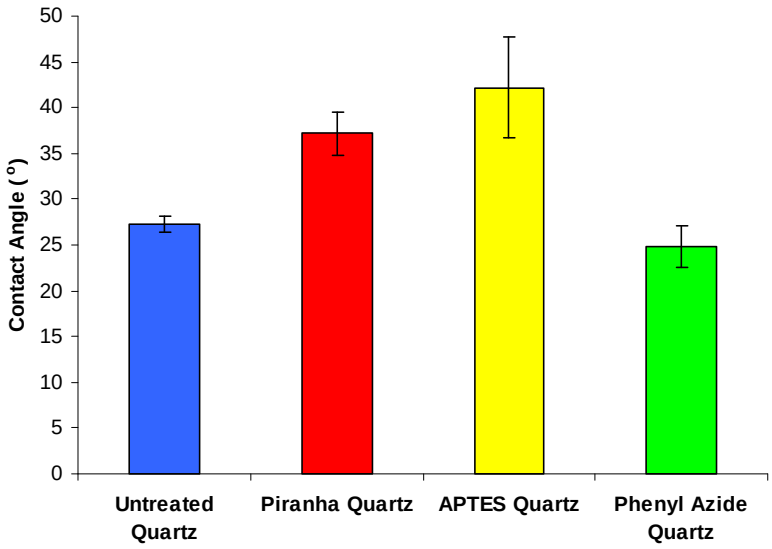

Figure 3.8: Average water contact angles with error bars

This result suggests that the new monolayer covalently bound to the APTES monolayer is significantly more hydrophilic, which is unrealistic as the phenyl azide is entirely organic. A more likely explanation for this is that the monolayer is not complete giving an irregular surface, which disrupts the surface tension of the water droplet causing it to collapse.

Photoimmobilisation of Single Stranded DNA

This approach was used to investigate the suitability of the phenyl azide photochemistry confirmed by the NMR study in chapter 2 for the photoimmobilisation of DNA. By attempting to immobilise a short oligonucleotide containing two labels (3' C_3-amino modification and 5' fluorescent dye modification) it is possible to detect by fluorescence spectroscopy or SERRS via the fluorescent dye where on the surface DNA has been immobilised (Scheme 3.8).

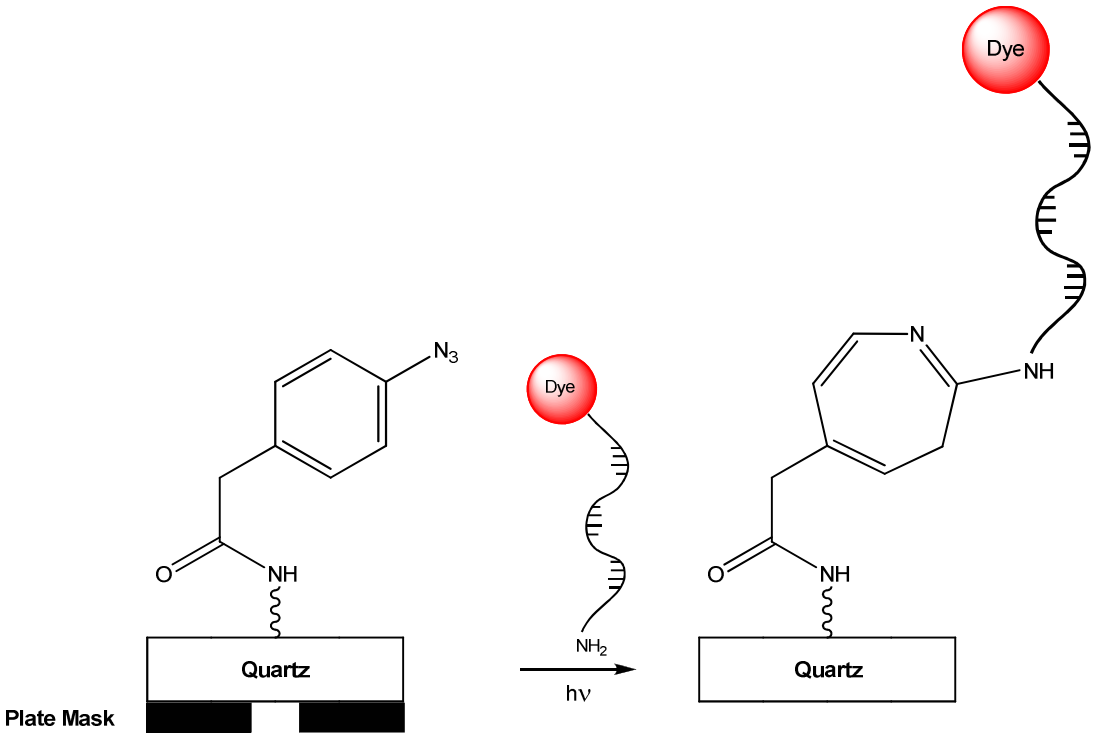

Scheme 3.8: Schematic representation of the photoimmobilisation of single stranded DNA onto quartz

Plate masks were used to photoimmobilise DNA on to the substrate. These masks were made out of metal which allowed for the photoimmobilisation to occur in a localised manner, as metal blocks out UV light entirely. The masks used had two regular patterns, spot and line with aperture sizes of 1.8 mm and 1.0 mm respectively (Figure 3.9).

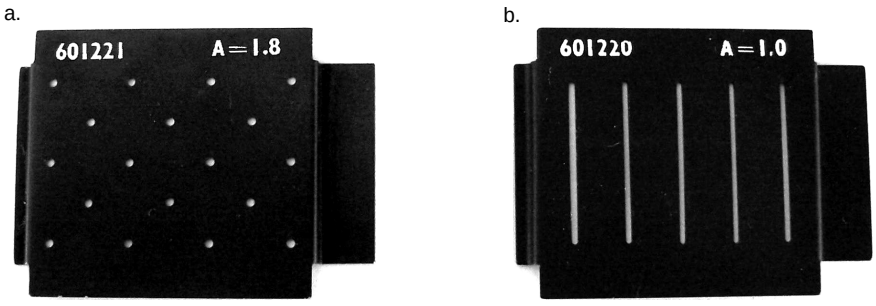

Figure 3.9: Plate masks used in DNA photoimmobilisation; a. spot mask; b. line mask

A 1 μM solution of the desired 5' dye 3' C_3-amino modified DNA was placed on the top surface of the phenyl azide modified quartz coverslip. The plate mask was then placed underneath the coverslip and both placed on the 365 nm UV lamp of the transilluminator. The lamp was then switched on for 5 minutes to allow for the photoimmobilisation of DNA. After this period the coverslip was sonicated twice in distilled water for 5 minutes, dried over nitrogen, and analysed immediately.

Raman spectrometers were then set to record extended scans of the fluorescence, 1 accumulation for 2 seconds using a 50 × objective, other specifications for the analysis are outlined in Table 3.1.

Dye	Extended Scan Spectra Range (nm)	Laser Used (nm)	Laser Power (%)
FAM	500-600	515	10
HEX	520-620	515	10
Cy3.5	580-680	515	50
Cy5	640-740	633	100

Table 3.1: Additional spectrometer specifications to analyse the photoimmobilised DNA using fluorescence

In total 10 scans were taken at each immobilisation site (on) and 10 scans were taken at random sites nearby each immobilisation site (off). This was to demonstrate that the DNA had been photoimmobilised and not just adsorbed on to the surface. Figure 3.10 shows the average fluorescence spectra at the on and off sites for each dye labelled DNA sequence.

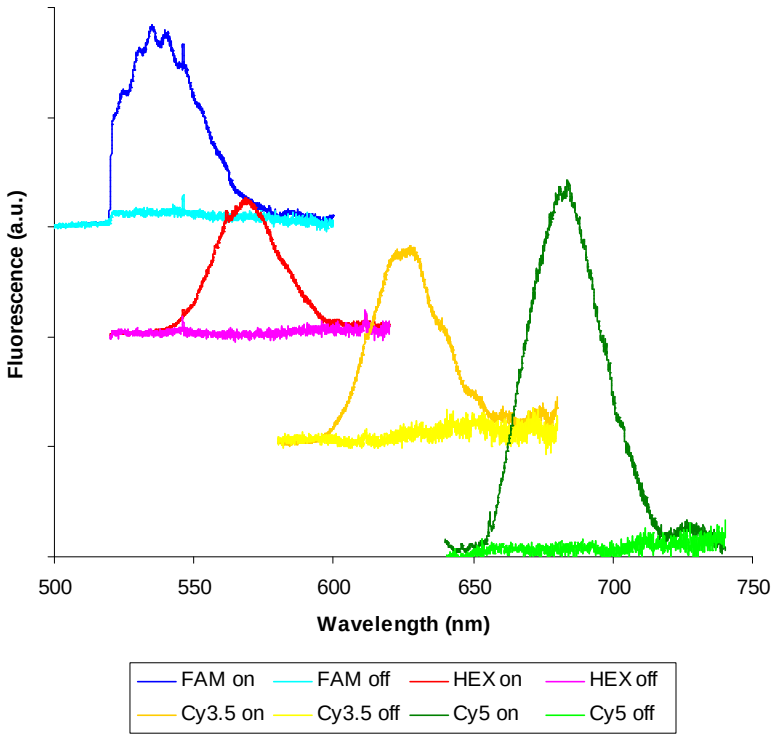

Figure 3.10: Fluorescence spectra of photoimmobilised DNA on quartz

Due to the processing of the raw data (baseline correction and zeroing) a marked difference between the expected emission maxima and observed emission maxima of each fluorophore was observed (Table 3.2). The difference may have been also due to a waterchromic effect, where the expected emission maxima are that for a solution phase where the observed emission maxima are measured in the solid phase since they have been immobilised on to a surface.

Dye	Established emission wavelength maximum (nm)	Observed emission wavelength maximum (nm)
FAM	520	535
HEX	556	570
Cy3.5	596	628
Cy5	667	685

Table 3.2: Established and observed emission wavelength maximum of the dyes on photoimmobilised DNA

For SERRS of DNA to occur, a roughened metal surface and an aggregation agent are required. Typically the roughened metal surface used in DNA analysis is silver colloid. Silver colloid synthesis was achieved by the reduction of silver nitrate with citric acid via a modified Lee *et al.* method [75] as described by Munro *et al.*[76] where Figure 3.11 shows the characteristic UV-vis spectrum obtained.

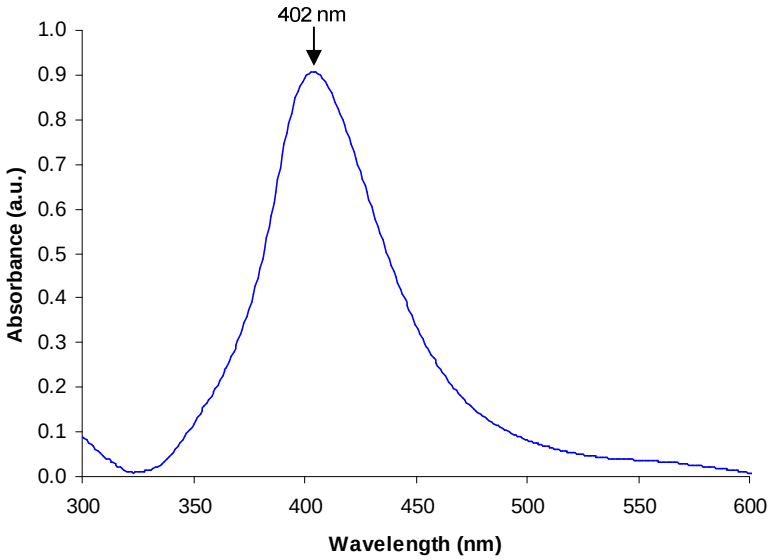

Figure 3.11: UV-vis absorption spectrum of synthesised citrated reduced silver colloid

An aggregation agent is added to the silver colloid because the negative charges surrounding the colloid and phosphate backbone of DNA repel each other. Therefore the role of the aggregation agent is to partially neutralise these charges so that the two are no longer repelling each other, this enables small aggregates to form upon which SERRS can occur. Graham *et al.* have reported using spermine as an aggregation agent with the result of improvement of SERRS signals.[77] Spermine is a low molecular weight polyamine that is positively charged in aqueous conditions and acts as a charge modifier of DNA (Figure 3.12).[78]

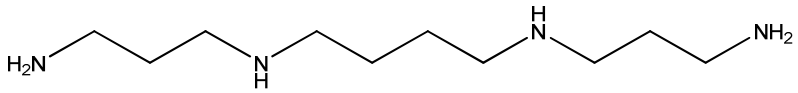

Figure 3.12: Spermine

In order to analyse the photoimmobilised DNA using SERRS, the successive addition of 1 μL 0.1 M solution of spermine in water followed by 1 μL of 10^{-9} M silver colloid to the site of photoimmobilisation took place and was allowed to dry under nitrogen gas.

Raman spectrometers were then set to record static scans of the Raman scattered light, 1 accumulation for 1 second using a 50 × objective, other specifications for the analysis are outlined in Table 3.3.

Dye	Centred Static Scan (nm)	Laser Used (nm)	Laser Power (%)
FAM	1400	515	10
HEX	1400	515	10
Cy3.5	1400	515	10
Cy5	1200	633	100

Table 3.3: Additional spectrometer specifications to analyse the photoimmobilised DNA using SERRS

Again 10 scans were taken at each immobilisation site (on) and 10 scans were taken at random sites nearby each immobilisation site (off). Figure 3.13 shows the average SERRS spectra at the on and off sites for each dye labelled DNA sequence.

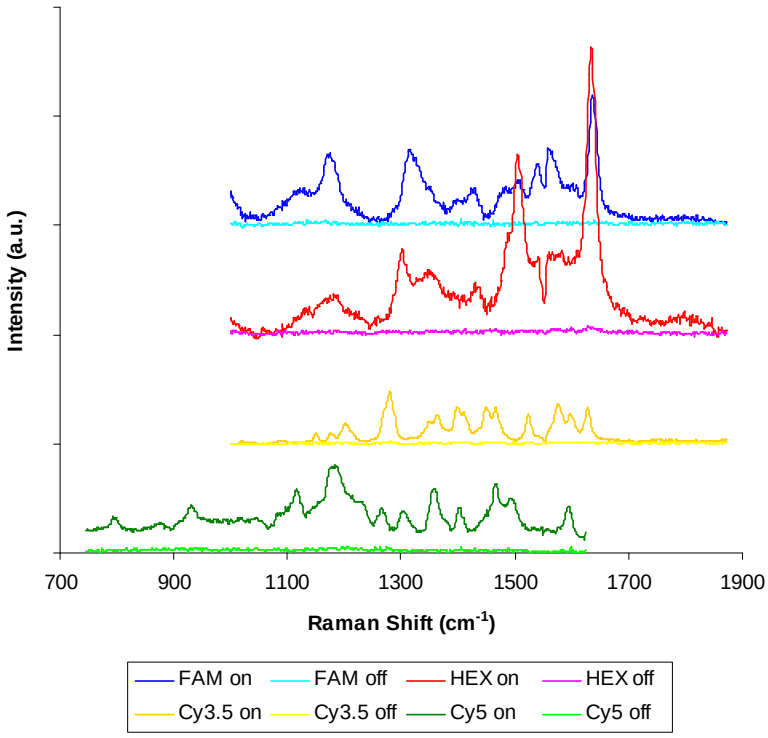

Figure 3.13: SERRS spectra of photoimmobilised DNA on quartz

The advantages of analysing DNA using SERRS as the detection method over fluorescence is that each individual dye has a characteristic spectrum that is unique to itself, whereas fluorescence spectra are broad and can be easily confused with other dyes. This discrimination and sensitivity enables a variety of dyes to be analysed at one time (multiplexing).

Photoimmobilisation of a Split Assay for the Detection of Chlamydia trachomatis

The previous section utilised synthetic DNA that had been modified with both a fluorescent dye and a primary amine. However if this method is to be used for testing disease states a way of introducing and detecting a non-modified piece of DNA is required, as natural DNA does not contain any modifications. To achieve this, a split assay approach has been adopted. This is where the complement to the desired target is split in half, one half has a modification for immobilisation and the other half has fluorescent dye modification for detection.

Also in the previous sections random DNA sequences were used, in this case a target probe sequence for *Chlamydia trachomatis* (CT) was used (Figure 3.14).

3'-TCT-CCG-TAG-GAA-TCA-GGG-ACA-GCG-TCG-5'

Figure 3.14: Target probe sequence for *Chlamydia trachomatis*

The complementary sequence to the target was split into two segments, one with a 5' Bodipy 650 (BD650) modification (Figure 3.15) the other with a 3' C_3-amino modification (Figure 3.16).

5'-BD650-AGA-GGC-ATC-CTT-A-3'

Figure 3.15: Split complement sequence with a 5' BD650 modification

5'-GT-CCC-TGT-CGC-AGC-NH_2-3'

Figure 3.16: Match split complement sequence with a 3' C_3-amino modification

Two other 3' C_3-amino modified strands of DNA were also synthesised, one with a single base mis-match at the 5' end (Figure 3.17) and the other was a nonsense strand, i.e. entirely uncomplementary (Figure 3.18).

5'-TT-CCC-TGT-CGC-AGC-NH_2-3'

Figure 3.17: Mis-match split complement sequence with a 3' C_3-amino modification

5'-CG-ACG-CTG-TCC-CTG-NH_2-3'

Figure 3.18: Nonsense split complement sequence with a 3' C_3-amino modification

A UV melting experiment was performed on the DNA sequences prior to performing any hybridisation onto the quartz coverslip to investigate whether the sequences chosen for the match would hybridise (Figure 3.19). This would also provide an approximate temperature to perform the hybridisation onto the quartz. By also performing a UV melting experiment on the mis-match (Figure 3.20) and nonsense (Figure 3.21) sequences it would give an indication whether they too would hybridise.

3'-TCT-CCG-TAG-GAA-TCA-GGG-ACA-GCG-TCG-5'
5'-BD650-AGA-GGC-ATC-CTT-A GT-CCC-TGT-CGC-AGC-NH_2-3'

Figure 3.19: Match CT split assay sequences

3'-TCT-CCG-TAG-GAA-TCA-GGG-ACA-GCG-TCG-5'
5'-BD650-AGA-GGC-ATC-CTT-A **T**T-CCC-TGT-CGC-AGC-NH_2-3'

Figure 3.20: Mis-match CT split assay sequences, highlighting position of mis-match

3'-TCT-CCG-TAG-GAA-TCA-GGG-ACA-GCG-TCG-5'
5'-BD650-AGA-GGC-ATC-CTT-A**CG-ACG-CTG-TCC-CTG**-NH_2-3'

Figure 3.21: Nonsense CT split assay sequences, highlighting uncomplementary section

20 μL aliquots of 10^{-4} M of each sequence of the split assay to be hybridised (i.e. target probe, 5' BD650 complement and 3' C_3-amino complement) were made up to 2 mL with pH 7 0.3 M PBS and placed into a sealed quartz cuvette. The temperature was then raised and lowered between the temperatures of 20 °C and 80 °C at a rate of 1 °C per minute, for 10 cycles, whilst monitoring the absorbance at 260 nm.

Figure 3.22 shows the characteristic sigmoidal shape of the UV melting curves obtained from the when match, mis-match and nonsense sequences hybridise. These curves are re-plotted as the first order derivative, as they give a better indication of the degree of hybridisation and exact melting temperature.

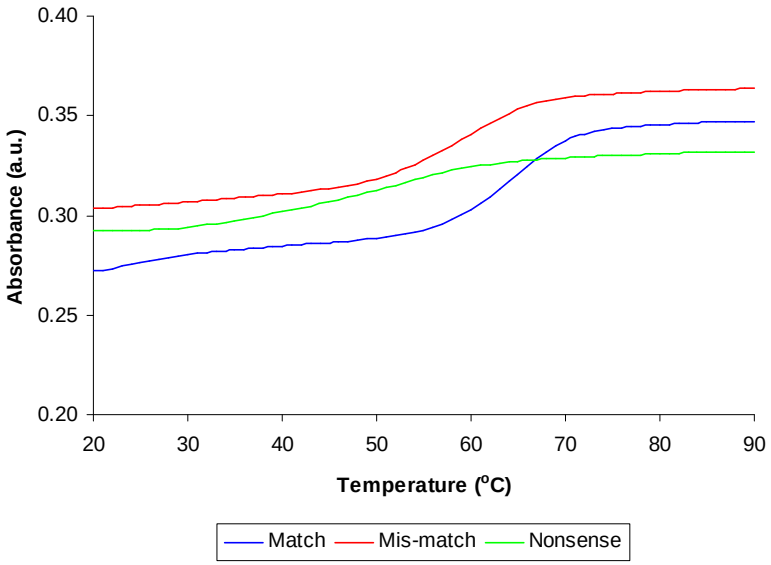

Figure 3.22: UV melting curve

From the first order derivative it can be seen that the match, mis-match and nonsense sequences hybridise (Figure 3.23), however the degree of hybridisation varied. Both the match and mis-match have characteristic first order derivative plots, where the match has a narrower peak, indicating that the hybridisation occurs within a smaller temperature range. Since the match hybridised at 64 °C compared to 61 °C of the mis-match, this demonstrates that the single base mis-match does affect the T_m, showing that the match is more stable. The nonsense sequences do hybridise, but it is only the target probe and BD650 complement sequences that hybridise, as the 3' C_3-amino complement is entirely uncomplementary. This results in a 12 °C drop in hybridisation temperature to 51 °C.

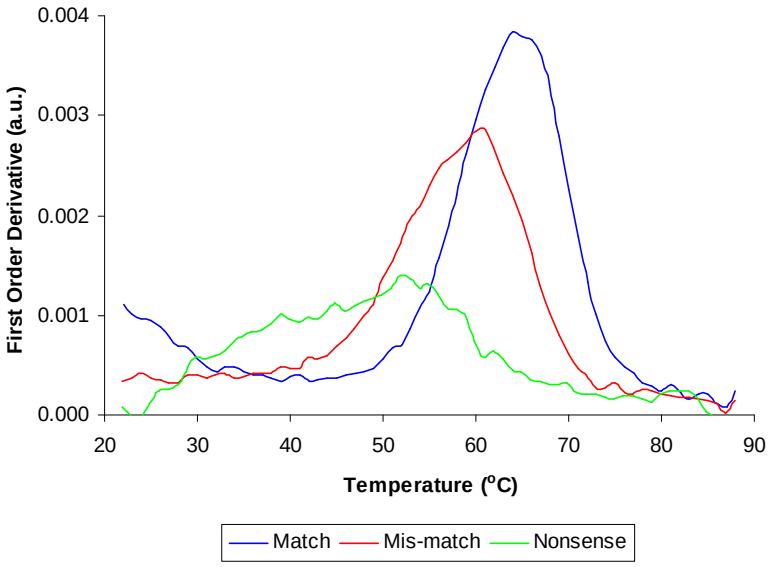

Figure 3.23: First order derivative of UV melting curve

In a similar manner to the single stranded immobilisation, the split assay immobilisation was achieved by first immobilising the C_3-amino modified DNA then the 5' fluorescent dye modified DNA along with the target DNA which have been prehybridised were added together on the surface (Scheme 3.9). The purpose of the prehybridisation is to partially overcome the diffusion limitation; this is where the rate limiting step is that of the diffusion of the complement and first base recognition to its target.[79-82]

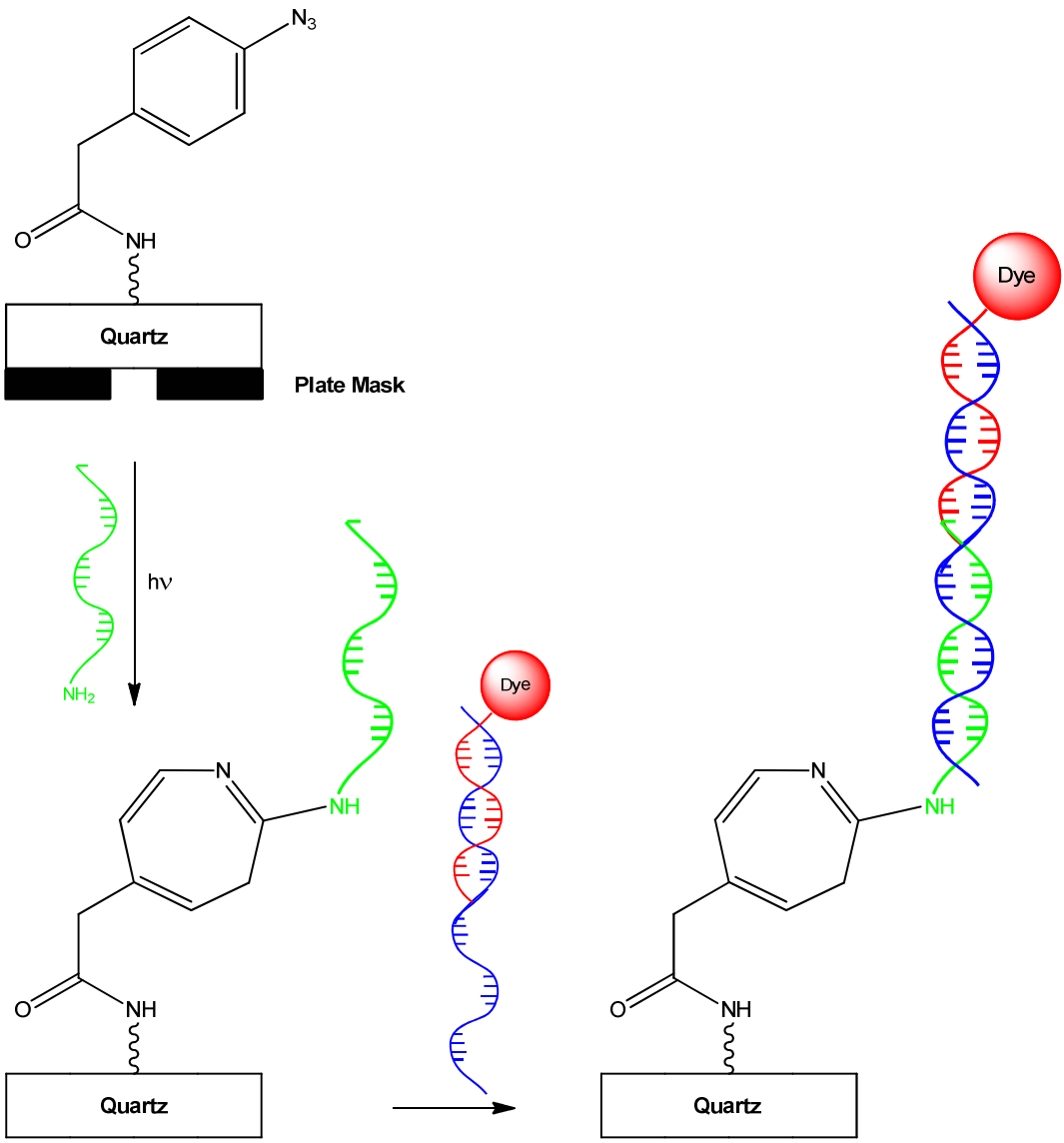

Scheme 3.9: Schematic representation of the photoimmobilisation of a split assay for the detection of *Chlamydia trachomatis* onto quartz

A 1 μM solution of 3' C_3-amino modified capture DNA was placed on the top surface of the phenyl azide modified quartz coverslip. The plate mask was then placed underneath the coverslip and both placed on the 365 nm UV lamp of the transilluminator. The lamp was then switched on for 5 minutes to allow for the photoimmobilisation of DNA. Prehybridisation was achieved by taking 2 μL aliquots of 10^{-4} M of each sequence; i.e. target probe and 5' BD650 complement, made up to 20 μL with pH 7 0.3 M PBS and subject to the following hybridisation conditions in a commercial PCR instrument (95 °C for 5 minutes and then slowly cooled down to 4

ºC). The hybridisation mixture was then used immediately by pipetting over the site of the photoimmobilised capture DNA. The coverslip was then placed in a water tight hybridisation chamber containing pH 7 0.3 M PBS in the wells. The hybridisation chamber was then immersed into an 80 °C water bath where the temperature was allowed to drop by 1 °C every 5 minutes to ambient temperature. After this period the coverslip was sonicated twice in distilled water for 5 minutes dried over nitrogen, and analysed immediately.

A Raman spectrometer was then set to record extended scans of the fluorescence between 640-740 nm, using a 633 nm laser at 100 % power, 1 accumulation for 2 seconds using a 50 × objective. In total 10 scans were taken at each immobilisation site; match, mis-match and nonsense. Figure 3.24 shows the average fluorescence spectrum obtained at each immobilisation site.

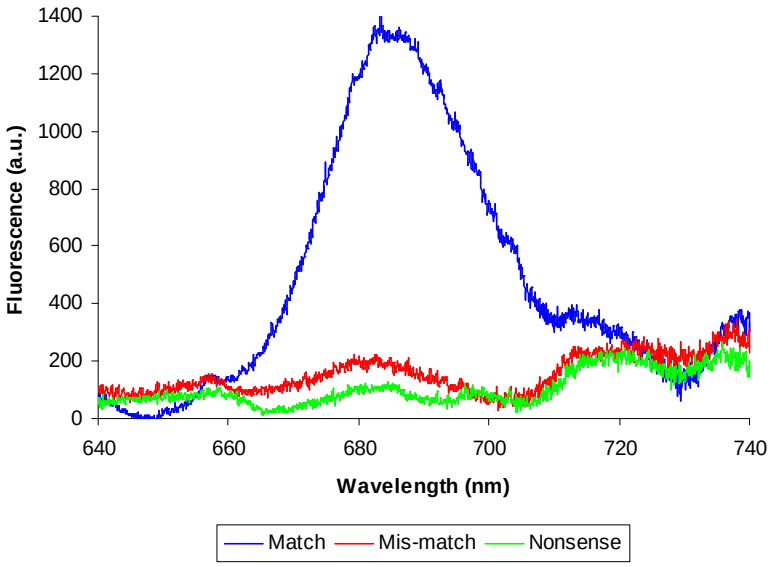

Figure 3.24: Fluorescence spectra of the photoimmobilisation of the split assay

After analysis by fluorescence, the successive addition of 1 μL 0.1 M solution of spermine in water followed by 1 μL of 10^{-9} M silver colloid to the sites of photoimmobilisation took place and was allowed to dry under nitrogen gas. The Raman spectrometer was then set to record static scans of the Raman scattered light, centred at 1400 cm^{-1}, using a 633 nm laser at 100 % power and 1 accumulation for 2 seconds using a 50 × objective. Again 10 scans were taken at each immobilisation site where Figure 3.25 shows the average SERRS spectra obtained at each immobilisation site.

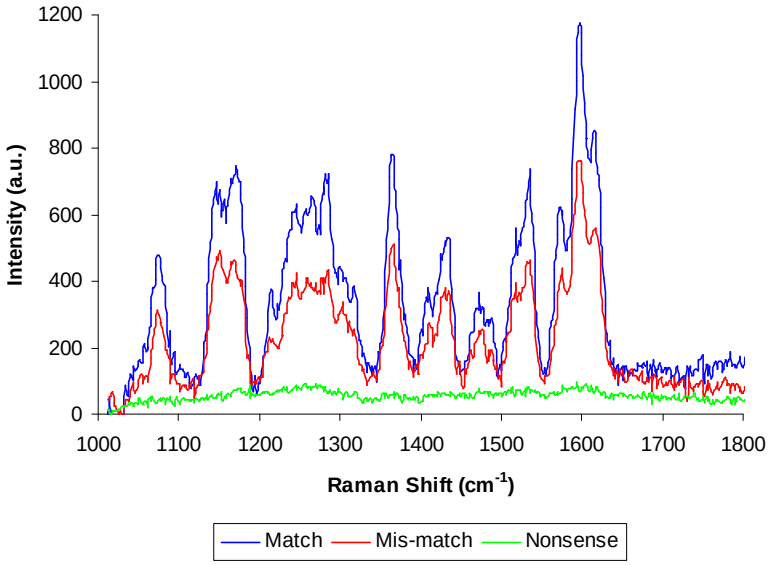

Figure 3.25: SERRS spectra of the photoimmobilisation of the split assay

After processing the raw data (baseline correction and zeroing) for fluorescence it was clear that only the match gave a positive result, although the unprocessed data did show a marked difference between the mis-match and nonsense. Again as with the single stranded immobilisation a waterchromic effect was observed where the emission maxima was different to the expected emission maxima, 685 nm and 664 nm respectively. This confirms analysis via fluorescence using Raman instruments and the data processing were unsuitable. However analysis of the split assay using SERRS verified the results obtained during the DNA hybridisation, in that the match and mis-match probe sequences do hybridise, with the match probe sequence hybridising to a greater degree than the mis-match.

3.2.2. Photoimmobilisation of DNA onto Epoxide Polymer

The epoxide polymer used in this section of work was synthesised by Dr Allan Mackintosh and Dr Alexander Kuehne, University of Strathclyde. It has been specifically designed to transmit UV light, which is somewhat unique as most polymer systems absorb UV light. Table 3.4 outlines the % UV transmission of the epoxide polymer films generated.[83]

Wavelength (nm)	Transmission (%)
> 350	> 98
270	45
230	35

Table 3.4: % UV transmission of epoxide polymer films

It is well known that primary amines react with epoxides, in basic conditions via a S_N2 type reaction process, where the nucleophile attacks at the least substituted carbon (Scheme 3.10).

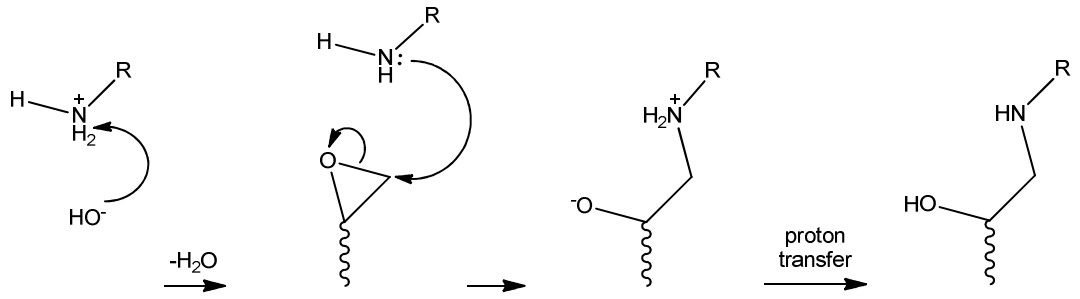

Scheme 3.10: Epoxide ring opening reaction with a primary amine as the nucleophile

Therefore the desired phenyl azide to be synthesised must contain a terminal primary amine group, for photoimmobilisation to occur at the epoxide polymer surface.

2-Aminoethanol (Figure 3.26) was first chosen as a suitable linker to attach to the phenyl azide, as the amino and hydroxyl functionality have different reactivity. This difference in relativities allows for the amine to be protected via common efficient protection strategies.

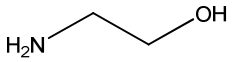

Figure 3.26: 2-Aminoethanol

tert-Butyloxycarbonyl (Boc) protection of 2-aminoethanol was achieved using di-*tert*-butyl dicarbonate following a method described by Debaene *et al.* (Scheme 3.11), and was purified via flash column chromatography, resulting in the desired product in a 97 % yield.[84]

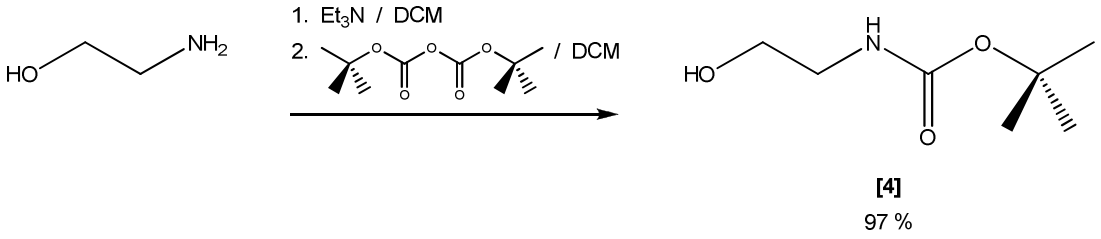

Scheme 3.11: Synthesis of *tert*-butyl 2-hydroxyethyl carbamate [4]

The Boc protected 2-aminoethanol was then reacted with CDI activated 2-(4-azidophenyl)acetic acid [3], in an ester formation reaction (Scheme 3.12). After purification via flash column chromatography a yield 64 % was achieved.

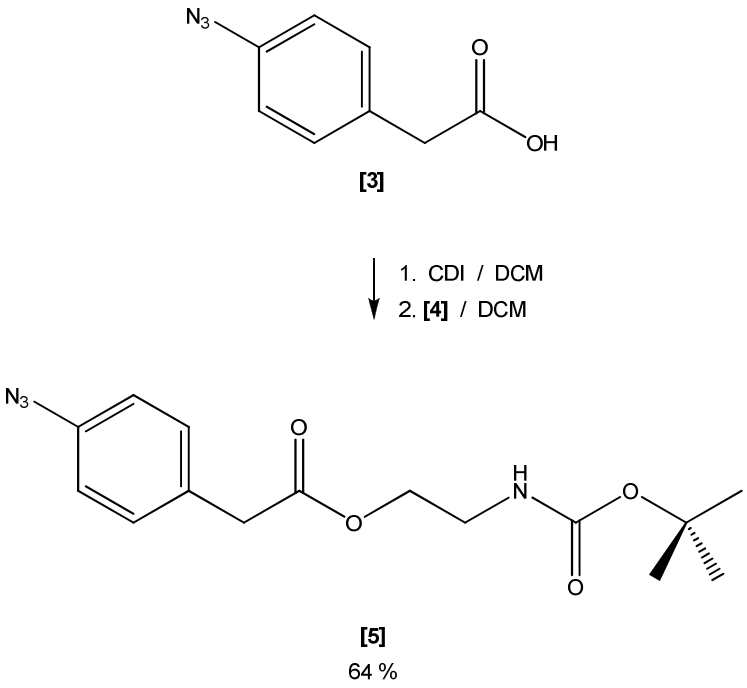

Scheme 3.12: Synthesis of 2-(*tert*-butoxycarbonylamino)ethyl 2-(4-azidophenyl)acetate [5]

To achieve the amino functionalised phenyl azide, a Boc deprotection step is required, which was attempted using 1% trifluoroacetic acid (TFA) in DCM (Scheme 3.13).

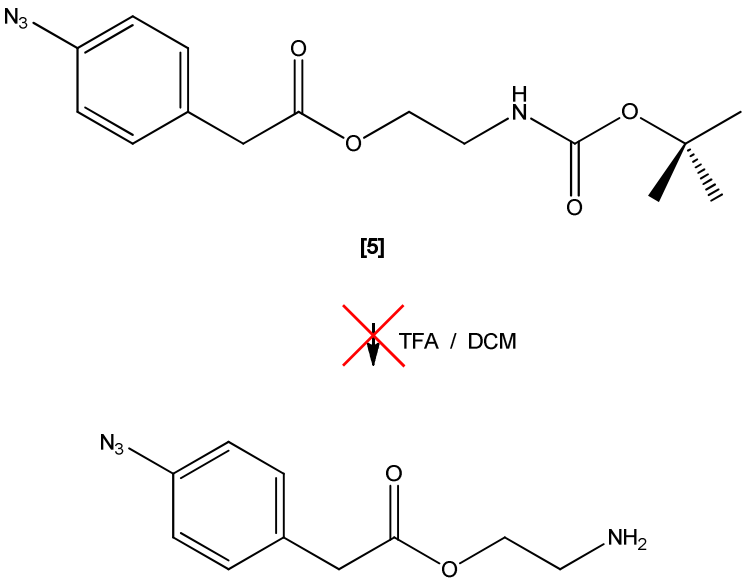

Scheme 3.12: Attempted synthesis of 2-aminoethyl 2-(4-azidophenyl)acetate

Analysis of the product using 1H NMR after purification via flash column chromatography, revealed that there was only one proton attached to the nitrogen. By further investigating the 1H NMR showed that the actual product from the deprotection step was 2-(4-azidophenyl)-*N*-(2-hydroxyethyl)acetamide (Figure 3.27), this was also confirmed by IR as the spectrum contained a broad OH stretch.

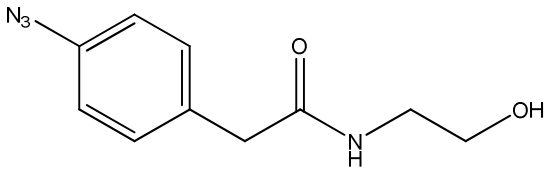

Figure 3.27: 2-(4-azidophenyl)-*N*-(2-hydroxyethyl)acetamide

This was more than likely due to the TFA catalysing the ester hydrolysis and then the subsequent amide formation between the recently deprotected 2-aminoethanol.

Therefore a new protection strategy was adopted, by using the 9*H*-fluorenylmethyloxycarbonyl (Fmoc) protected 2-aminoethanol, where the Fmoc group is removed by base. The Fmoc protected 2-aminoethanol was reacted with CDI activated 2-(4-azidophenyl)acetic acid [3], in an ester formation reaction (Scheme 3.13), and then purified via flash column chromatography.

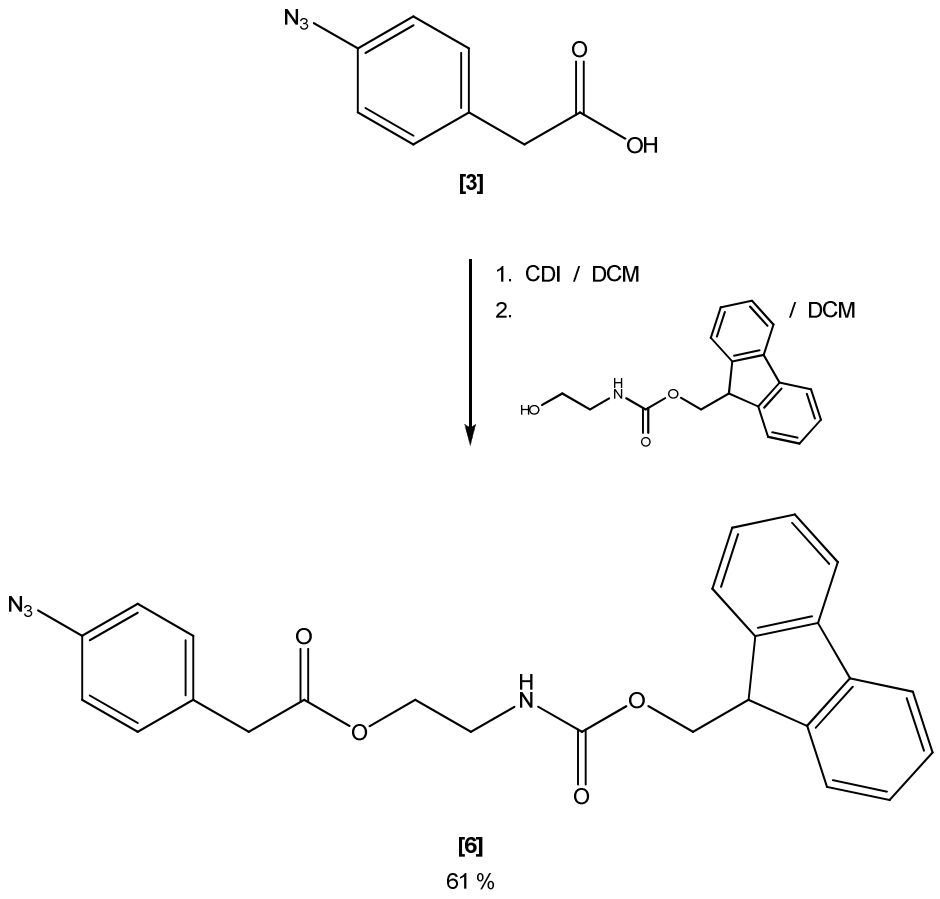

Scheme 3.13: Synthesis of 2-(((9*H*-fluoren-9-yl)methoxy)carbonylamino)ethyl 2-(4-azidophenyl) acetate [6]

After purification a yield of 61 % was achieved and a sample was recrystallised from EtOAc to obtain a crystal for analysis via X-ray diffraction. The resulting ellipsoidal crystal structure is shown in Figure 3.28 where the bulky Fmoc group is causing a slight folding over towards the flat phenyl azide structure

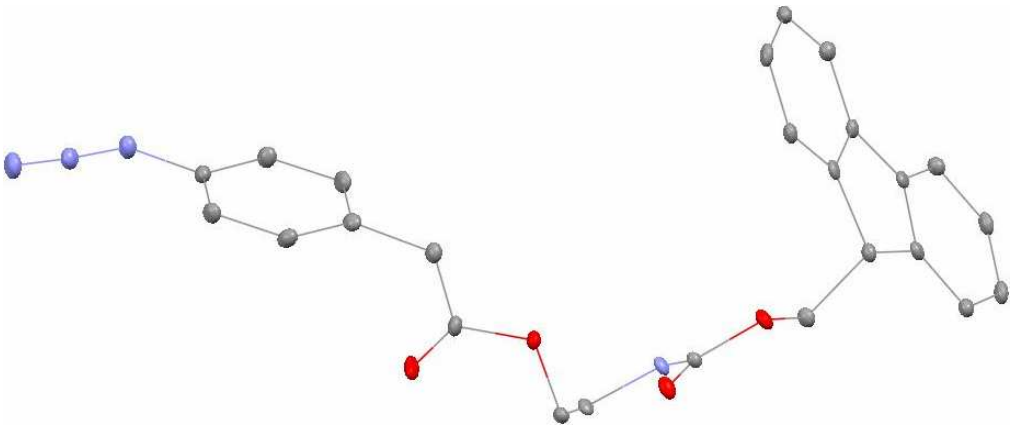

Figure 3.28: Ellipsoidal crystal structure of 2-(((9*H*-fluoren-9-yl)methoxy)carbonylamino)ethyl 2-(4-azidophenyl)acetate [6]

The final step to achieve the amino functionalised phenyl azide was Fmoc deprotection which was attempted using 20 % piperidine in MeCN (Scheme 3.14).

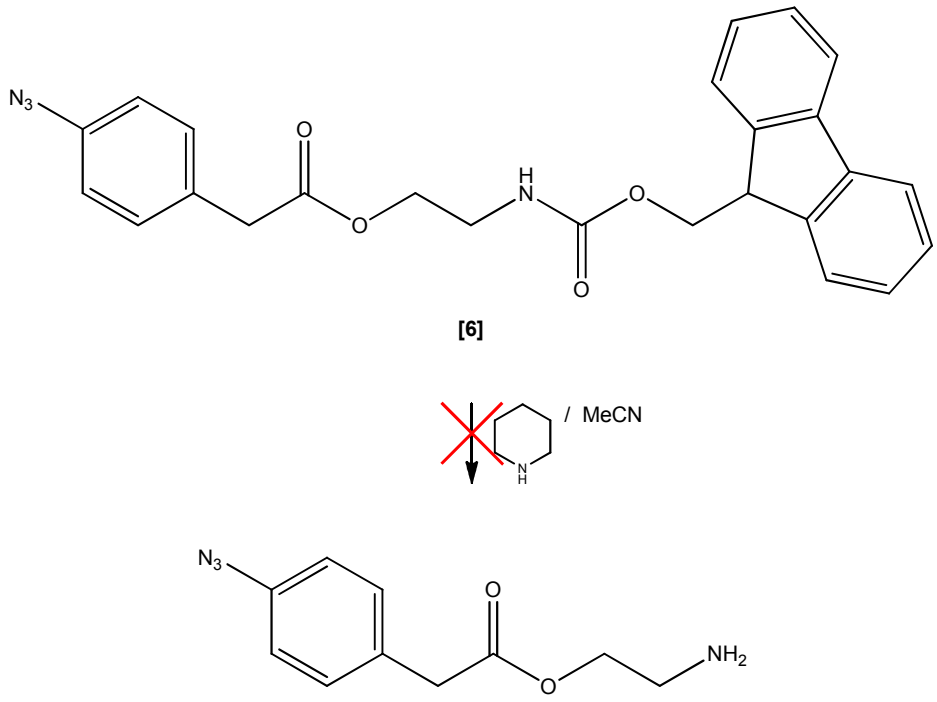

Scheme 3.14: Attempted synthesis of 2-aminoethyl 2-(4-azidophenyl)acetate

Again analysis of the product using 1H NMR and IR after purification via flash column chromatography, revealed that the same 2-(4-azidophenyl)-*N*-(2-hydroxyethyl)acetamide product was formed.

Since it was obvious that both acid and base appear to catalyse the hydrolysis and subsequent amide formation of the products, an alternative linker 1,2-ethanediamine was employed (Figure 3.29).

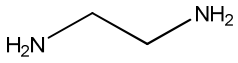

Figure 3.29: 1,2-Ethanediamine

This was chosen as an amide group formed with a carboxylic acid is less reactive than the ester formed with the same carboxylic acid, this is due to the resonance stabilisation (Scheme 3.15).[85]

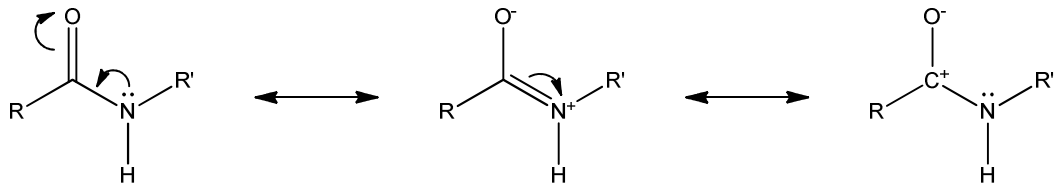

Scheme 3.15: Resonance stabilisation of an amide

Boc protected 1,2-ethanediamine was reacted with CDI activated 2-(4-azidophenyl)acetic acid [3], in an amide formation reaction (Scheme 3.16), and purified via flash column chromatography.

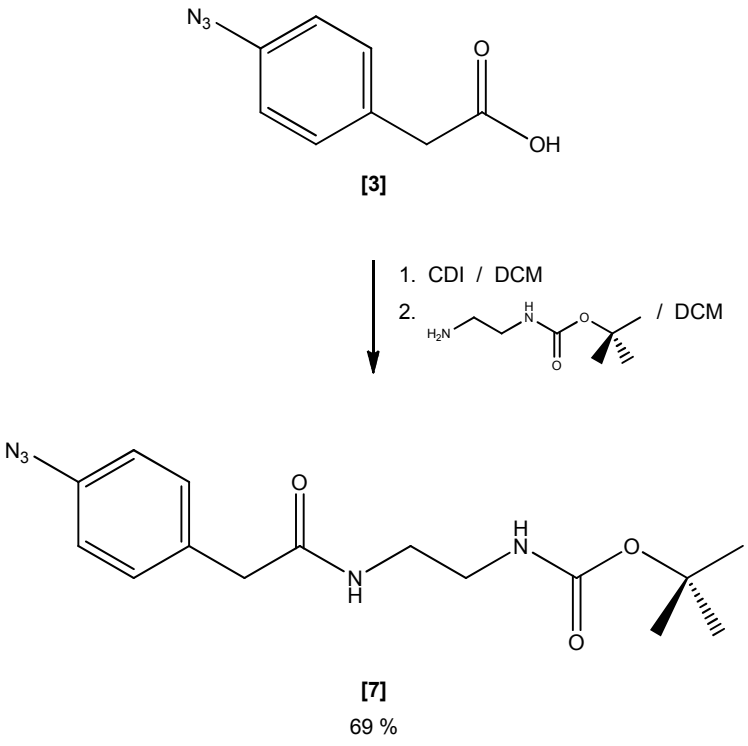

Scheme 3.16: Synthesis of *tert*-butyl 2-(2-(4-azidophenyl)acetamido)ethylcarbamate [7]

Following purification a yield of 69 % was achieved and a sample was recrystallised from EtOAc to obtain a crystal for analysis via X-ray diffraction. The resulting ellipsoidal crystal structure is shown in Figure 3.30 where the structure appears as a relatively straight alkyl chain with the phenyl azide as a planar structure.

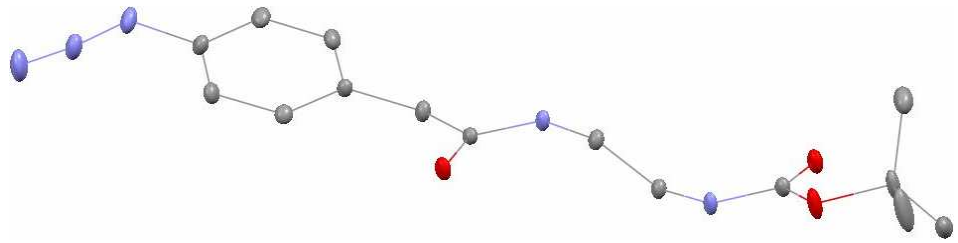

Figure 3.30: Ellipsoidal crystal structure of tert-butyl 2-(2-(4-azidophenyl)acetamido) ethyl carbamate [7]

Then removal of the Boc group was required and attempted using 1% TFA in DCM (Scheme 3.17).

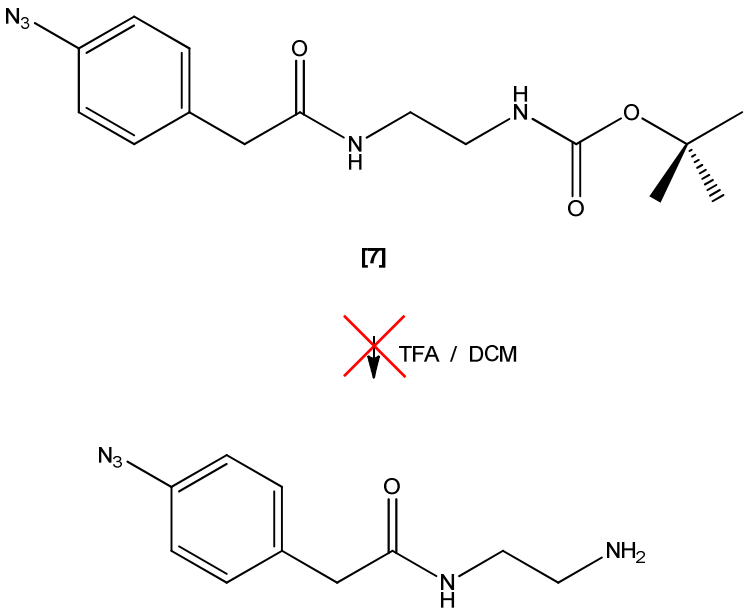

Scheme 3.17: Attempted synthesis of *N*-(2-aminoethyl)-2-(4-azidophenyl)acetamide

Although the product was visualised towards the baseline of a TLC, attempts to purify via flash column chromatography were unsuccessful, as the product had the tendency to remain on the silica gel even with a variety of polarities and solvent systems.

Preparation of Phenyl Azide Functionalised Epoxide Polymer

Unfortunately the three proposed routes of creating a phenyl azide containing a primary amine to react with the epoxide polymer were unsuccessful. So it was proposed to achieve this via a two step process.

A freshly prepared epoxide polymer sheet on a quartz coverslip was immersed into a 1 mM solution of 2-aminoethanol in a 0.1 % w/v NaOH in distilled water solution for 3 hours at 40 °C. After this period the polymer was washed with distilled water, MeCN and finally DCM and dried over nitrogen, resulting in the S_N2 ring opening of the epoxide, leaving hydroxyl functionality on the surface (Scheme 3.18).

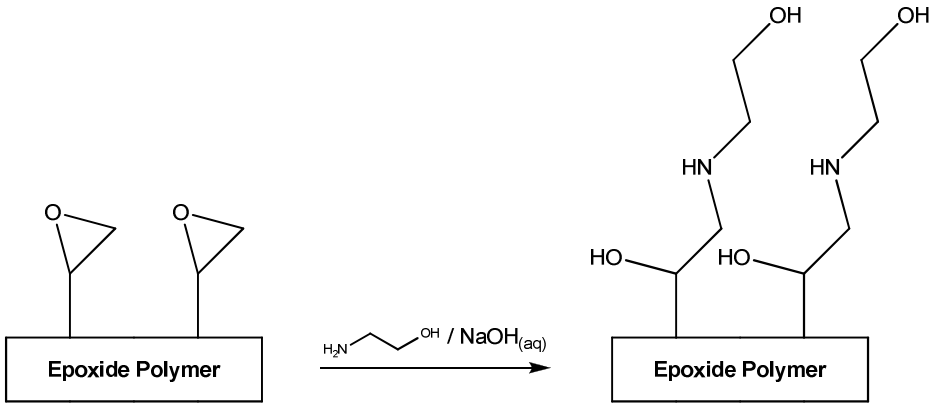

Scheme 3.18: S_N2 ring opening of epoxide polymer with 2-aminoethanol

A 1:1.2 solution of 2-(4-azidophenyl) acetic acid [3] and CDI in DCM was prepared, on a 1 mM scale, and stirred for 30 minutes. The epoxide polymer was immersed into the prepared solution and agitated for 1 hour. The polymer was then sonicated twice in DCM for 5 minutes dried over nitrogen which results in the epoxide polymer functionalised with the desired phenyl azide (Scheme 3.19).

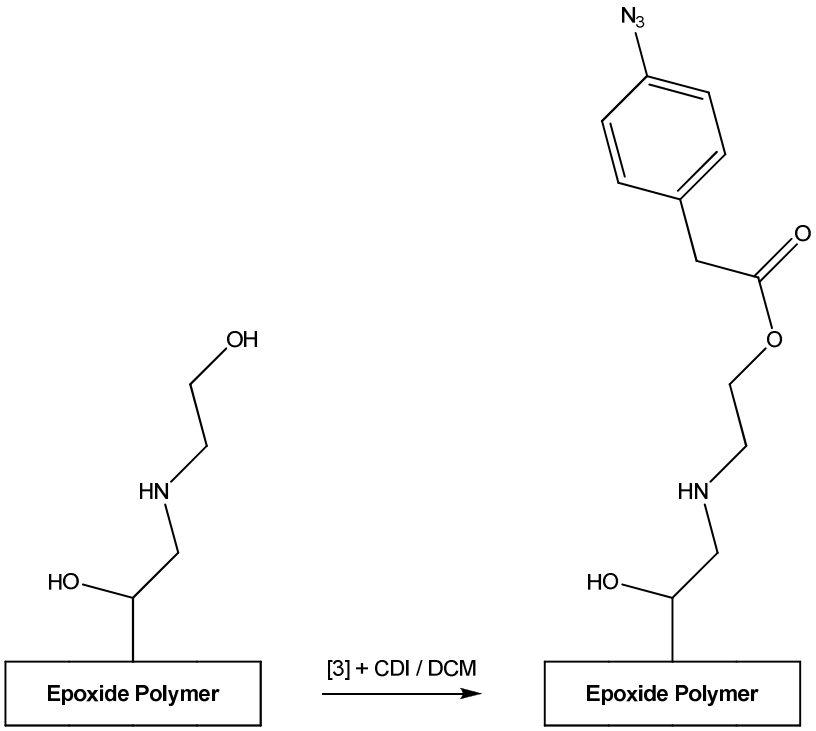

Scheme 3.19: Phenyl azide functionalisation of epoxide polymer

Scheme 3.19 illustrates that the phenyl azide has only attached on the free hydroxyl of the 2-aminoethanol. It could theoretically attach at the hydroxyl of the ring opened epoxide, however this is unlikely as it more sterically hindered.

Photoimmobilisation of Single Stranded DNA

The photoimmobilisation of DNA onto the epoxide polymer was achieved in a similar method to that of the photoimmobilisation of DNA onto quartz (Scheme 3.20).

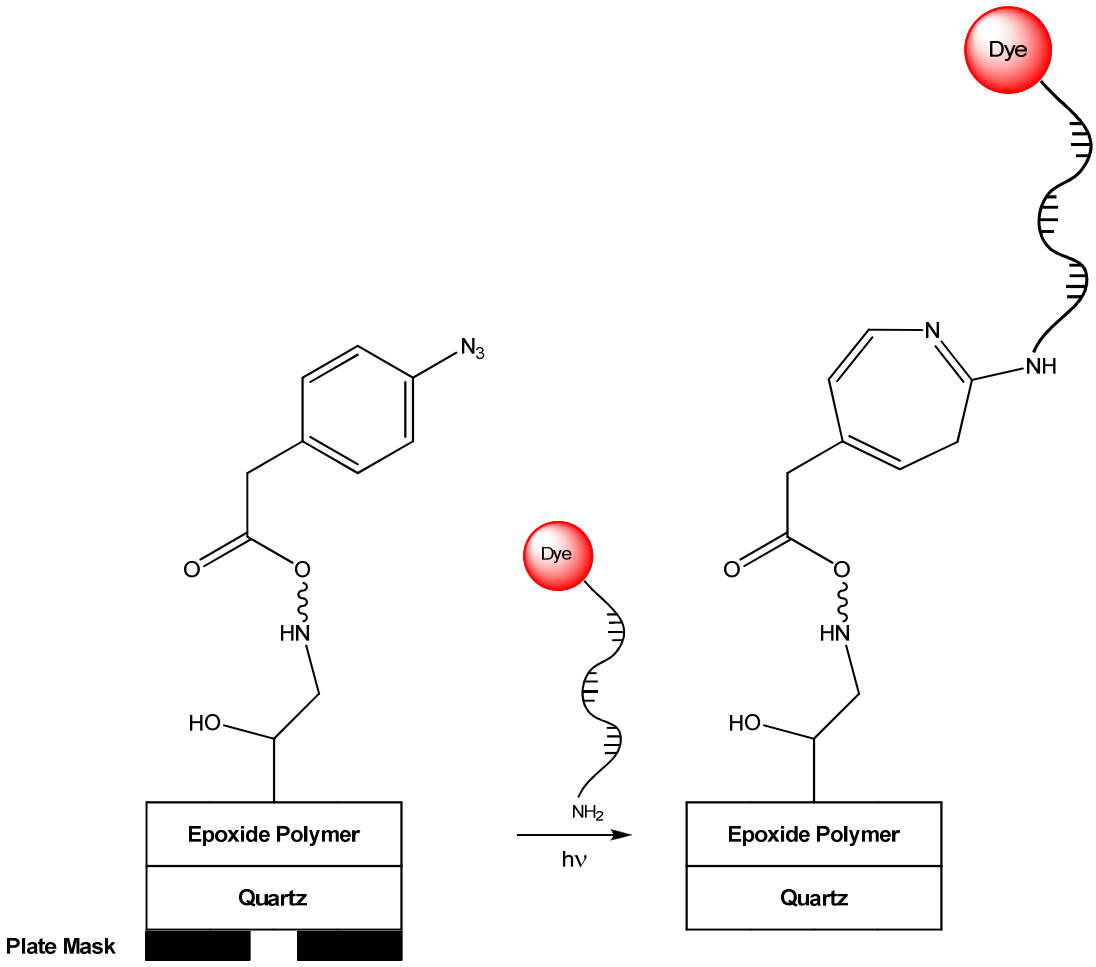

Scheme 3.20: Schematic representation of the photoimmobilisation of single stranded DNA onto epoxide polymer

A 1 μM solution of 5' Cy5 3' C_3-amino modified DNA was placed in the top surface of the phenyl azide modified epoxide polymer. The plate mask was then placed underneath the quartz coverslip upon which the polymer had been synthesised on, and both placed on the 365 nm UV lamp of the transilluminator. The lamp was then switched on for 10 minutes to allow for the photoimmobilisation of DNA. After this period the epoxide polymer was sonicated twice in distilled water for 5 minutes dried over nitrogen, and analysed immediately.

A StreamLine™ Plus Raman imaging system was then set up to record static scans of the Raman scattered light using a 633 nm laser at 100 % power, using a 5 × objective, 1 accumulation for 2 seconds every 100 μm in the x-axis and 10.6 μm in the y-axis.

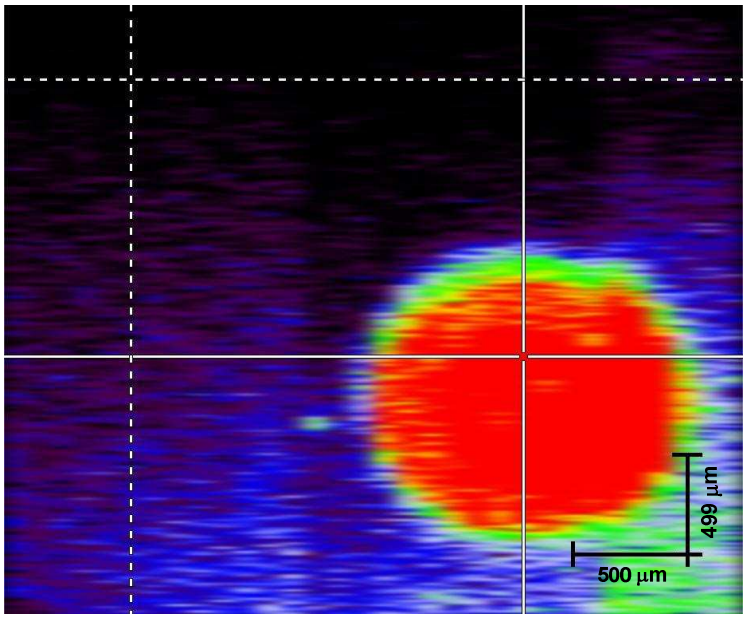

Figure 3.31: StreamLine™ map at 633 nm of the photoimmobilisation of DNA through 'spot' mask

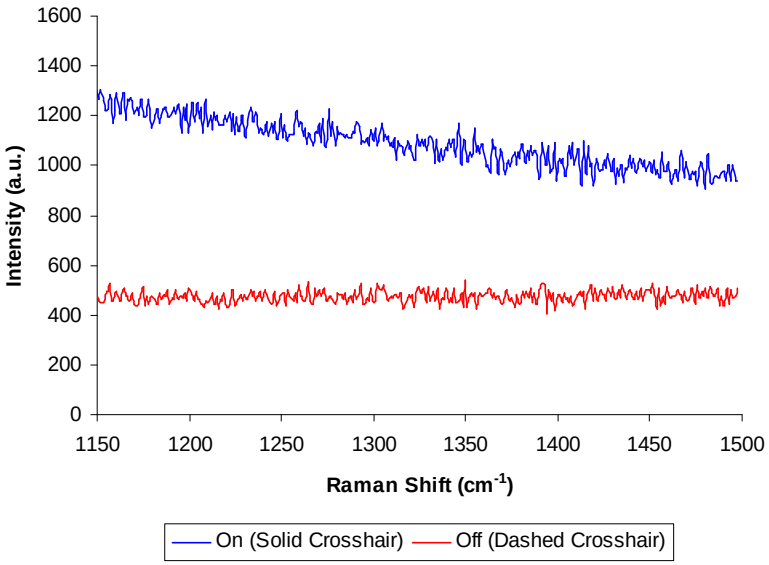

Figure 3.32: RRS spectra at 633 nm of the photoimmobilisation of DNA through 'spot' mask

It is clear that photoimmobilisation has occurred on to the epoxide polymer as the StreamLine™ map clearly shows the shape and position of the mask used (Figure 3.29). The diameter of the 'spot' calculated from the scale bar was 1.4 mm which is approximately 20 % smaller than that of the aperture sizes of the mask used of 1.8 mm. Unfortunately no resonance Raman scattering was observed, just an increase in background as the competing fluorescence of the Cy5 dye that strongly absorbs at the excitation wavelength of 633 nm, is swamping the signal (Figure 3.32).

3.3.3. Photoimmobilisation of DNA onto Gold

The gold substrate used for the photoimmobilisations was the novel SERS substrate, Klarite™ (Figure 3.33). Klarite™ substrates are gold coated microstructured silicon substrates, containing a 4 mm^2 active area of thousands of regular spaced 1 μm^2 wells. These wells control the surface plasmons in order for SERS to occur.[86]

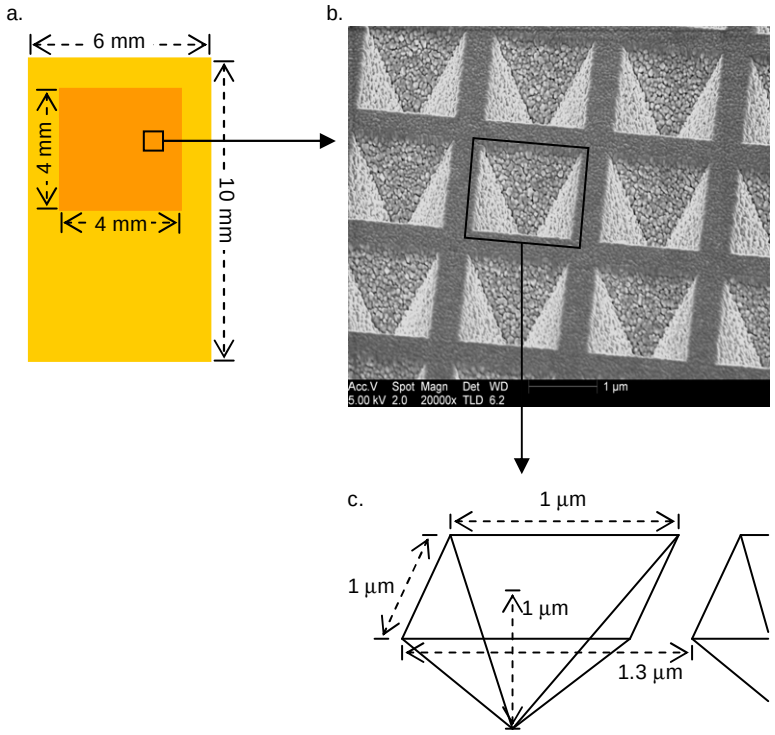

Figure 3.33: Klarite™ SERS substrate; a. schematic representation with dimensions; b. SEM of active surface; c. schematic representation of individual well with dimensions

The immobilisation of BD650, ROX and Cy7 labelled DNA onto Klarite™ surfaces and subsequent detection via SERRS has been previously reported by Stokes *et al.*[87] Given that the exploitation of the strong coordinate covalent bond between gold and sulfur has been long established, especially when in preparing SAMs, the phenyl azide to be synthesised must contain a terminal sulfur group, in order for photoimmobilisation to occur at the gold surface.[88]

3-Sulfanylpropanoic acid was chosen as a suitable linker to attach to the phenyl azide, as the sulfur and carboxylic acid have different functionalities (Figure 3.34). However the sulfur needed to be protected, as the ester and amide formation chemistries required to attached the subsequent linker 2-aminoethanol for the attachment of the phenyl azide, would result in a thioether linkage between the unprotected sulfur and that of the free carboxylic acid of the 2-(4-azidophenyl)acetic acid [3] and 3-sulfanylpropanoic acid.

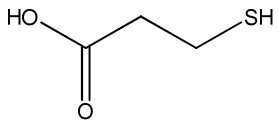

Figure 3.34: 3-Sulfanylpropanoic acid

Protection of 3-sulfanylpropanoic acid was achieved using a trityl protection group following the method outline by Polidori *et al.* (Scheme 3.21), where purification was achieved via recrystallisation in DCM, resulting in a 91 % yield.[89]

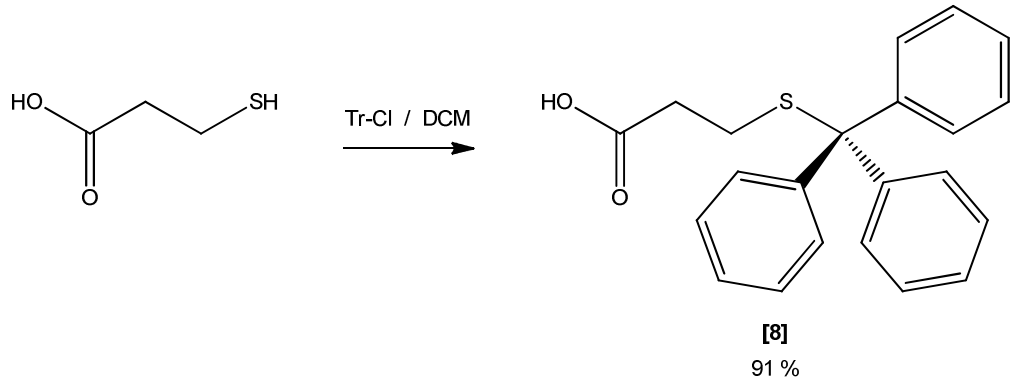

Scheme 3.21: Synthesis of 3-(tritylsulfanyl)propanoic acid

A sample was then recrystallised from DCM to obtain a crystal for analysis via X-ray diffraction. The resulting ellipsoidal crystal structure is shown in Figure 3.35 where the bulky trityl group is tetrahedrally arranged so that the phenyl groups are spaced the furthest away from each other to avoid any steric interactions.

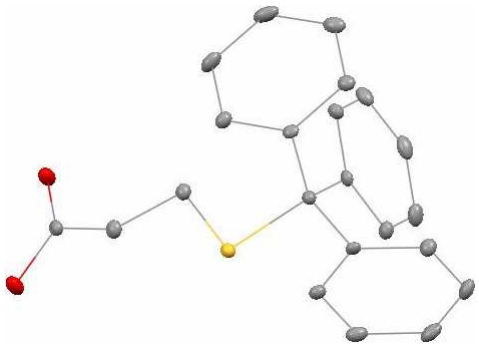

Figure 3.35: Ellipsoidal crystal structure of 3-(tritylsulfanyl)propanoic acid [8]

2-Aminoethanol was then reacted with CDI activated 3-(tritylsulfanyl)propanoic acid [8], in an amide formation reaction (Scheme 3.22).

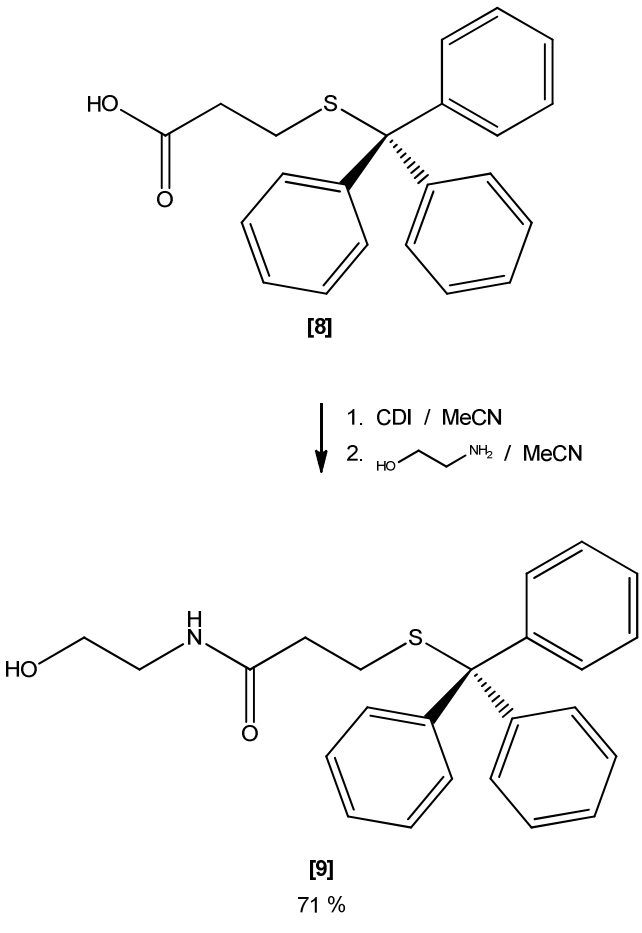

Scheme 3.22: Synthesis of *N*-(2-hydroxyethyl)-3-(tritylthio)propanamide [9]

Following purification via flash column chromatography a yield of 71 % was achieved and a sample was recrystallised from EtOAc to obtain a crystal for analysis via X-ray diffraction. The resulting ellipsoidal crystal structure is shown in Figure 3.36 where the structure is of similar shape to that of 3-(tritylsulfanyl)propanoic acid [8].

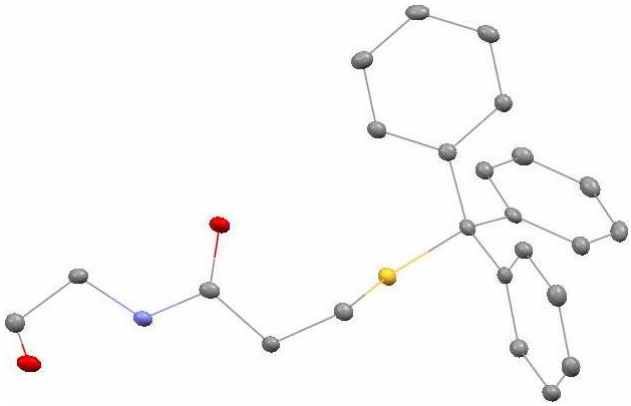

Figure 3.36: Ellipsoidal crystal structure of *N*-(2-hydroxyethyl)-3-(tritylthio)propanamide [9]

N-(2-hydroxyethyl)-3-(tritylthio)propanamide [9] was then reacted with CDI activated 2-(4-azidophenyl)acetic acid [3], in an ester formation reaction (Scheme 3.23), and purified via flash column chromatography resulting in a 54 % yield.

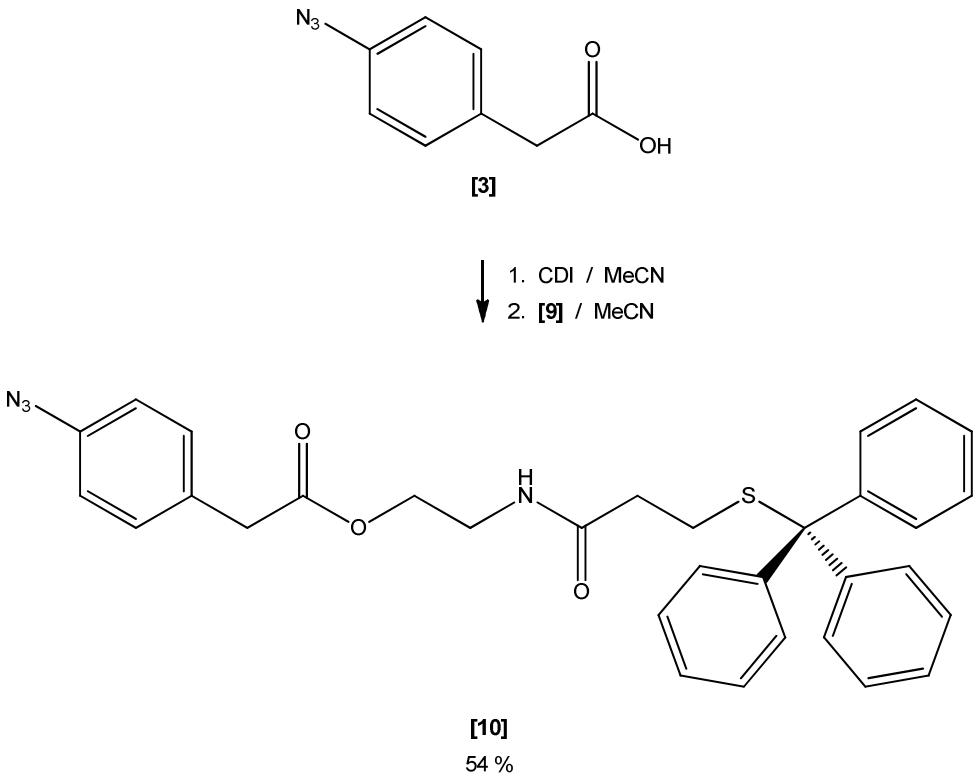

Scheme 3.23: Synthesis of 2-(3-(tritylthio)propanamido)ethyl 2-(4-azidophenyl) acetate [10]

A sample was then recrystallised from DCM to obtain a crystal for analysis via X-ray diffraction. The resulting ellipsoidal crystal structure is shown in Figure 3.37 where the large molecule has folded over to provide an overall more compact structure.

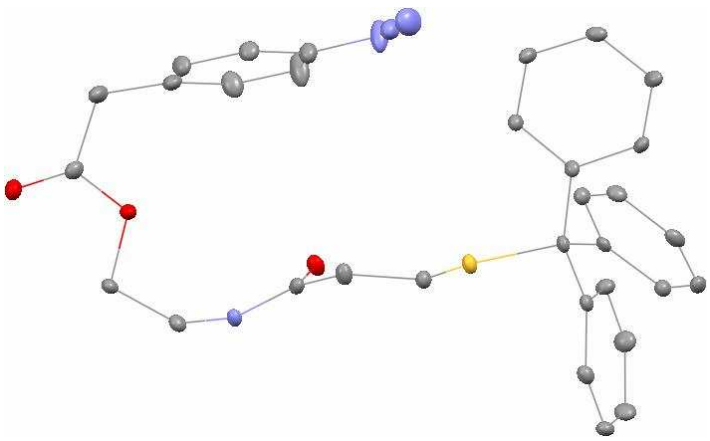

Figure 3.37: Ellipsoidal crystal structure of 2-(3-(tritylthio)propanamido)ethyl 2-(4-azidophenyl) acetate [10]

The trityl group is typically removed by a 10 % v/v TFA in DCM, in the presence of triethylsilane (Et_3SiH) as a cation scavenger.[89] However in the previous section where TFA was used to remove a Boc protecting group it was found that the acid catalysed the hydrolysis of the ester. As the typical concentrations required to remove the trityl are 10 times higher than in the previous section, an alternative method was required.

In DNA synthesis it is common to remove the trityl protection group of sulfur via oxidation with aqueous silver nitrate. An attempt to deprotect the thiol by using silver nitrate on silica gel was made, although it was not done under aqueous conditions, it was thought that the residual water in the solvents used would be enough to achieve this (Scheme 3.24). The benefit of using this method is that there would be no requirement to purify the product, as the deprotection method inherently does it at the same time due to the passing of the product through silica gel, just like flash column chromatography.

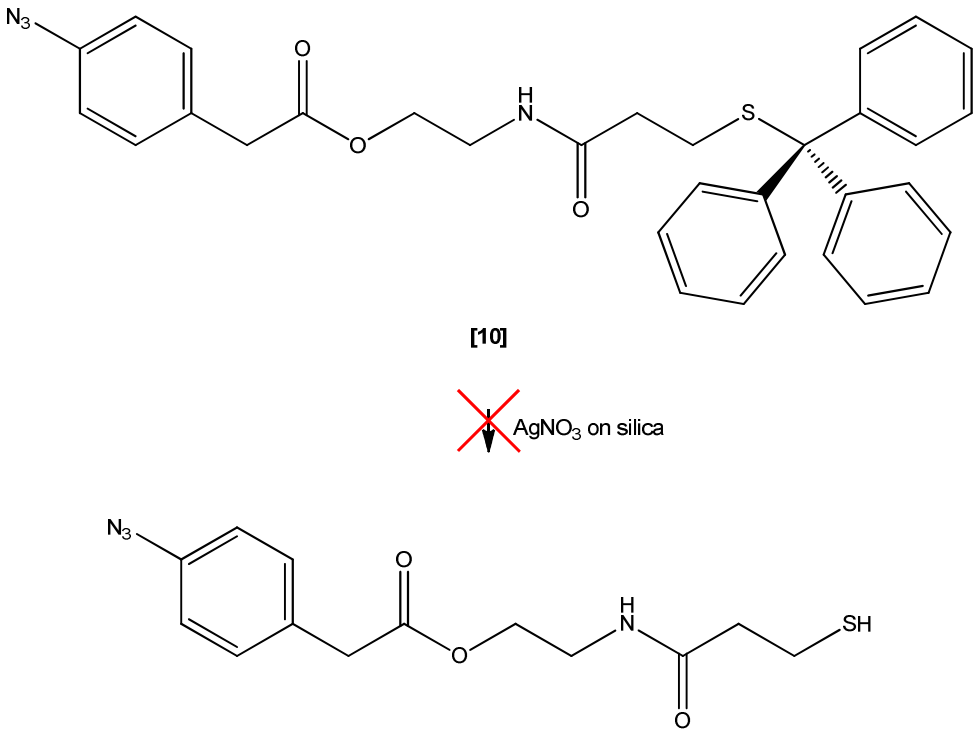

Scheme 3.24: Attempted synthesis of 2-(3-mercaptopropanamido)ethyl 2-(4-azidophenyl)acetate

At the start of the deprotection two distinct yellow bands were clearly visible, which could possibly be the product and the trityl group. Unfortunately as these bands moved down the column they became faded in colour and upon collection of the bands, the only compound observed on a TLC was that of the trityl protected compound. It may be conceivable that the product had decomposed on the silica gel, but a more likely outcome is that the reaction did not occur, and that the two bands observed were a contamination and the original trityl protected compound.

An alternative sulfur containing group that has been widely used within the group is thioctic acid (Figure 3.38). It is a bidentate ligand that forms stronger covalent bonds to gold, compared to the monodentate equivalent.

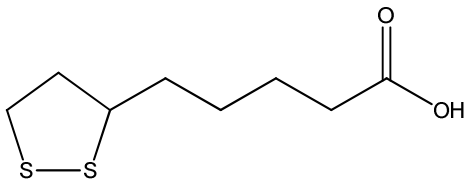

Figure 3.38: Thioctic acid

2-Aminoethanol was again chosen as a linker between thioctic acid and 2-(4-azidophenyl)acetic acid [3]. To achieve this 2-aminoethanol was reacted with CDI activated thioctic acid, in an amide formation reaction (Scheme 3.25).

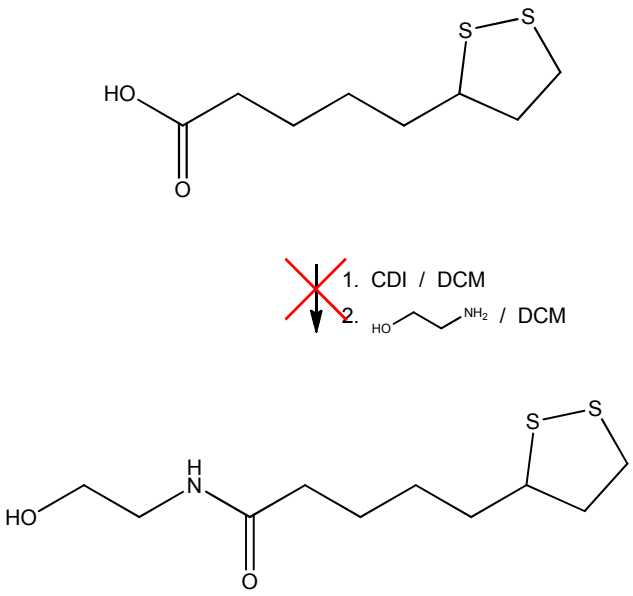

Scheme 3.25: Attempted synthesis of 5-(1,2-dithiolan-3-yl)-*N*-(2-hydroxyethyl)pentanamide

Unfortunately after evaporation of the solvent following a mild work up and drying, the resultant impure product was incapable of being redissolved back into DCM. It was more than likely due to the disulfide polymerising, as this has been previously been observed within the research group.

Preparation of Phenyl Azide Functionalised Gold

The two planned routes of synthesising a phenyl azide containing a sulfur to react with gold were unsuccessful. So just like the epoxide polymer it was proposed to achieve this via a two step process.

A 1 % w/v thioctic acid solution in DCM was pipetted over the Klarite™ and then placed in a water tight hybridisation chamber containing distilled water in the wells for 30 minutes, which functionalises the Klarite™ with a carboxylic acid (Scheme 3.26).

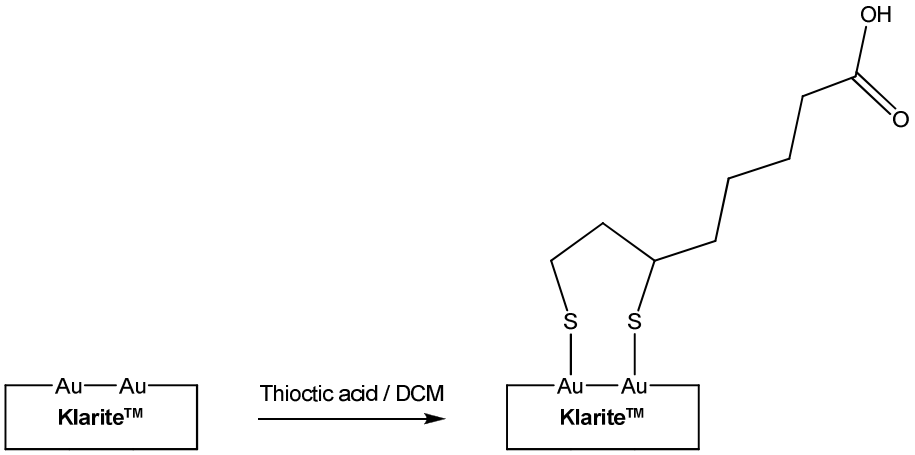

Scheme 3.26: Thioctic acid immobilisation to the gold surface

2-Aminoethanol was then reacted with CDI activated 2-(4-azidophenyl)acetic acid [3], in an amide formation reaction (Scheme 3.27), and purified via flash column chromatography to afford a yield of 78 %.

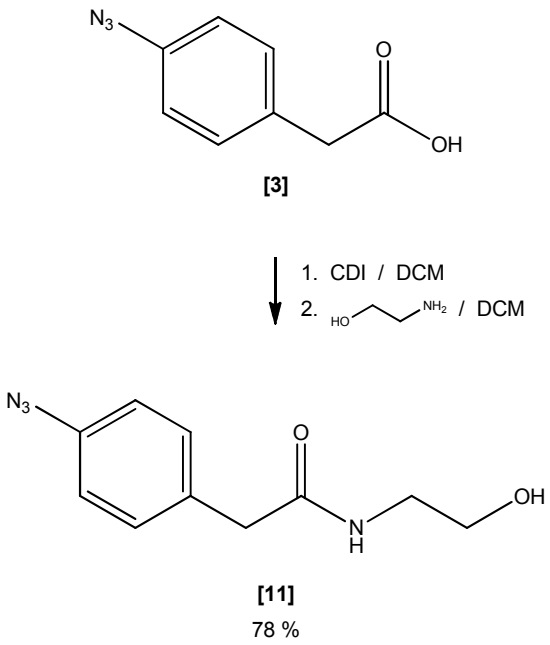

Scheme 3.27: Synthesis of 2-(4-azidophenyl)-*N*-(2-hydroxyethyl)acetamide [11]

The Klarite™ was first immersed into a 1 % w/v solution of CDI in DCM stirred for 30 minutes followed by being immersed into a 1 % w/v solution of [11] in DCM. After this period the Klarite™ was then sonicated twice in DCM for 5 minutes dried over nitrogen which results in the Klarite™ functionalised with the desired phenyl azide (Scheme 3.28).

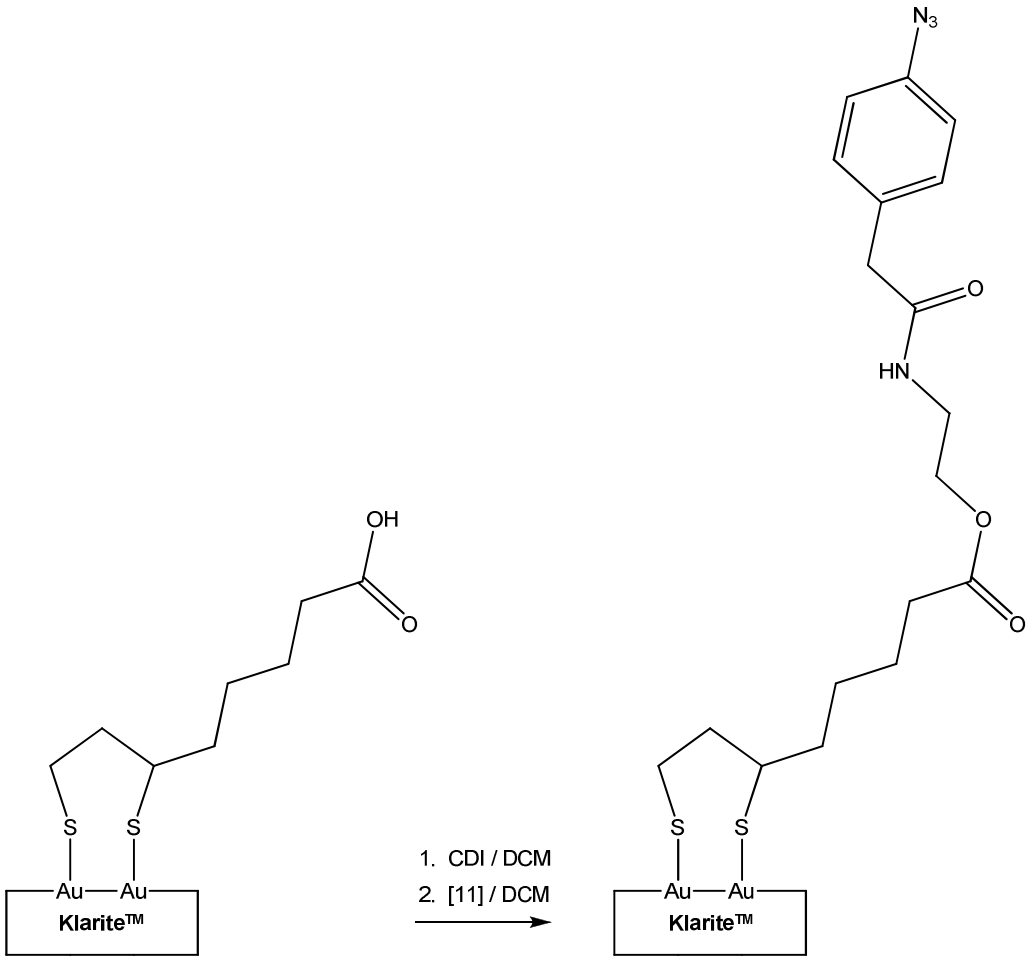

Scheme 3.28: Phenyl azide functionalisation of gold

Photoimmobilisation of Single Stranded DNA

The method for photoimmobilisation of DNA onto the Klarite™ is slightly different to that of the photoimmobilisation onto quartz and epoxide polymer. This is because the active surface of the Klarite™ is made from silicon coated with gold and hence is not UV penetrable. Therefore the immobilisation of the DNA must happen in a two step process, first by UV activating the phenyl azide and then introducing the DNA to the activated Klarite™ surface (Scheme 3.29).

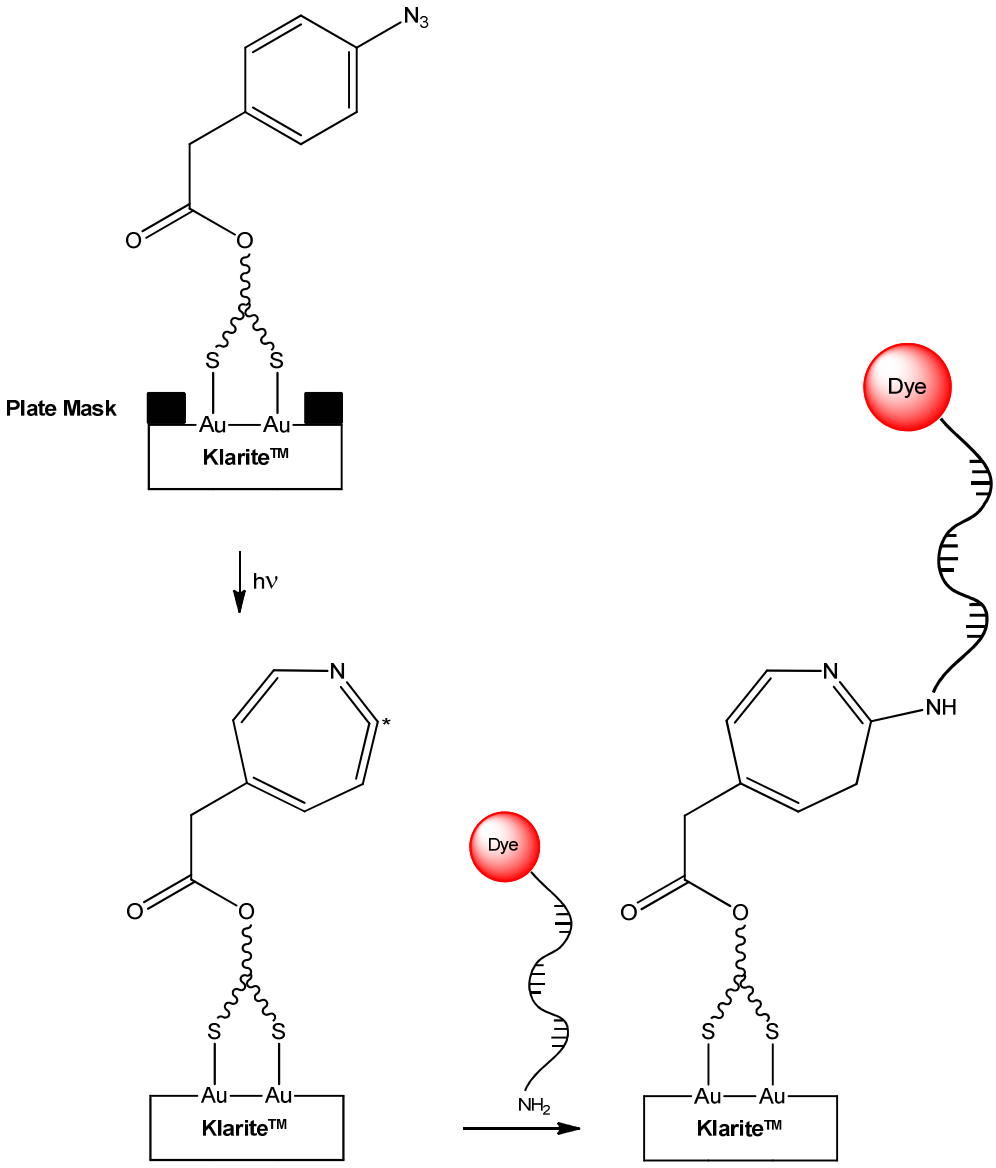

Scheme 3.29: Schematic representation of the photoimmobilisation of single stranded DNA onto gold

The desired plate mask was placed on the 365 nm UV lamp of the transilluminator followed by the Klarite™ placed on top of the mask, face down towards the UV lamp. The lamp was then switched on for 5 minutes to allow activation of the phenyl azide. The Klarite™ was then immersed into a 1 μM solution of 5' Cy5 3' C_3-amino modified for 30 minutes. After this period the Klarite™ was sonicated twice in distilled water for 5 minutes and analysed immediately.

A StreamLine™ Plus Raman imaging system was then set up to record static scans of the Raman scattered light using a 633 nm laser at 100 % power, using a 5 × objective, 1 accumulation for 2 seconds every 100 μm in the x-axis and 10.6 μm in the y-axis.

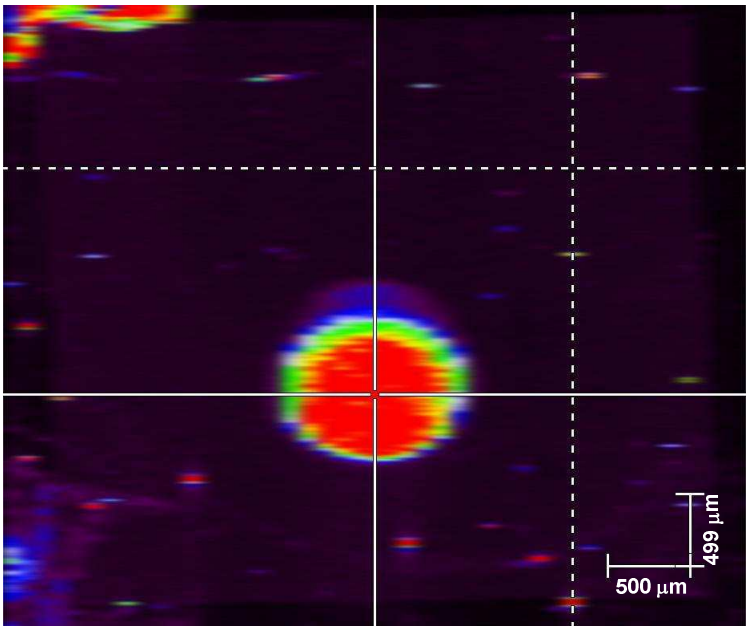

Figure 3.39: StreamLine™ map at 633 nm of the photoimmobilisation of DNA through 'spot' mask

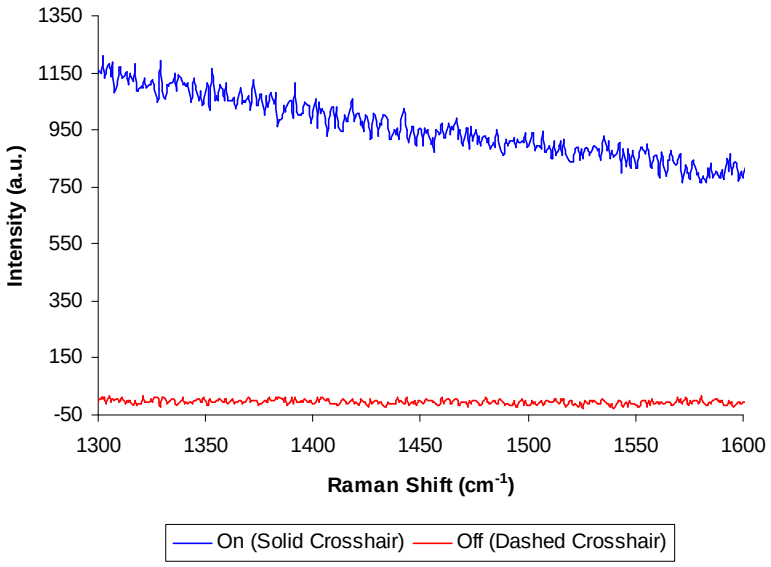

Figure 3.40: SERRS spectra at 633 nm of the photoimmobilisation of DNA through 'spot' mask

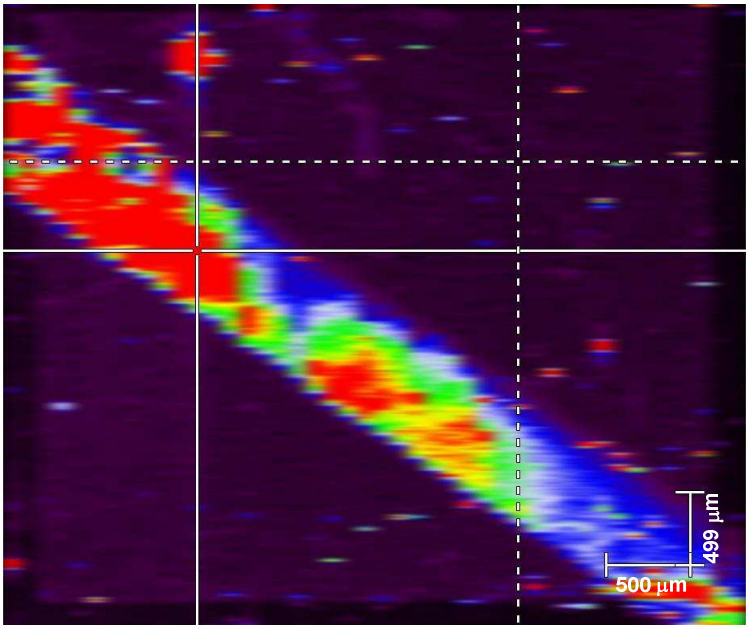

Figure 3.41: StreamLine™ map at 633 nm of the photoimmobilisation of DNA through 'line' mask

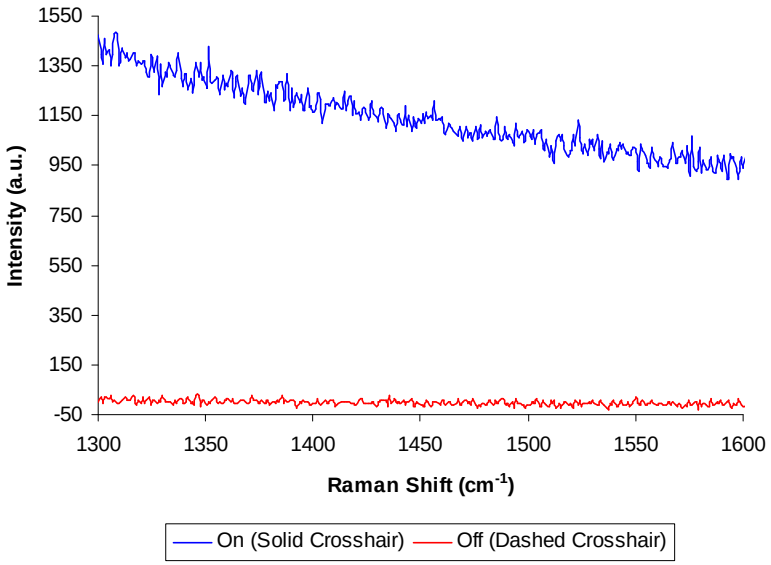

Figure 3.42: SERRS spectra at 633 nm of the photoimmobilisation of DNA through 'line' mask

It is clear that photoimmobilisation has occurred on to the Klarite™ surface as the StreamLine™ maps clearly show the shape and position of the masks used (Figure 3.39 and Figure 3.41). The diameter of the 'spot' calculated from the scale bar was 1.2 mm and the width of the 'line' was 0.7 mm, these are approximately 30 % smaller than that of the aperture sizes of the masks used of 1.8 mm and 1.0 mm respectively. Both masks appear to be focusing the UV light onto the Klarite™ rather than dispersing it. Unfortunately no SERRS was observed, just an increase in background coming from fluorescence of the Cy5 dye as it strongly absorbs at the excitation wavelength of 633 nm (Figure 3.40 and Figure 3.42).

To overcome the fluorescence, the StreamLine™ maps were repeated using 785 nm as the excitation source, keeping the all imaging system set up the same as for 633 nm (Figure 3.43 and Figure 3.45). This wavelength is far enough away from the excitation wavelength of Cy5 to prevent fluorescence, but it is still within the range for SERRS to occur.

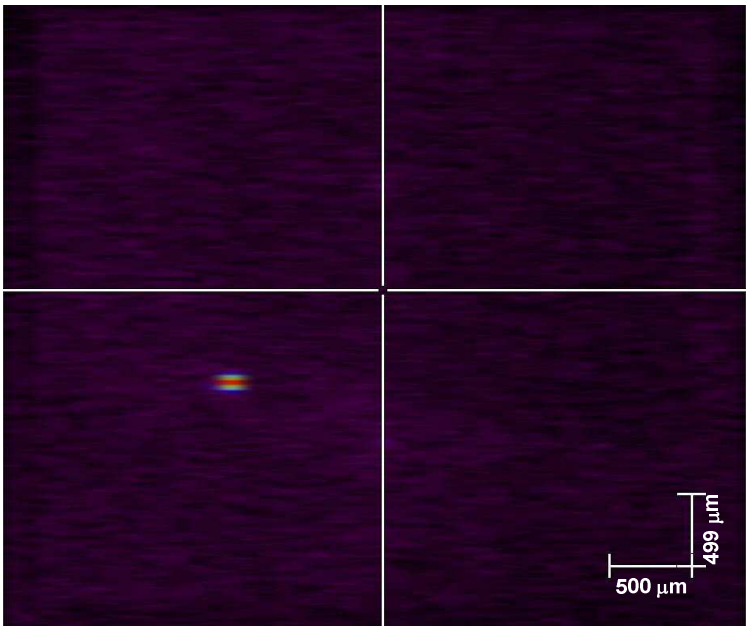

Figure 3.43: StreamLine™ map at 785 nm of the photoimmobilisation of DNA through 'spot' mask

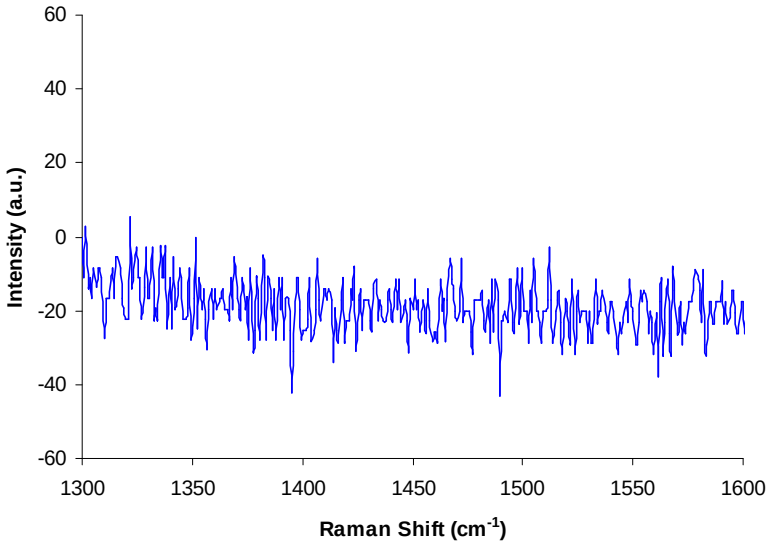

Figure 3.44: SERRS spectrum at 785 nm of the photoimmobilisation of DNA through 'spot' mask

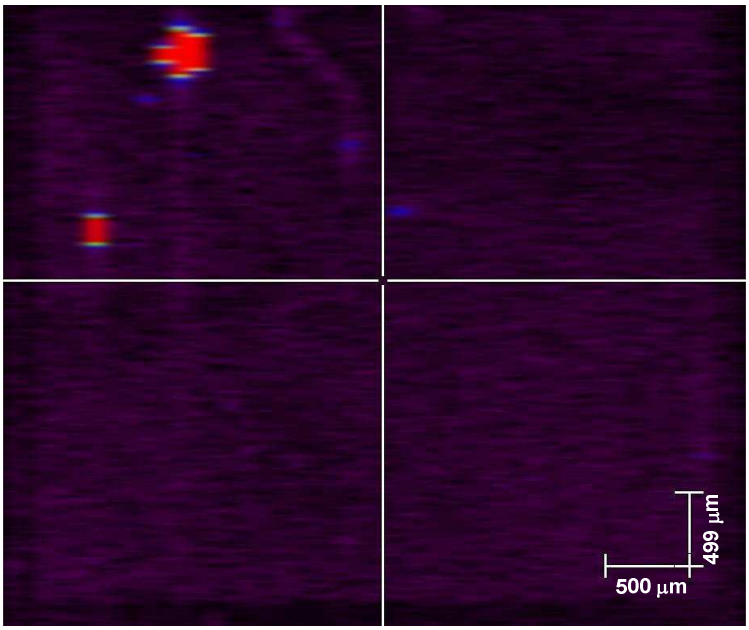

Figure 3.45: StreamLine™ map at 785 nm of the photoimmobilisation of DNA through 'line' mask

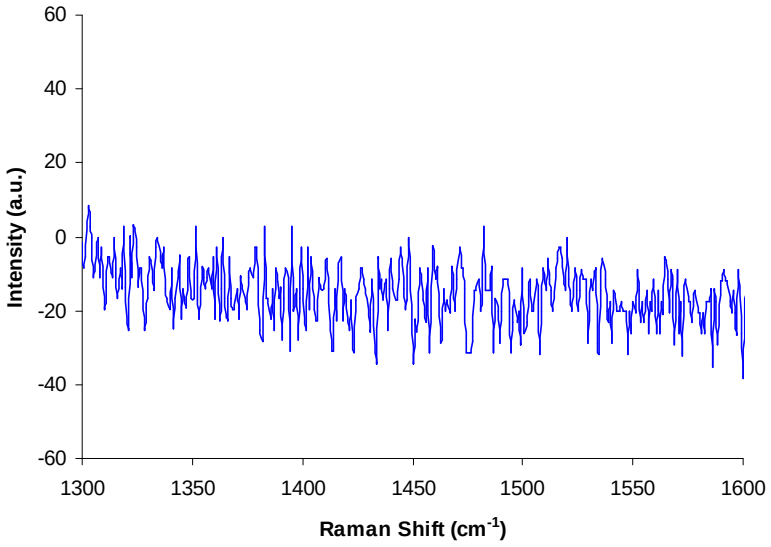

Figure 3.46: SERRS spectrum at 785 nm of the photoimmobilisation of DNA through 'spot' mask

Analysing the Klarite™ at 785 nm instead of 633 nm did not result in any SERRS (Figure 3.44 and Figure 3.46), this maybe due to the fact that not enough DNA has been photoimmobilised to the Klarite™ so it can not be detected. This is highly unlikely as SERRS is a sensitive technique and D3 Technologies Ltd. have previously reported SERRS from a Cy5 modified oligonucleotide on Klarite™ at levels as low as femtomolar (10^{-15} M).[90] What is the more likely explanation for the lack of SERRS signal is that the Cy5 molecule is too far off the surface and hence away from the surface plasmons in order to get the surface enhancement.

3.3. Experimental

3.3.1. Solvents and Reagents

Solvents and reagents used were as previous section.

Anhydrous DCM and Et_3N were prepared from reflux over CaH_2, distilled and collected under a N_2 atmosphere and used immediately.

Anhydrous MeCN was purchased from Link Technologies in sealed bottles.

APTES was purchased from Aldrich in SureSeal™ bottles.

Unmodified, dye modified and amino modified oligonucleotides were purchased from MWG Biotech in a lyophilised state, and rehydrated to the desired concentration using diethylpyrocarbonate (DEPC) treated water.

DEPC treated water was purchased from Bioline.

Quartz glass microscope coverslips (22 mm × 22 mm × 0.2 mm) were purchased from Agar Scientific.

Klarite™ SERS substrates were purchased from D3 Technologies Ltd.

3.3.2. Chromatography and Recrystallisation

Recrystallisation was carried out using specific solvent systems expressed in Table 3.5.

Flash column chromatography, TLC and plate detection tests were carried out as previous section where specific solvent systems are expressed in Table 3.5.

Code	Solvents	Ratios
[D]	DCM	100
[E]	DCM:MeOH	90:10
[F]	Pet Ether 60-80:EtOAc	50:50
[G]	EtOAc	100
[H]	EtOAc:MeOH	90:10
[I]	EtOAc:MeOH	95:5
[J]	Pet Ether 60-80:EtOAc	100-0:0-100
[K]	EtOAc:MeOH	100-95:0-5

Table 3.5: Chromatography and recrystallisation solvent systems

3.3.3. Chemical Analysis, Spectroscopy and Instrumentation

Chemical analysis, spectroscopy and instrumentation were carried out as in the previous section.

Contact angles were measured using an FTA200 contact angle instrument (Camtel, UK), a University of Strathclyde service.

Fluorescence spectroscopy and SERRS were performed on two systems:

1. 515 nm argon ion laser coupled to a Renishaw inVia microscope system,
2. 633 nm helium-neon laser coupled to a Renishaw Ramascope microscope system.

Prehybridisations for the split assay were performed in a Stratagene Mx4000™ multiplex quantitative PCR system.

Streamline maps were made using a StreamLine™ Plus Raman imaging system using a 633 nm helium-neon laser and a 785 nm diode laser.

3.3.4 DNA Concentration [91]

The concentration of the purified and desalted sample of synthetic DNA can be accurately determined by measuring its absorbance at 260 nm. The Beer-Lambert law (Equation 3.3) is used to calculate the concentration of DNA as each nitrogenous base absorbs at 260 nm.

$$A = \varepsilon \cdot c \cdot l$$

Equation 3.3: Beer-Lambert law

Since molar extinction coefficients are additive; the molar extinction for a DNA sequence can be obtained by combining the values for the individual DNA nitrogenous bases (Table 3.6) and multiplying it by the hypochromicity factor, 0.9 (Equation 3.4). This is because base-stacking interactions suppress the absorbance of DNA relative to the value calculated from the extinction coefficients of the individual nucleosides.

DNA Nitrogenous Base	Molar extinction coefficient at 260 nm ($mol^{-1}dm^3cm^{-1}$)
A	15,400
C	7,400
G	11,500
T	8,700

Table 3.6: Molar extinction coefficients of the DNA nitrogenous bases at 260 nm

$$\varepsilon_{DNA} = [(n \cdot \varepsilon_A) + (n \cdot \varepsilon_C) + (n \cdot \varepsilon_G) + (n \cdot \varepsilon_T)] \times 0.9$$

Equation 3.4: Molar extinction coefficient for a given DNA sequence

3.3.5. Synthetic Procedures

Prior to synthesis round bottomed flasks were flame dried under a N_2 atmosphere, whilst syringes and other glassware were dried in an oven at 140 °C overnight.

tert-butyl 2-hydroxyethyl carbamate [4]

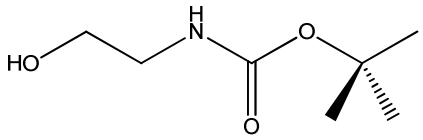

[4]

To a solution of 2-aminoethanol (2.01 g, 33 mmol, 2.0 mL, 1 eq) in 100 mL anhydrous DCM, anhydrous Et_3N (5.06g, 50 mmol, 3.7 mL, 1.5 eq) followed by di-*tert*-butyl dicarbonate (7.20 g, 33 mmol, 1 eq) was slowly added. The reaction mixture was then stirred at ambient temperature overnight under a N_2 atmosphere and was then quenched with saturated NH_4Cl solution (100 mL). The aqueous phase was extracted with EtOAc (100 mL × 3). The combined organic phases were washed with saturated NaCl solution (100 mL × 3) and dried immediately with Na_2SO_4 and then concentrated *in vacuo*. Purification was achieved by flash column chromatography [D] to afford title compound [4] (5.14 g, 97 %, R_f = 0.51 [D]) as a colourless oil (Found: C, 51.0; H, 8.55; N, 8.5 % $C_7H_{15}NO_3$ requires C, 52.2; H, 9.4; N, 8.7 %); δ_H(400 MHz; $CDCl_3$) 1.42 (9H, s, CH_3), 3.16 (1H, s, OH), 3.23-3.27 (2H, m, CH_2), 3.64-3.68 (2H, m, CH_2), 5.15 (1H, s, NH); δ_C(100 MHz; $CDCl_3$) 28.5, 43.3, 62.5, 79.8, 157.0; m/z (MS-ESI) 162.1123 ($[M+H]^+$ $C_7H_{16}NO_3^+$ requires 162.1125); ν_{max} (NaCl/film)/cm^{-1} 3467 st, br (–OH), 1693 st, sh (C=O, OCONH).

2-(tert-butoxycarbonylamino)ethyl 2-(4-azidophenyl)acetate [5]

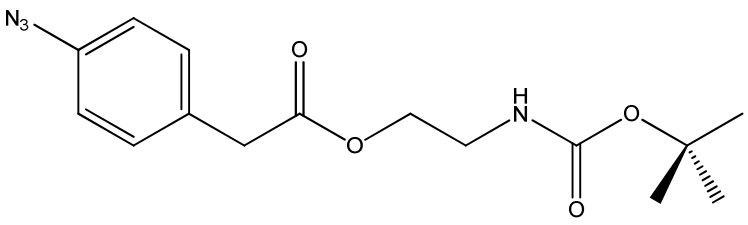

[5]

A solution of 2-(4-azidophenyl)acetic acid [3] (1.77 g, 10 mmol, 1 eq) in 10 mL anhydrous DCM was slowly added to a solution of CDI (1.95 g, 1.20 mmol, 1.20 eq) in 10 mL anhydrous DCM. The reaction mixture was then stirred at ambient temperature for 2 hrs under a N_2 atmosphere. Then a solution of *tert*-butyl 2-hydroxyethyl carbamate [4] (2.32 g, 1.05 mmol, 1.05 eq) in 10 mL anhydrous DCM slowly was added and stirred at ambient temperature overnight under a N_2 atmosphere. The reaction mixture was then diluted with DCM (100 mL) and washed with 10 % w/v NaOH (50 mL × 2) and with saturated NaCl solution (50 mL × 2). The organic phase was dried immediately with Na_2SO_4 and concentrated *in vacuo*. Purification was achieved by flash column chromatography [D] to afford title compound [5] (2.05 g, 64 %, R_f = 0.77 [E]) as a cream solid (Found: C, 56.75; H, 7.4; N, 17.4 % $C_{15}H_{20}N_4O_4$ requires C, 56.2; H, 6.3; N, 17.5 %); δ_H(400 MHz; DMSO-d_6) 1.38 (9H, s, CH_3), 3.14-3.18 (2H, q, *J*5.7, CH_2), 3.66 (2H, s, CH_2), 4.00-4.03 (2H, t, *J*5.8, CH_2); 6.91-6.93 (1H, t, *J*5.4, CONH); 7.05-7.08 (2H, m, AA'BB' splitting, ArH), 7.29-7.33 (2H, m, AA'BB' splitting, ArH); δ_C(100 MHz; DMSO-d_6) 28.2, 38.8, 39.4, 63.2, 77.8, 118.9, 131.0, 131.3, 137.9, 155.6, 171.0; m/z (MS-ESI) 338.1825 ($[M+NH_4]^+$ $C_{15}H_{24}N_5O_4^+$ requires 338.1823); ν_{max} (NaCl/nujol)/cm^{-1} 3376 med (–NH), 2117 st, sh (–N_3), 1740 st, sh (C=O, CO_2R), 1683 st, sh (C=O, OCONR); mp 46-48 ºC.

2-aminoethyl 2-(4-azidophenyl)acetate

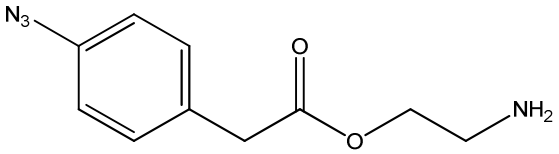

A solution of 2-(*tert*-butoxycarbonylamino)ethyl 2-(4-azidophenyl)acetate [5] (1.60 g, 5 mmol, 1 eq) in 1 % v/v TFA in DCM (5 mL, excess) was stirred for 1 hr at ambient temperature under a N_2 atmosphere. After this the reaction mixture was then diluted with DCM (50 mL) and washed with 10 % w/v NaOH (25 mL × 2) and with saturated NaCl solution (25 mL × 2). The organic phase was dried immediately with Na_2SO_4 and concentrated *in vacuo*. The described procedure did not result in the title compound.

2-(((9H-fluoren-9-yl)methoxy)carbonylamino)ethyl 2-(4-azidophenyl)acetate [6]

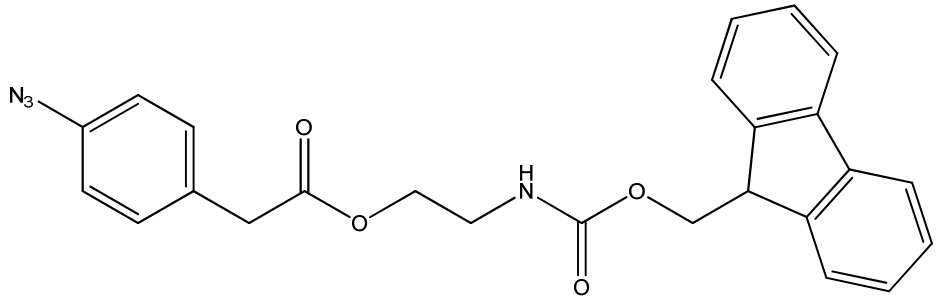

[6]

A solution of 2-(4-azidophenyl)acetic acid [3] (1.77 g, 10 mmol, 1 eq) in 10 mL anhydrous DCM was slowly added to a solution of CDI (1.95 g, 1.20 mmol, 1.20 eq) in 10 mL anhydrous DCM. The reaction mixture was then stirred at ambient temperature for 2 hrs under a N_2 atmosphere. Then a solution of 9*H*-fluoren-9-ylmethyl 2-hydroxyethyl carbamate (2.32 g, 1.05 mmol, 1.05 eq) in 10 mL anhydrous DCM slowly was added and stirred at ambient temperature overnight under a N_2 atmosphere. The reaction mixture was then diluted with DCM (100 mL) and washed with saturated $NaHCO_3$ solution and with saturated NaCl solution (50 mL × 2). The organic phase was dried immediately with Na_2SO_4 and concentrated *in vacuo*. Purification was achieved by flash column chromatography [F] to afford title compound [6] (2.72 g, 61 %, R_f = 0.77 [G]) as a cream solid (Found: C, 67.6; H, 5.0; N, 12.4 % $C_{25}H_{22}N_4O_4$ requires C, 67.9; H, 5.0; N, 12.7 %); δ_H(400 MHz; DMSO-d_6) 3.23-3.27 (2H, q, *J*5.7, CH_2), 3.66 (2H, s, CH_2), 4.04-4.07 (2H, t, *J*5.8, CH_2), 4.20-4.23 (1H, t, *J*6.6, CH), 4.32-4.33 (2H, d, *J*6.8, CH_2), 7.02-7.04 (2H, d, *J*8.4, ArH), 7.28-7.34 (4H, m, ArH), 7.40-7.45 (3H, m, ArH), 7.68-7.70 (2H, d, *J*7.6, ArH), 7.88-7.90 (2H, d, *J*7.6, ArH); δ_C(100 MHz; DMSO-d_6) 39.2, 39.4, 46.7, 63.0, 65.4, 118.9, 120.1, 125.1, 127.0, 127.6, 131.0, 131.2, 137.9, 140.7, 143.8, 156.2, 171.0; m/z (MS-ES) 460.1972 ($[M+NH_4]^+$ $C_{25}H_{26}N_5O_4^+$ requires 460.1979); ν_{max} (NaCl/nujol)/cm^{-1} 3325 med sh (–NH), 3066 wk (–NH), 2109 st, sh (–N_3), 1729 st, sh (C=O, CO_2R), 1678 st, sh (C=O, OCONR); mp 96-98 ºC.

2-aminoethyl 2-(4-azidophenyl)acetate

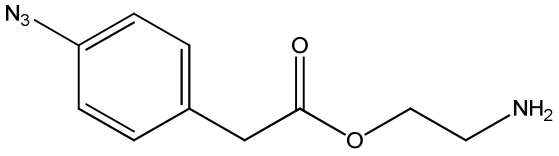

A solution of 2-(((9*H*-fluoren-9-yl)methoxy)carbonylamino) ethyl 2-(4-azidophenyl) acetate [6] (2.22 g, 5 mmol, 1 eq) in 20 % v/v piperidine in MeCN (5 mL, excess) was stirred for 3 hrs at ambient temperature under a N_2 atmosphere. After this the reaction mixture was then concentrated *in vacuo* and the residue subsequently diluted with DCM (50 mL). The organic phase was then washed with 10 % w/v HCl (25 mL × 2) and with saturated NaCl solution (25 mL × 2) and then immediately with Na_2SO_4 and concentrated *in vacuo*. The described procedure did not result in the title compound.

tert-butyl 2-(2-(4-azidophenyl)acetamido)ethylcarbamate [7]

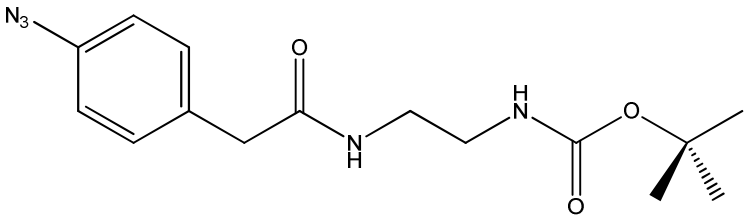

[7]

A solution of 2-(4-azidophenyl)acetic acid [3] (1.77 g, 10 mmol, 1 eq) in 10 mL anhydrous DCM was slowly added to a solution of CDI (1.95 g, 1.20 mmol, 1.20 eq) in 10 mL anhydrous DCM. The reaction mixture was then stirred at ambient temperature for 2 hrs under a N_2 atmosphere. Then a solution of *tert*-butyl 2-aminoethyl carbamate (1.68 g, 1.05 mmol, 1.05 eq) in 10 mL anhydrous DCM slowly was added and stirred at ambient temperature overnight under a N_2 atmosphere. The reaction mixture was then diluted with DCM (100 mL) and washed with 10 % w/v NaOH (50 mL × 2) and with saturated NaCl solution (50 mL × 2). The organic phase was dried immediately with Na_2SO_4 and concentrated *in vacuo*. Purification was achieved by flash column chromatography [G] to afford title compound [7] (2.20 g, 69 %, R_f = 0.71 [H]) as a cream solid (Found: C, 56.7; H, 6.55; N, 21.4 % $C_{15}H_{21}N_5O_3$ requires C, 56.4; H, 6.6; N, 21.9 %); δ_H(400 MHz; DMSO-d_6) 1.37 (9H, s, CH_3), 2.94-2.99 (2H, q, *J*6.1, CH_2), 3.04-

3.09 (2H, q, *J*6.1, CH_2), 3.38 (2H, s, CH_2), 6.77-6.79 (2H, t, *J*5.4, CONH); 7.02-7.06 (2H, m, AA'BB' splitting, ArH), 7.26-7.30 (2H, m, AA'BB' splitting, ArH), 8.02-8.04 (2H, t, *J*4.8, CONH); δ_C(100 MHz; DMSO-d_6) 28.2, 38.8, 39.6, 41.6, 77.6, 118.8, 130.6, 133.4, 137.4, 155.6, 170.0; m/z (MS-ESI) 320.1722 ($[M+H]^+$ $C_{15}H_{22}N_5O_3^+$ requires 320.1717); ν_{max} (NaCl/nujol)/cm^{-1} 3324 st, sh (–NH), 3309 med (–NH), 2116 st, sh ($–N_3$), 1681 st, sh (C=O, CO_2R), 1649 st, sh (C=O, OCONR); mp 140-141 ºC.

N-(2-aminoethyl)-2-(4-azidophenyl)acetamide

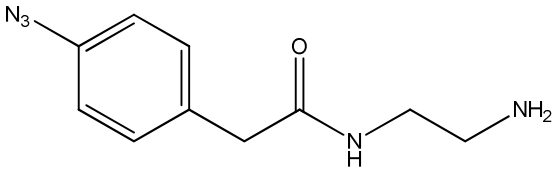

A solution of *tert*-butyl 2-(2-(4-azidophenyl)acetamido)ethyl carbamate [7] (1.60 g, 5 mmol, 1 eq) in 1 % v/v TFA in DCM (5 mL, excess) was stirred for 1 hr at ambient temperature under a N_2 atmosphere. After this the reaction mixture was then diluted with DCM (50 mL) and washed with 10 % w/v NaOH (25 mL × 2) and with saturated NaCl solution (25 mL × 2). The organic phase was dried immediately with Na_2SO_4 and concentrated *in vacuo*. The described procedure did not result in the title compound.

3-(tritylsulfanyl)propanoic acid [8]

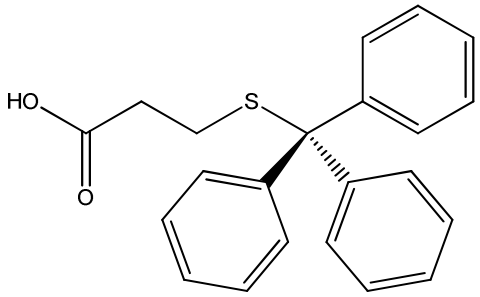

[8]

A solution of triphenylmethyl chloride (17.34 g, 62.2 mmol, 1 eq) in 50 mL anhydrous DCM was added dropwise to a solution of 3-sulfanylpropanoic acid (6.60 g, 62.2 mmol, 8.0 mL, 1 eq) in 30mL anhydrous DCM. The reaction mixture was then stirred at ambient temperature overnight. At the end of this period, a precipitate had formed,

which was separated from the solvent by filtration. Purification was achieved by recrystallisation [D] to afford title compound [8] (19.67 g, 91 %,) as a white solid (Found: C, 75.35; H, 5.6; S, 9.2 % $C_{22}H_{20}O_2S$ requires C, 75.8; H, 5.8; S, 9.2 %); δ_H(400 MHz; DMSO-d_6) 2.15-2.18 (2H, m, CH_2), 2.27-2.31 (2H, m, CH_2), 7.23-7.36 (15H, m, ArH), 12.19 (1H, s, CO_2H); δ_C(100 MHz; DMSO-d_6) 26.7, 32.9, 66.1, 126.7, 128.0, 129.1, 144.3, 172.6; m/z (MS-FAB) 347.1111 ($[M–H]^-$ $C_{22}H_{19}O_2S^-$ requires 347.1111); ν_{max} (NaCl/nujol)/cm^{-1} 1703 st, sh (C=O, CO_2H); mp 211-213 ºC.

N-(2-hydroxyethyl)-3-(tritylthio)propanamide [9]

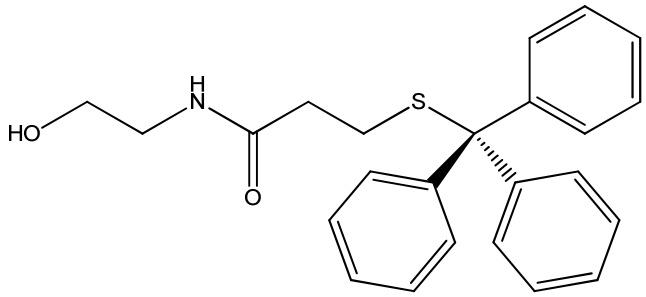

[9]

A solution of 3-(tritylsulfanyl)propanoic acid [8] (6.97 g, 20 mmol, 1 eq) in 20 mL anhydrous MeCN was slowly added to a solution of CDI (3.89 g, 24 mmol, 1.20 eq) in 20 mL anhydrous MeCN. The reaction mixture was then stirred at 40 °C for 2 hrs under a N_2 atmosphere. Then a solution of 2-aminoethanol (1.28 g, 21 mmol, 1.3 mL, 1.05 eq) in 20 mL anhydrous MeCN slowly was added and stirred at 40 °C overnight under a N_2 atmosphere. The reaction mixture was then concentrated *in vacuo* and the residue subsequently diluted with DCM (200 mL). This was then washed with 10 % v/v HCl (100 mL × 2), 10 % w/v NaOH (100 mL × 2) and finally with saturated NaCl solution (100 mL × 2). The organic phase was dried immediately with Na_2SO_4 and concentrated *in vacuo*. Purification was achieved by flash column chromatography [G] to afford title compound [9] (5.59 g, 71 %, R_f = 0.37 [I]) as a white solid (Found: C, 73.7; H, 6.0; N, 4.0; S, 8.3 % $C_{24}H_{25}NO_2S$ requires C, 73.6; H, 6.4; N, 3.6; S, 8.2 %); δ_H(400 MHz; DMSO-d_6) 2.14-2.17 (2H, m, CH_2), 2.22-2.26 (2H, m, CH_2), 3.04-3.08 (2H, q, *J*5.9, CH_2), 3.33-3.73 (2H, q, *J*5.9, CH_2), 4.59-4.62 (1H, t, *J*5.6, OH), 7.22-7.35 (15H, m, ArH), 7.78-7.80 (1H, t, *J*5.4, CONH); δ_C(100 MHz; DMSO-d_6) 27.4, 33.9, 41.4, 59.8, 65.9, 126.7, 128.0, 129.0, 144.4, 170.0; m/z (MS-ESI) 414.1490 ($[M+Na]^+$

$C_{24}H_{25}NNaO_2S^+$ requires 414.1498); νmax (NaCl/nujol)/cm^{-1} 3394 wk (–NH), 3282 med (–NH), 1653 st, sh (C=O, CONR); mp 130-131 ºC.

2-(3-(tritylthio)propanamido)ethyl 2-(4-azidophenyl)acetate [10]

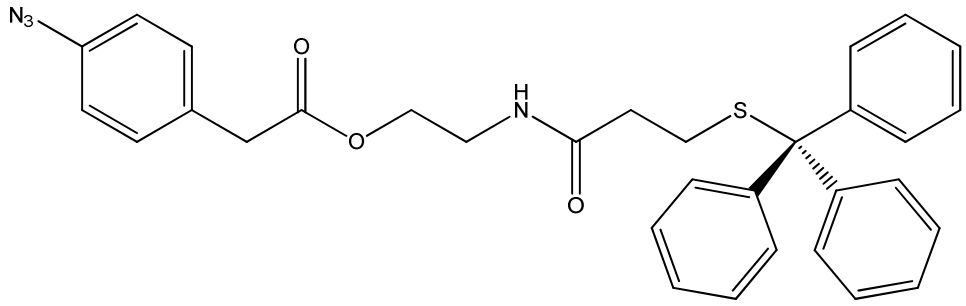

[10]

A solution of 2-(4-azidophenyl)acetic acid [3] (1.77 g, 10 mmol, 1 eq) in 10 mL anhydrous MeCN was slowly added to a solution of CDI (1.95 g, 12.0 mmol, 1.20 eq) in 10 mL anhydrous MeCN. The reaction mixture was then stirred at ambient temperature for 2 hrs under a N_2 atmosphere. Then a solution of *N*-(2-hydroxyethyl)-3-(tritylthio)propanamide [9] (4.11 g, 10.5 mmol, 1.05 eq) in 10 mL anhydrous MeCN slowly was added and stirred at ambient temperature overnight under a N_2 atmosphere. The reaction mixture was then concentrated *in vacuo* and the residue subsequently diluted with DCM (100 mL). This was then washed with 10 % w/v NaOH (50 mL × 2) and with saturated NaCl solution (50 mL × 2). The organic phase was dried immediately with Na_2SO_4 and concentrated *in vacuo*. Purification was achieved by flash column chromatography [J] to afford title compound [10] (2.96 g, 54 %, R_f = 0.74 [I]) as a cream solid (Found: C, 70.45; H, 5.2; N, 9.6; S, 6.1 % $C_{32}H_{30}N_4O_3S$ requires C, 69.8; H, 5.5; N, 10.2; S, 5.8 %); δ_H(400 MHz; DMSO-d_6) 2.14-2.17 (2H, m, CH_2), 2.25-2.28 (2H, m, CH_2), 3.24-3.28 (2H, q, *J*5.7, CH_2), 3.63 (2H, s, CH_2), 3.99-4.02 (2H, t, *J*5.8, CH_2), 7.03-7.06 (2H, m, AA'BB' splitting, ArH), 7.21-7.35 (17H, m, ArH), 7.93-7.96 (1H, t, *J*5.6 CONH); δ_C(100 MHz; DMSO-d_6) 27.3, 33.9, 37.5, 39.7, 62.8, 66.0, 118.9, 126.7, 128.0, 129.0, 131.0, 131.2, 137.9, 144.4, 170.3, 170.9; m/z (MS-EI) 550.2027 ($[M]^+$ $C_{32}H_{30}N_4O_3S^+$ requires 550.2033); ν_{max} (NaCl/nujol)/cm^{-1} 3272 med (–NH), 3092 wk (–NH), 2118 st, sh (–N_3), 1728 st, sh (C=O, CO_2R), 1643 st, sh (C=O, CONR); mp 101-103 ºC.

2-(3-mercaptopropanamido)ethyl 2-(4-azidophenyl)acetate

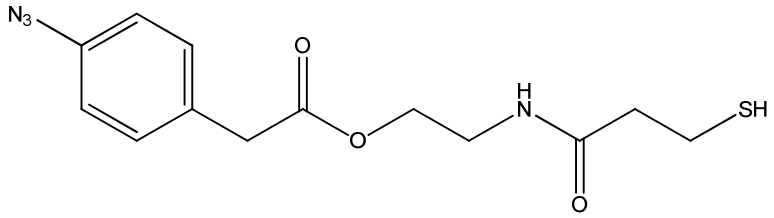

2-(3-(tritylthio)propanamido)ethyl 2-(4-azidophenyl)acetate [10] (1.38 g, 2.5 mmol) was dry loaded onto a packed flash chromatography column filled with silver nitrite on silica. Deprotection and purification was achieved by flash column chromatography [F]. The described procedure did not result in the title compound.

5-(1,2-dithiolan-3-yl)-N-(2-hydroxyethyl)pentanamide

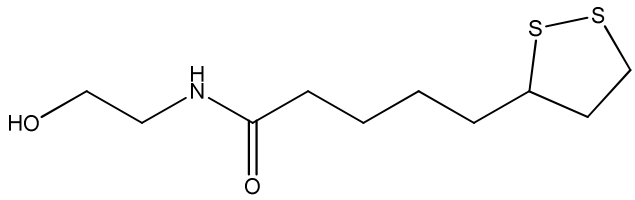

A solution of 5-(1,2-dithiolan-3-yl)pentanoic acid (2.06 g, 10 mmol, 1 eq) in 10 mL anhydrous DCM was slowly added to a solution of CDI (1.95 g, 12.0 mmol, 1.20 eq) in 10 mL anhydrous DCM. The reaction mixture was then stirred at ambient temperature for 2 hrs under a N_2 atmosphere. Then a solution of 2-aminoethanol (0.64 g, 10.5 mmol, 0.65 mL, 1.05 eq) in 10 mL anhydrous DCM slowly was added and stirred at ambient temperature overnight under a N_2 atmosphere. The reaction mixture was then diluted with DCM (100 mL) and washed with 10 % v/v citric acid (50 mL × 2), saturated $NaHCO_3$ solution (50 mL × 2) and finally with saturated NaCl solution (50 mL × 2). The organic phase was dried immediately with Na_2SO_4 and concentrated *in vacuo*. The described procedure did not result in the title compound.

2-(4-azidophenyl)-N-(2-hydroxyethyl)acetamide [11]

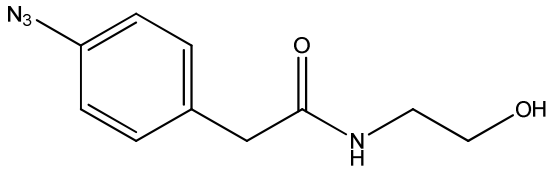

[11]

A solution of 2-(4-azidophenyl)acetic acid [3] (1.77 g, 10 mmol, 1 eq) in 10 mL anhydrous DCM was slowly added to a solution of CDI (1.95 g, 12.0 mmol, 1.20 eq) in 10 mL anhydrous DCM. The reaction mixture was then stirred at ambient temperature for 2 hrs under a N_2 atmosphere. Then a solution of 2-aminoethanol (0.64 g, 10.5 mmol, 0.65 mL, 1.05 eq) in 10 mL anhydrous DCM slowly was added and stirred at ambient temperature overnight under a N_2 atmosphere. The reaction mixture was then diluted with DCM (100 mL) and washed with 10 % v/v HCl (50 mL × 2), 10 % w/v NaOH (50 mL × 2) and finally with saturated NaCl solution (50 mL × 2). The organic phase was dried immediately with Na_2SO_4 and concentrated *in vacuo*. Purification was achieved by flash column chromatography [K] to afford title compound [11] (1.71 g, 78 %, R_f = 0.26 [I]) as a cream solid (Found: C, 54.7; H, 5.1; N, 25.0 % C10H12N4O2 requires C, 54.5; H, 5.5; N, 25.4 %); δ_H(400 MHz; DMSO-d_6); 3.08-3.13 (2H, q, *J*5.9, CH_2), 3.37-3.41 (4H, m, CH_2), 4.64-4.67 (1H, t, *J*5.4, OH), 7.03-7.06 (2H, m, AA'BB' splitting, ArH), 7.27-7.31 (2H, m, AA'BB' splitting, ArH), 8.03 (1H, br s, CONH); δ_C(100 MHz; DMSO-d_6) 41.5, 41.6, 118.8, 130.5, 133.5 137.4, 170.0; m/z (MS-ESI) 221.1034 ($[M+H]^+$ $C_{10}H_{13}N_4O_2^+$ requires 221.1033); ν_{max} (NaCl/nujol)/cm^{-1} 3294 med (–NH), 3079 wk (–NH), 2146 st, sh (–N_3), 1639 st, sh (C=O, CONH); mp 74-76 ºC.

3.3.6. Colloid Preparation

Prior to synthesis a 1 L round bottomed flask was cleaned scrupulously with *aqua regia* and then rinsed with copious amount of distilled water.

Citrate Reduced Silver Colloid

90 mg silver nitrate was added to 500 mL of distilled water heated to 40 °C with constant vigorous stirring. The solution was then rapidly heated to 98 °C and a 10 mL solution of 1 % w/v trisodium citrate in distilled water was added. The solution was maintained at 96-98 °C with constant vigorous stirring for 75 minutes, by which time a dull-green colour had developed and then allowed to cool to room temperature overnight.

CHAPTER 4

DEPOSITION OF PHENYL AZIDES ON A NANOSCALE

4. Deposition of Phenyl Azides on a Nanoscale

4.1. Introduction

Due to the increasing demand for high density DNA microarrays, the need for the deposition of small quantities of materials to a substrate is required. Two methods of achieving this have been developed from existing technologies; ink-jet printing and dip-pen nanolithography (DPN), where feature sizes can be deposited in the low micro- to nanoscale respectively.

4.1.1. Ink-jet Printing [92]

Although ink-jet technology has been used to control the deposition of small volumes of liquid to 2-D substrates for 30 years, it is still a well used technique at present. A typical ink-jet printer consists of a static pressure ink reservoir, a small diameter orifice and a pressure generating element. The size of the orifice controls the eventual diameter of the droplet ejected from the device. GeneJet is a commercially available ink-jet printer specifically designed for the deposition of DNA and takes advantage of the piezoelectric capillary jet's ability to generate small precisely placed droplets at high speed. As a result feature sizes of approximately 150 μm in diameter with a typical standard deviation of 13 % can be deposited, with up to 2000 droplets deposited from a single load before any dilution of the sample can be seen.

4.1.2. Dip-pen Nanolithography (DPN)

Dip-pen nanolithography is a soft lithography technique that originally derived from atomic force microscopy (AFM), where an AFM tip is used for the deposition of nanoscale materials onto a substrate. The individual molecules are transferred from the tip to the surface through a water meniscus which forms in ambient conditions as the tip nears the surface (Figure 4.1).

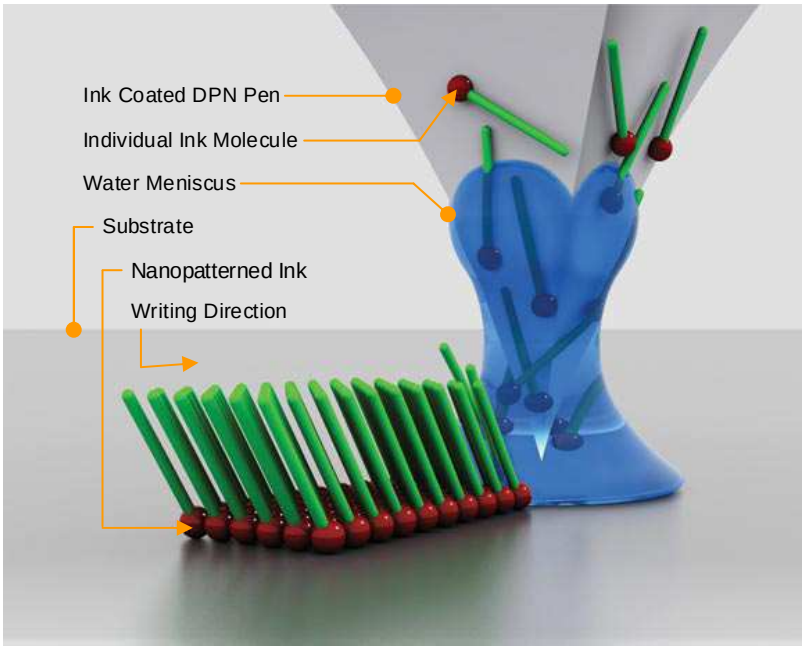

Figure 4.1: Schematic representation of DPN [93]

The term dip-pen nanolithography was first coined by Mirkin *et al.* however the technique of depositing organic molecules via a SFM tip was first achieved by Jaschke *et al.* 4 years earlier.[94, 95] But it is Prof. Chad A. Mirkin, Northwestern University, that has patented and pioneered this process and co-founded the spinout company NanoInk Inc.®, who now exclusively supply the instrumentation, hardware, software and even consumables, such as tips and substrates, for DPN. The instrumentation for the DPN is kept in an environmental chamber where humidity and temperature can be controlled. This is essential as each individual ink has a specific affinity to a particular surface at a specific humidity and temperature, which in turn dictates its inking rate. This is especially important if the ink is water soluble or if detailed patterns are to be written.

DPN Substrates [96]

There are two types of DPN substrates available from NanoInk Inc.®, silicon dioxide and gold. Silicon dioxide substrates are produced from thermally grown silicon dioxide on a silicon wafer, whereas the gold substrates are produced from evaporated gold on a titanium coated silicon wafer (Figure 4.2).

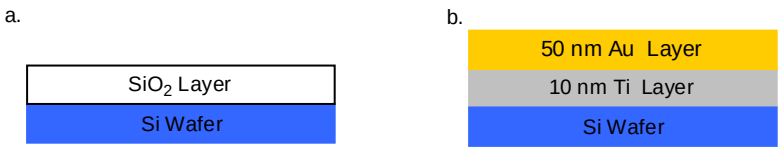

Figure 4.2: DPN substrate composition; a silicon dioxide, b. gold

These substrates have been specifically designed to incorporate 240 unique alignment markings (pairs of letters) spaced 250 µm apart and are raised 200 nm above the flat substrate areas (Figure 4.3). The alignment markings help locate where you have written, so if further analysis or steps are required, the area can be easily found.

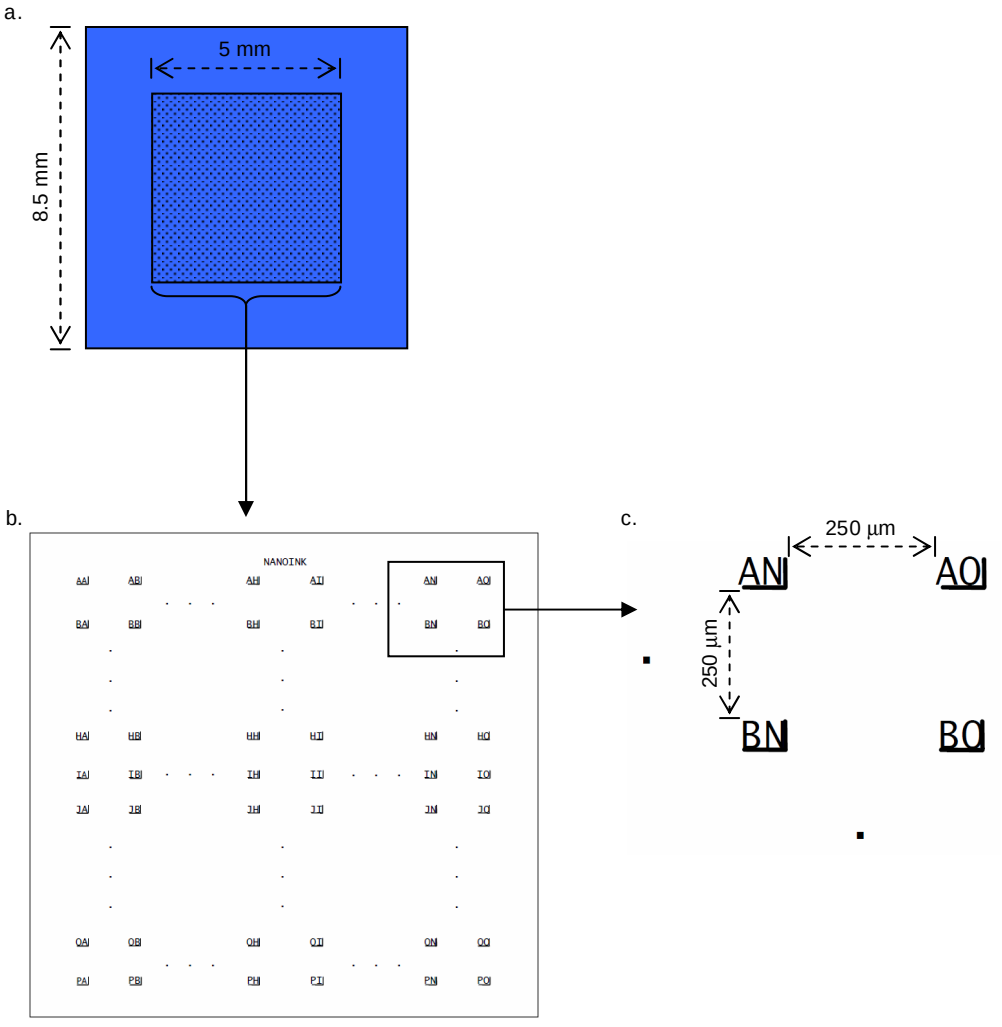

Figure 4.3: Silicon dioxide DPN substrate; a. dimensions of die and patterned area; b. abbreviated map of the pattern; c. dimensions between pattern

DPN Cantilevers [97, 98]

DPN cantilevers are made from silicon nitride probes coated with gold; this provides a more reflective surface enabling the laser to be aligned more readily.[99] The most frequently used cantilever for DPN is the A-Type S-1 cantilever ("diving board"), as it has a relative average spring constant, with the pyramidal based tip sharpened to radius of ~15 nm (Figure 4.4).

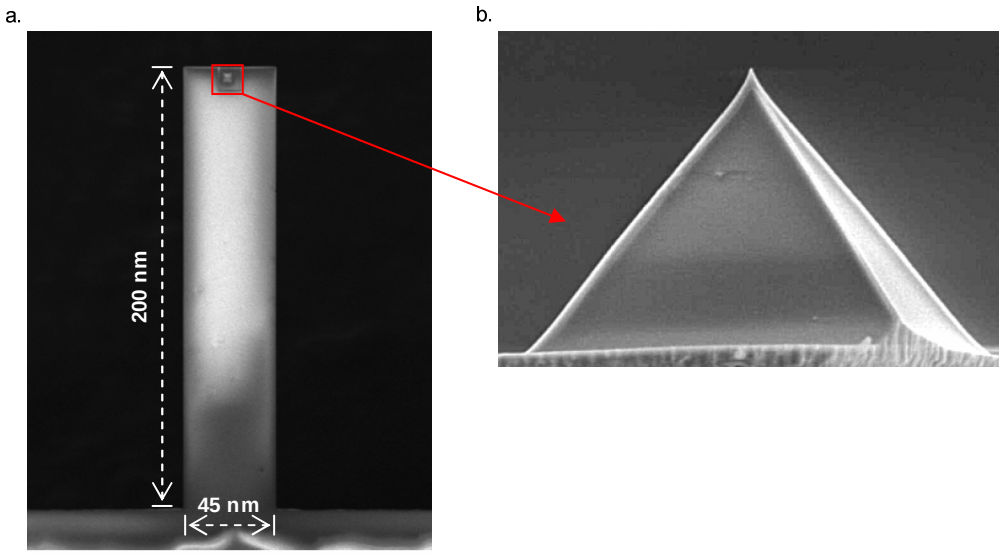

Figure 4.4: A-Type S-1 cantilever; a. SEM with dimensions, b. FESEM of tip

DPN Ink Calibration [100]

Before any DPN ink can be used for lithography it must be calibrated first by calculating the diffusion coefficient. Using the InkCAD™ design software and the InkCal™ calibration wizard (Figure 4.5) a series of lines are written at various speeds.

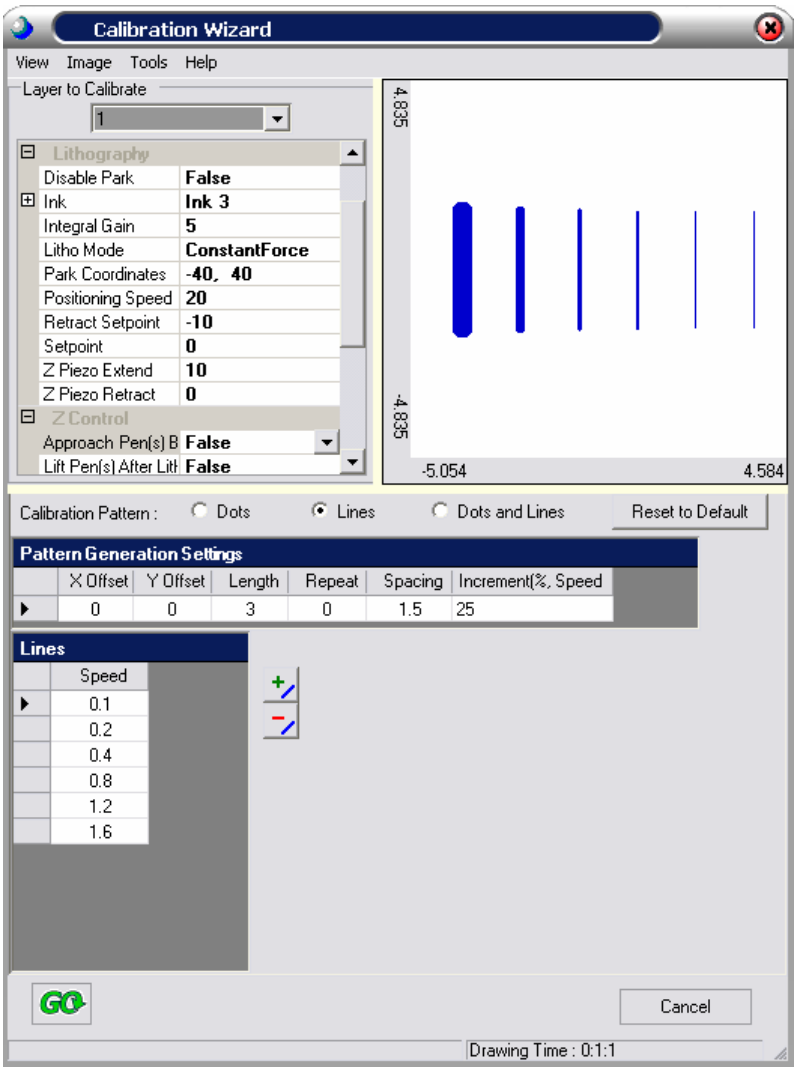

Figure 4.5: InkCal™ calibration wizard setup screen

The series of lines are then analysed in full AFM mode and a set of lateral force microscopy (LFM), topography and error images are obtained, where the LFM images are used for obtaining calibration results. LFM measures two forces (lateral and normal) through the bending and twisting of the cantilever during the imaging process.[101, 102] Forward and reverse images are obtained as the tip rasters over the calibration lines (left to right and vice versa), if there is a correlation between the two images then the feature imaged is genuine. Using the calibration wizard, the line width can be measured and inserted into the software where it automatically calculates the diffusion coefficient ($\mu m^2 s^{-1}$). Alternatively the diffusion coefficient ($\mu m^2 s^{-1}$) can be calculated from the slope when the line width (μm) is plotted against inverse speed ($s/\mu m$).

4.2. Results and Discussion

The aim of this chapter was to synthesise two novel DPN inks containing the chosen azide for use on silicon dioxide and gold flat DPN substrates, with the intention of using them to create nanoarrays of photoimmobilised DNA

4.2.1. Novel DPN Inks

In chapter 3 the photoimmobilisation of DNA on to a quartz and gold substrates was successfully achieved via a common two step process:

1. reaction of surface reactive group on to surface,
2. reaction of phenyl azide to the surface reactive group.

However in order to be used in DPN, a single molecule containing a surface reactive group and the chosen phenyl azide must be synthesised.

Silicon Dioxide Substrate

In chapter 3 the quartz was functionalised with the desired phenyl azide in a two step process. Firstly by the reaction of APTES with the quartz and then the subsequent reaction with the CDI activated 2-(4-azidophenyl) acetic acid [3]. By simply reacting the CDI activated 2-(4-azidophenyl)acetic acid [3] with APTES in an amide formation reaction (Scheme 4.1), the desired phenyl azide containing a silicon dioxide reactive group was synthesised.

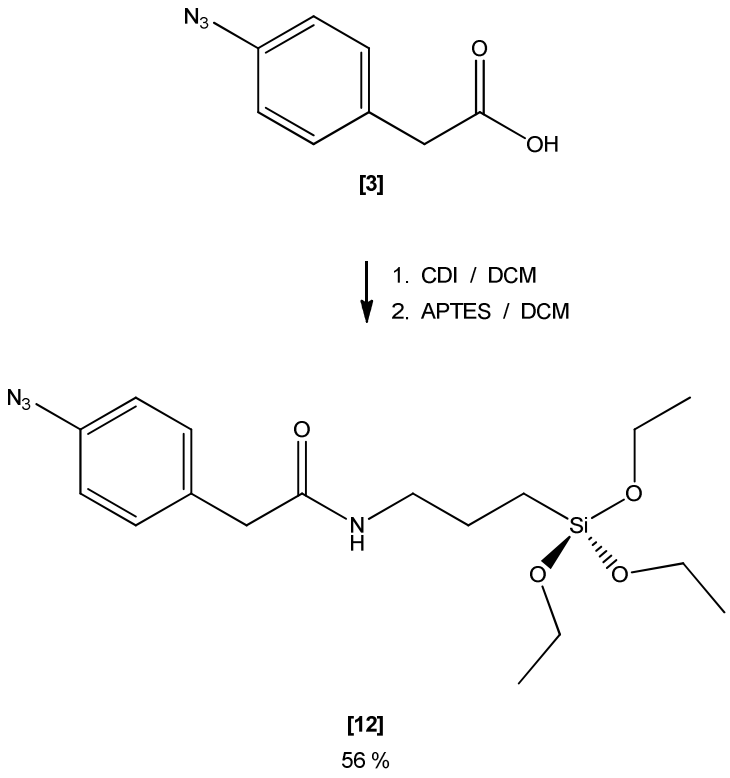

Scheme 4.1: Synthesis of 2-(4-azidophenyl)-*N*-(3-(triethoxysilyl)propyl)acetamide [12]

Purification was achieved via flash column chromatography, this was done quickly to prevent the silane portion of the compound interacting or reacting with the silica gel. As a result a yield of only 56 % was achieved as a solid, which was unexpected as most low molecular weight silanes are liquids. It was also noted that the compound failed to dissolve in any solvent after several of months of storage. This was more than likely due to the silane portion oxidising, rather than UV exposure to the phenyl azide as it was stored in the dark.

A diving board DPN cantilever was then coated in a 5 % w/v solution of [12] in MeOH using the 'double dip method'. This is where the cantilever is dipped into the desired ink solution for 10 seconds then dried over nitrogen gas and repeated. An illustrative LFM image of the line calibration is shown in Figure 4.6 which shows that the ink does not particularly diffuse very well on the surface.

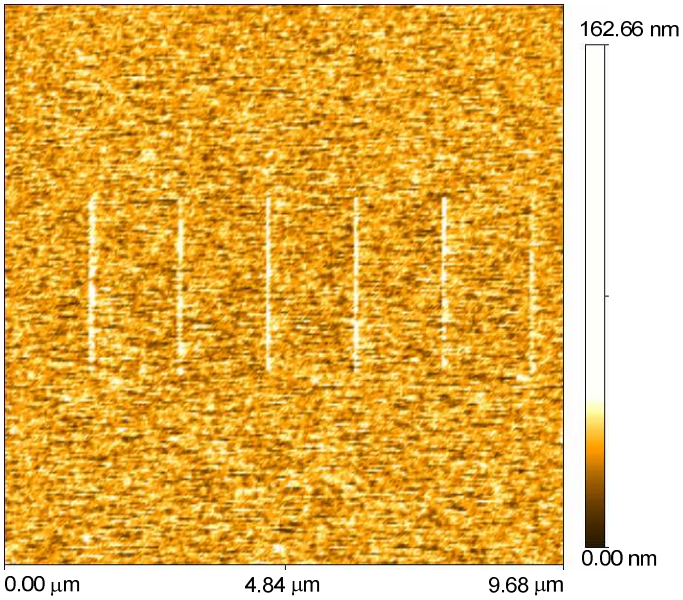

Figure 4.6: Illustrative LFM image for line calibration of [12]

This was confirmed by the calibration graph as the line width range was only 57-78 nm from faster to shortest speeds (Figure 4.7). This is due to when the solvent is evaporating on the surface, it leaves behind the solid silane in the smallest area possible, as a result a small diffusion coefficient of 0.002 $\mu m^2 s^{-1}$ with an overall % RSD of 21.6 was obtained.

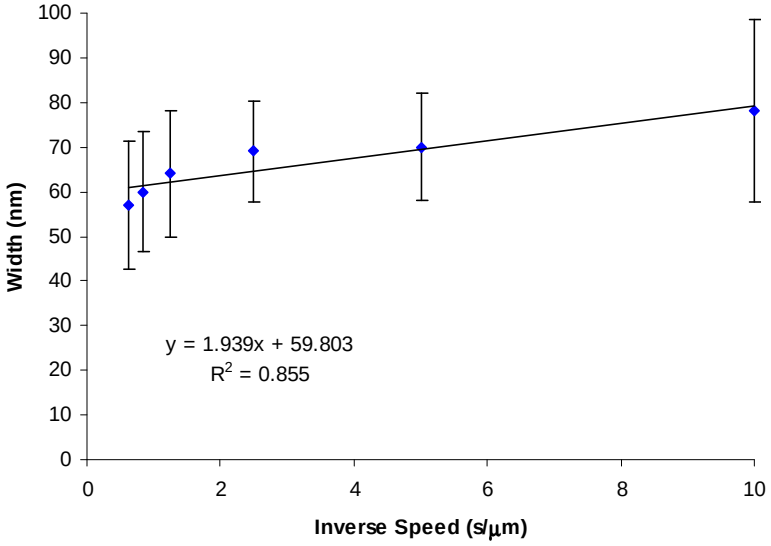

Figure 4.7: Calibration graph of [12]

This small diffusion coefficient has an advantage, as the ink can be used to draw small feature sizes. However this can be as a major drawback too, as the lithography of larger feature sizes would take a long time to complete.

Gold Substrate

Similarly in chapter 3 the gold was functionalised with the desired phenyl azide in a three step process. Firstly by the reaction of thioctic acid with the gold, then the amide formation reaction between 2-aminoethanol and the CDI activated 2-(4-azidophenyl)acetic acid [3] to form 2-(4-azidophenyl)-N-(2-hydroxyethyl)acetamide [11] and finally by the reaction of this with CDI activated thioctic acid. By just reacting 2-(4-azidophenyl)-*N*-(2-hydroxyethyl)acetamide [11] with the CDI activated thioctic acid in an ester forming reaction (Scheme 4.2), the desired phenyl azide containing a gold reactive group was synthesised.

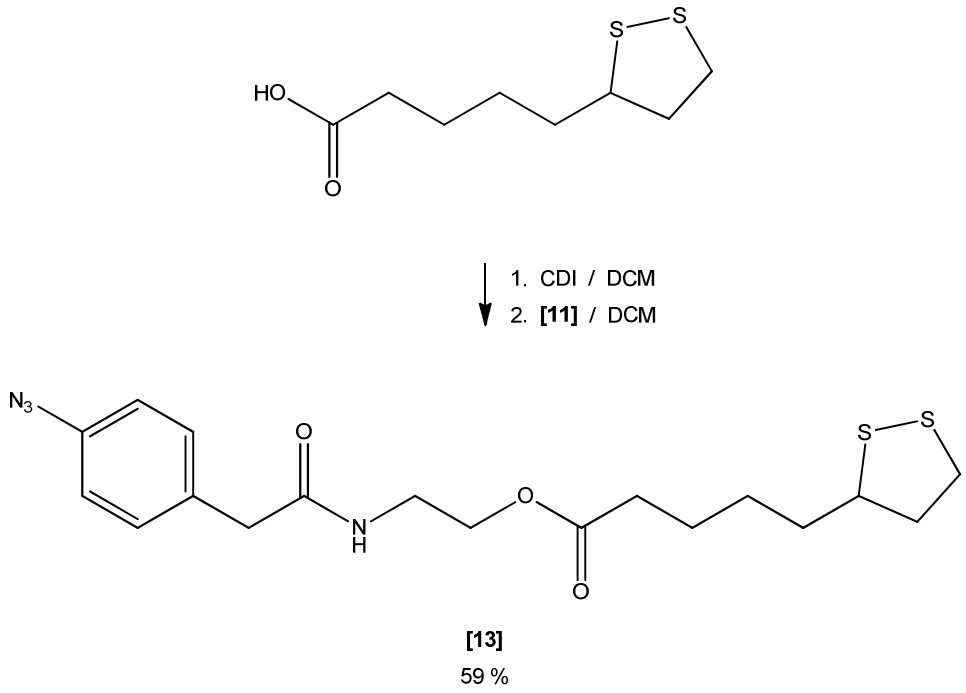

Scheme 4.2: Synthesis of 2-(2-(4-azidophenyl)acetamido)ethyl 5-(1,2-dithiolan-3-yl) pentanoate [13]

After purification a yield of 59 % was achieved, where the product formed was a viscous oil that was barely resoluble in DCM. In reality, after less than a week of storage, it was completely insoluble in any aqueous or organic solvents. This was almost certainly due to the disulfide polymerising, rather than UV exposure to the phenyl azide as it was stored in the dark.

A diving board DPN cantilever was coated in a ~1 % w/v solution of [13] in DCM using the 'double dip method'. An illustrative LFM image of the line calibration is shown in Figure 4.8 which shows that the ink does diffuse well on the surface.

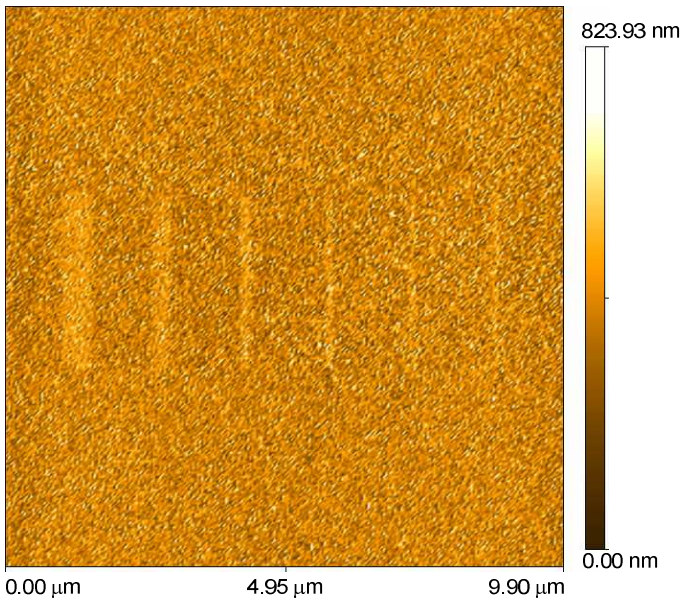

Figure 4.8: Illustrative LFM image for line calibration of [13]

This was confirmed by the calibration graph as the diffusion coefficient calculated was 0.098 $\mu m^2 s^{-1}$ with an overall % RSD of 26.6, which was 10 times larger than that of the silane ink (Figure 4.9).

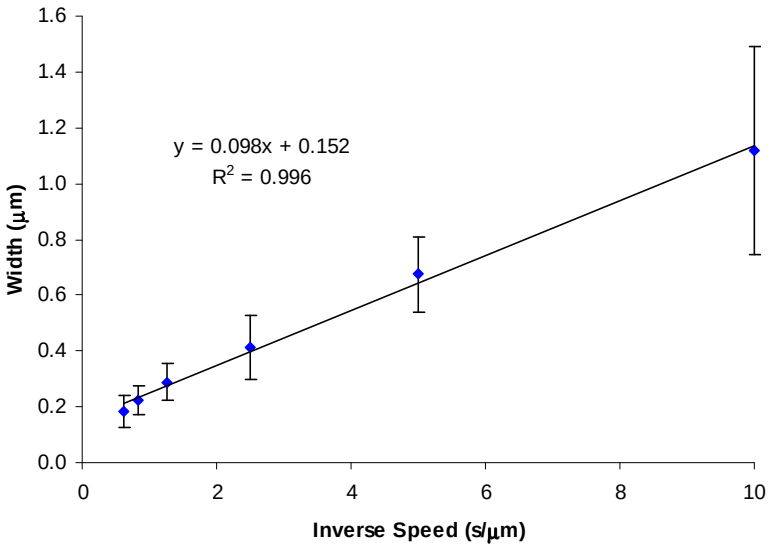

Figure 4.9: Calibration graph of [13]

This larger diffusion coefficient allows for a greater degree of control over line widths between ~200-1000 nm. This is due to the ink being a viscous oil and also having a greater affinity to the gold substrate, than that of the silane to the silicon dioxide substrate.

4.3. Experimental

4.3.1. Solvents and Reagents

Solvents and reagents used were as previous sections.

4.3.2. Chromatography

Flash column chromatography and TLC and plate detection tests were carried out as previous sections where specific solvent systems are expressed in Table 4.1.

Code	Solvents	Ratios
[L]	DCM:MeOH	90:10
[M]	DCM:MeOH	100-90:0-10
[N]	Pet Ether 60-80:EtOAc	50:50
[O]	EtOAc:MeOH	95:5

Table 4.1: Chromatography solvent systems

4.3.3. Chemical Analysis, Spectroscopy and Instrumentation

Chemical analysis, spectroscopy and instrumentation were carried out as in the previous sections.

DPN was performed DPN NScriptor™ DPN® system (NanoInk, Inc.®), using an A-Type S-1 ("diving board") cantilever on silicon dioxide and gold DPN substrates.

4.3.4. Synthetic Procedures

Prior to synthesis round bottomed flasks were flame dried under a N_2 atmosphere, whilst syringes and other glassware were dried in an oven at 140 °C overnight.

2-(4-azidophenyl)-N-(3-(triethoxysilyl)propyl)acetamide [12]

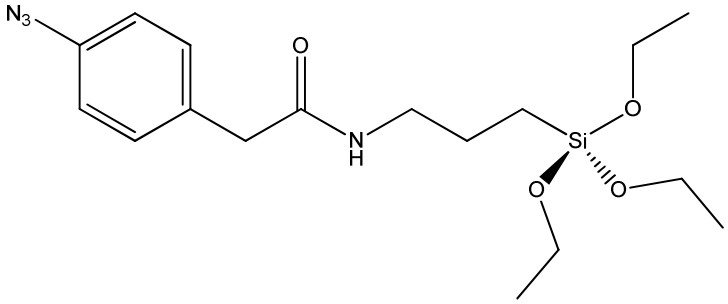

[12]

Prior to synthesis all glassware was silanised with a solution of HMDS (5 % v/v) in DCM overnight.

A solution of 2-(4-azidophenyl) acetic acid [3] (1.77 g, 10 mmol, 1 eq) in 10 mL anhydrous DCM was slowly added to a solution of CDI (1.95 g, 1.20 mmol, 1.20 eq) in 10 mL anhydrous DCM. The reaction mixture was then stirred at ambient temperature for 2 hrs under a N_2 atmosphere. Then a solution of APTES (2.32 g, 1.05 mmol, 2.2 mL, 1.05 eq) in 10 mL anhydrous DCM slowly was added and stirred at ambient temperature overnight under a N_2 atmosphere. The reaction mixture was then diluted with DCM (100 mL) and washed with 10 % v/v HCl (50 mL × 2), 10 % w/v NaOH (50 mL × 2) and finally with saturated NaCl solution (50 mL × 2). The organic phase was dried immediately with Na_2SO_4 and concentrated *in vacuo*. Purification was achieved by flash column chromatography [L] to afford title compound [12] (2.13 g, 56 %, R_f = 0.73 [M]) as a cream solid (Found: C, 53.8; H, 7.25; N, 14.7 % $C_{17}H_{28}N_4O_4Si$ requires C, 53.7; H, 7.4; N, 14.7 %); δ_H(400 MHz; DMSO-d_6) 0.48-0.52 (2H, m, CH_2), 1.11-1.14 (9H, t, *J*7.0, CH_3), 1.38-1.46 (2H, m, CH_2), 2.98-3.03 (2H, q, *J*6.5, CH_2), 3.37 (2H, s, CH_2), 3.68-3.74 (6H, q, J6.9, CH_2), 7.02-7.06 (2H, m, AA'BB' splitting, ArH), 7.27-7.31 (2H, m, AA'BB' splitting, ArH), 8.00-8.03 (1H, t, *J*5.4, CONH); δ_C(100 MHz; DMSO-d_6) 7.2, 18.2, 22.7, 41.3, 41.7, 57.7, 118.9, 130.5, 133.7, 137.4, 169.7; m/z (MS-CI) 381.1958 ($[M+H]^+$ $C_{17}H_{29}N_4O_4Si^+$ requires 381.1953); ν_{max} (NaCl/nujol)/cm^{-1} 3288 med (–NH), 3034 wk (–NH), 2122 st, sh ($–N_3$), 1641 st, sh (C=O, CONH); mp 74-75 ºC.

2-(2-(4-azidophenyl)acetamido)ethyl 5-(1,2-dithiolan-3-yl)pentanoate [13]

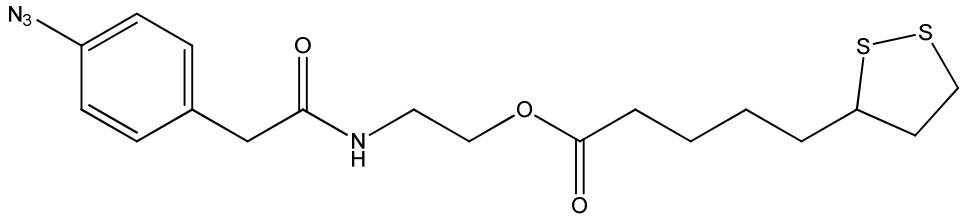

[13]

A solution of 5-(1,2-dithiolan-3-yl)pentanoic acid (1.03 g, 5 mmol, 1 eq) in 5 mL anhydrous DCM was slowly added to a solution of CDI (0.97 g, 6 mmol, 1.20 eq) in 5 mL anhydrous DCM. The reaction mixture was then stirred at ambient temperature for 2 hrs under a N_2 atmosphere. Then a solution of 2-(4-azidophenyl)-*N*-(2-hydroxyethyl)acetamide [11] (1.16 g, 5.25 mmol, 1.05 eq) in 5 mL anhydrous DCM slowly was added and stirred at ambient temperature overnight under a N_2 atmosphere. The reaction mixture was then diluted with DCM (50 mL) and washed with saturated $NaHCO_3$ solution (25 mL × 2) and with saturated NaCl solution (25 mL × 2). The organic phase was dried immediately with Na_2SO_4 and concentrated *in vacuo*. Purification was achieved by flash column chromatography [N] to afford title compound [13] (1.21 g, 59 %, R_f = 0.67 [O]) as a yellow viscous oil (Found: C, 52.1; H, 5.8; N, 13.3; S, 15.3 % $C_{18}H_{24}N_4O_3S_2$ requires C, 52.9; H, 5.9; N, 13.7; S, 15.7 %); δ_H(400 MHz; DMSO-d_6) 1.31-1.69 (6H, m) 1.82-1.90 (1H, m, CH) 2.23-2.27 (2H, t, *J*7.4, CH_2), 2.36-2.44 (1H, m, CH), 3.08-3.21 (2H, m, CH), 3.26-3.31 (2H, q, *J*5.6, CH_2), 3.40 (2H, s, CH_2), 3.56-3.63 (1H, m, CH), 3.99-4.02 (2H, t, *J*5.6, CH_2), 7.03-7.05 (2H, d, *J*8.4, ArH), 7.27-7.29 (2H, d, *J*8.4, ArH), 8.17-8.19 (1H, t, *J*5.4 CONH); δ_C(100 MHz; DMSO-d_6); 24.1, 28.1, 33.2, 34.1, 37.7, 38.1, 38.9, 39.9, 41.5, 56.0, 62.4, 118.9, 130.5, 133.3, 137.5, 170.2, 172.7; m/z (MS-ESI) 409.1368 ($[M+H]^+$ $C_{18}H_{25}N_4O_3S_2^+$ requires 409.1363); ν_{max} (NaCl/film)/cm^{-1} 3295 med (–NH), 3078 wk (–NH), 2115 st, sh (–N_3), 1735 st, sh (C=O, CO_2R), 1650 st, sh (C=O, CONH).

CHAPTER 5

CONCLUSIONS

5. Conclusions

Three phenyl azides have been successfully synthesised to contain a para carboxylic acid; 4-azido-2-hydroxybenzoic acid [1], 4-azidobenzoic acid [2] and 2-(4-azidophenyl)acetic acid [3]. The UV activation rate constants were calculated for all three phenyl azides with and without the present of 1-hexylamine. When illuminated at 365 nm they were shown to follow a first order reaction rate, with the exception of 4-azidobenzoic acid without the present of 1-hexylamine. But when the phenyl azides were illuminated at 302 nm they did not follow any reaction order. The investigation into the suitability of the synthesised phenyl azides for further modification resulted in 2-(4-azidophenyl) acetic acid [3] to be selected as the core structure for future applications. Spectroscopic proof of the chosen phenyl azide reacting with 1-hexylamine when illuminated at 365 nm was obtained by 1H NMR, where the disappearance of starting materials and appearance of the product were observed.

Through the functionalisation of quartz, epoxide polymer and gold with the chosen phenyl azide 2-(4-azidophenyl)acetic acid [3], the successful photoimmobilisation of single stranded DNA was achieved. When the single stranded DNA was photoimmobilised onto the quartz, clear and unique fluorescence and SERRS spectra were obtained at the site of immobilisation. However when the photoimmobilised DNA on the epoxide polymer and gold was analysed, the patterns immobilised were clear but no there was no RRS or SERRS spectra observed, just an increase background. The successful photoimmobilisation of a split-assay for the detection of *Chlamydia trachomatis* with the sensitivity of detecting a single base mis-match was also achieved on quartz. The SERRS spectra obtained confirmed the results from the DNA melt, that is the mis-match does partially hybridised, giving a positive result, but of less intensity to that of the full match.

Two novel photoactive DPN inks were synthesised containing the chosen phenyl azide 2-(4-azidophenyl)acetic acid [3], for the use on silicon dioxide and gold DPN substrates. Both inks were calibrated in order to obtain their diffusion coefficients, where the thioctic acid based ink for the gold substrate had a 10 times larger diffusion coefficient, than that of the silane based for the silicon dioxide substrate. These entirely novel inks can then be used to draw nano-sized features with the intention to photoimmobilise DNA in a similar manner to the previous chapter.

CHAPTER 6

REFERENCES

6. References

1. J. D. Watson and F. H. C. Crick, *Nature*, 1953, **171**, 737-738.
2. J. D. Watson and F. H. C. Crick, *Nature*, 1953, **171**, 738-740.
3. J. D. Watson and F. H. C. Crick, *Nature*, 1953, **171**, 964-967.
4. Available from: <http://www.biotechnologyonline.gov.au/popups/img_helix.cfm> [Retrieved: 20/11/2007].
5. E. Chargaff, *Experientia*, 1950, **6**, 201-240.
6. R. E. Franklin and R. G. Gosling, *Nature*, 1953, **171**, 740-741.
7. M. D. Matteucci and M. H. Caruthers, *J. Am. Chem. Soc.*, 1981, **103**, 3185-3191.
8. S. L. Beaucage and M. H. Caruthers, *Tetrahedron Lett.*, 1981, **22**, 1852-1861.
9. L. J. McBride and M. H. Caruthers, *Tetrahedron Lett.*, 1983, **24**, 245-248.
10. M. H. Caruthers, *Acc. Chem. Res.*, 1983, **24**, 278-284.
11. X. Gao, P. Yu, E. LeProust, L. Sonigo, J. P. Pellois and H. Zhang, *J. Am. Chem. Soc.*, 1998, **120**, 12698-12699.
12. E. LeProust, J. P. Pellois P. Yu, H. Zhang and X. Gao, *J. Comb. Chem.*, 2000, **2**, 349-354.
13. A. C. Pease, D. Solas, E. J. Sullivan, M. T. Cronin, C. P. Holmes and S. P. A. Fodor, *Proc. Natl. Acad. Sci. USA*, 1994, **91**, 5022-5026.
14. G. H. McGall, A. D. Barone, M. Diggelmann, S. P. A. Fodor, E. Gentalen and N. Ngo, *J. Am. Chem. Soc.*, 1997, **119**, 5081-5090.
15. M. F. Holick, *Am. J. Clin. Nutr.*, 1994, **60**, 619-630.
16. M. Shirai and M. Tsunooka, *Prog. Polym. Sci.*, 1996, **21**, 1-45.
17. A. Blanc and C. G. Bochet, *J. Org. Chem.*, 2002, **67**, 5567-5577.
18. A. Hasan, K. Stengele, H. Giegrich, P. Cornwell, K. R. Isham, R. A. Sachleben, W. Pfleiderer and R. S. Foote, *Tetrahedron*, 1997, **53**, 4247-4264.
19. C. G. Bochet, *J. Chem. Soc. Perkin Trans. 1*, 2002, **2**, 125-142.

20. P. Klán, M. Zabadal and D. Heger , *Org. Lett.*, 2000, **2**, 1569-1571.

21. C. Walling and M. J. Gibian, *J. Am. Chem. Soc.*, 1965, **87**, 3413-3417.

22. G. T. Hermanson, *Bioconjugate Techniques*, 2nd Edition 2008, Academic Press.

23. W. von E. Doering and R. A. Odum, *Tetrahedron*, 1966, **22**, 81-93.

24. P. Griess, Philos. Trans. R. Soc. (London), 1864, **13**, 377.

25. M. F. Budyka, M. M. Kantor and M. V. Alfimov, *Russ. Chem. Rev.*, 1992, **61**, 25-39.

26. N. P. Gritsan and E. A. Pritchina, *Russ. Chem. Rev.*, 1992, **61**, 500-516.

27. G. B. Schuster and M. S. Platz, *Adv. Photochem.*, 1992, **17**, 69-143.

28. N. P. Gritsan and M. S. Platz, *Chem. Rev.*, 2006, **106**, 3844-3867.

29. N. P. Gritsan, T. Yuzawa and M. S. Platz, *J. Am. Chem. Soc.*, 1997, **119**, 5059-5060.

30. W. L. Karney and W. T. Borden, *J. Am. Chem. Soc.*, 1997, **119**, 1378-1387.

31. I. R. Dunkin and P. C. P. Thomson, *J. Chem. Soc., Chem. Comm.*, 1980, **11**, 499-501.

32. E. Leyva, M. S. Platz, G. Persy and J. Wirz, *J. Am. Chem. Soc.*, 1986, **108**, 3783-3790.

33. G. T. Hermanson, *Bioconjugate Techniques*, 1st Edition 1996, Academic Press.

34. Crosslinking Reagents: Technical Handbook, Pierce Biotechnology Inc., 2006, USA.

35. K. W. Gano, H. G. Monbouquette and D. C. Myles, *Tetrahedron Lett.*, 2001, **42**, 2249-2251.

36. A. Sasaki, L. Mahé, A. Izuoka and T. Sugawara, *Bull. Chem. Soc. Jpn.*, 1998, **71**, 1259-1275.

37. CIE-IEC, *International Lighting Vocabulary*, 3rd Edition 1970.

38. Benchtop UV Transilluminator Operating Instruction, Revision C, UVP Incorporated, California.

39. P. Atkins and J. de Paula, *Atkins' Physical Chemistry*, 8th Edition 2006, Oxford Unversity Press.

40. P. Atkins and J. de Paula, *Elements of Physical Chemistry*, 5th Edition 2009, Oxford University Press.

41. D. A. Skoog, E. J. Holler and T. A. Nieman, *Principles of Instrumental Analysis*, 5th Edition 1998, Brooks Cole.

42. Available from: <http://www.ccdc.cam.ac.uk/products/mercury/>.

43. R. Taylor and C. F. Macrae, *Acta Cryst.*, 2001, **B57**, 815-827.

44 I. J. Bruno, J. C. Cole, P. R. Edgington, M. K. Kessler, C. F. Macrae, P. McCabe, J. Pearson and R. Taylor, *Acta Cryst.*, 2002, **B58**, 389-397.

45. C. F. Macrae, P. R. Edgington, P. McCabe, E. Pidcock, G. P. Shields, R. Taylor, M. Towler and J. van de Streek, *J. Appl. Cryst.*, 2006, **39**, 453-457.

46. C. F. Macrae, I. J. Bruno, J. A. Chisholm, P. R. Edgington, P. McCabe, E. Pidcock, L. Rodriguez-Monge, R. Taylor, J. van de Streek and P. A. Wood, *J. Appl. Cryst.*, 2008, **41**, 466-470.

47. Y. Rogers, P. Jiang-Baucom, Z. Huang, V. Bogdanov, S. Anderson and M. T. Boyce-Jacino, *Anal. Biochem.*, 1999, **266**, 23-30.

48. K. L. Mittal, *Silanes and Other Coupling Agents: Volume 4*, 1st Edition 2007, VSP International Science Publishers.

49. C. A. Mirkin, R. L. Letsinger, R. C. Mucic and J. J. Storhoff, *Nature*, 1996, **382**, 607-609.

50. J. A. Dougan, C. Karlsson, W. E. Smith and D. Graham, *Nucleic Acids Res.*, 2007, **35**, 3668-3675.

51. J. Sharma, R. Chhabra, H. Yan and Y. Liu, *Chem. Commun.*, 2008, 2140-2142.

52. J. R. Lakowicz, B. Shen, Z. Gryczynski, S. D'Auria and I. Gryczynski, *Biochem. Biophys. Res. Co.,* 2001, **285**, 875-879.

53. X. Zhao, R. Tapec-Dytioco and W. Tan, *J. Am. Chem. Soc.*, 2003, **125**, 11474-11475.

54. C. V. Raman and K. S. Krishnan, *Nature*, 1928, **121**, 501-502.

55. M. Fleischmann, P. J. Hendra and A. J. McQuillan, *Chem. Phys. Lett.*, 1974, **26**, 163-166.

56. D. C. Jeanmarie and R. P. van Duyne, *J. Electroanal. Chem.*, 1977, **84**, 1-20.

57. M. Moskovits, *Rev. Mod. Phys.*, 1985, **57**, 783-823.

58. M. G. Albrecht and J. A. Creighton, *J. Am. Chem. Soc.*, 1977, **99**, 5215-5217.

59. A. Otto, I. Mrozek, H. Grabhorn and W. Akemann, *J. Phys. Condens. Matter*, 1992, **4**, 1143-1212.

60. W. E. Doering and S. Nie, *J. Phys. Chem. B*, 2002, **106**, 311-317.

61 C. Tran, *Anal. Chem.*, 1984, **56**, 824-826.

62. Y. W. C. Cao, R. C. Jin and C. A. Mirkin, *Science*, 2002, **297**, 1536-1540.

63. Y. Sun and Y. Xia, *Analyst*, 2003, **128**, 686-691.

64. A. M. Stacy and R. P. van Duyne, *Chem. Phys. Lett.*, 1983, **102**, 365-370.

65. K. Faulds, W. E. Smith and D. Graham, *Anal. Chem.*, 2004, **76**, 412-417.

66. K. Faulds, R. P. Barbagallo, J. T. Keer, W. E. Smith and D. Graham, *Analyst*, 2004, **129**, 567-568.

67. K. Faulds, L. Stewart, W. E. Smith and D. Graham, *Talanta*, 2005, **67**, 667-671.

68. R. J. Stokes A. Ingram J. Gallagher, D. Armstrong, W. E. Smith and D. Graham, *Chem. Commun.*, 2008, 567-569.

69. B. D. Hames and S. J. Higgins, *Gene Probes 2: A Practical Approach*, 1st Edition 1995, Oxford University Press.

70. Available from:
<https://ecom.mwgdna.com/help/oligo/formula-tm>
[Retrieved: 11/07/2007].

71. S. Tyagi and F. R. Kramer, *Nat. Biotechnol.*, 1996, **14**, 303-308.

72. S. Tyagi, S. A. E. Marras and F. R. Kramer, *Nat. Biotechnol.*, 2000, **18**, 1191-1196.

73. X. Zhou and J. Zhou, *Anal. Chem.*, 2004, **76**, 5302-5312.

74. T. Cass and F. S. Ligler, *Immobilized Biomolecules in Analysis: A Practical Approach*, 1st Edition 1998, Oxford University Press.

75. P. C. Lee and D. Meisel, *J. Phys. Chem.*, 1982, **86**, 3391-3395.

76. C. H. Munro, W. E. Smith, M. Garner, J. Clarkson and P. C. White, *Langmuir*, 1995, **11**, 3712-3720.

77. D. Graham, W. E. Smith, A. M. T. Linacre, C. H. Munro, N. D. Watson and P. C. White, *Anal. Chem.*, 1997, **69**, 4703-4707.

78. H. S. Basu and L. J. Marton, *Biochem. J.*, 1987, **244**, 243-246.

79. V. Chan, D. J. Graves and S. E. McKenzie, *Biophys. J.*, 1995, **69**, 2243-2255.

80. K. Pappaert, P. van Hummelen, J. Vanderhoevena, G. V. Barona and G. Desmet, *Chem. Eng. Sci.*, 2003, **58**, 4921-4930.

81. C. Gadgil, A. Yeckel and J. J. Derby, W. S. Hu, *J. Biotechnol.*, 2004, **114**, 31-45.

82. J. R. Borden, C. J. Paredes and E. T. Papoutsakis, *Biophys. J.*, 2005, **89**, 3277-3284.

83. A. R. Mackintosh, A. J. C. Kuehne, R. A. Pethrick, B. Guilhabert, E. Gu, C. L. Lee, M. D. Dawson, G. Heliotis and D. D. C. Bradley, *J. Phys. D: Appl. Phys.*, 2008, **41**, 094007.

84. F. Debaene, J. A. Da Silva, Z. Pianowski, F. J. Duran and N. Winssinger, *Tetrahedron*, 2007, **63**, 6577-6586.

85. E. V. Anslyn and D. A. Dougherty, *Modern Physical Organic Chemistry*, 1st Edition 2005, University Science Books, US.

86. N. M. B. Perney, J. J. Baumberg, M. E. Zoorob, M. D. B. Charlton, S. Mahnkopf and C. M. Netti, *Opt. Express*, 2006, **14**, 847-857.

87. R. J. Stokes, A. Macaskill, J. A. Dougan, P. G. Hargreaves, H. M. Stanford, W. E. Smith, K. Faulds and D. Graham, *Chem. Commun.*, 2007, 2811-2813.

88. J. C. Love, L. A. Estroff, J. K. Kriebel, R. G. Nuzzo and G. M. Whitesides, *Chem. Rev.*, 2005, **105**, 1103-1169.

89. A. Polidori, N. Michel, A. S. Fabiano and B. Pucci, *Chem. Phys. Lipids*, 2005, **136**, 23-46.

90. DNA Detection Application Note, D3 Technologies Ltd. Glasgow, UK.

91. B. D. Hames and S. J. Higgins, *Gene Probes 1: A Practical Approach*, 1st Edition 1995, Oxford University Press.

92. M. Schena, *DNA Microarrays: A Practical Approach*, 1st Edition 1999, Oxford University Press.

93. Available from:
<http://images.iop.org/dl/nano/DPN.jpg>
[Retrieved: 12/05/2009].

94. R. D. Piner, J. Zhu, F. Xu, S. Hong and C. A. Mirkin, *Science*, 1999, **283**, 661-663.

95. M. Jaschke and H. J. Butt, *Langmuir*, 1995, **11**, 1061-1064.

96. DPN® Sample Substrate Datasheet (Reference: DS-subst), NanoInk Inc.®, Skokie, IL, USA.

97. DPN® Probes Product Data Sheet (Reference: DS009), NanoInk Inc.®, Skokie, IL, USA.

98. DPN® Probes: Type A Datasheet (Reference: DS-apen), NanoInk Inc.®, Skokie, IL, USA.

99. K. B. Lee, J. H. Lim and C. A. Mirkin, *J. Am. Chem. Soc.*, 2003, **125**, 5588-5589.

100. InkCAD™ Software Product Data Sheet (Reference: DS008), NanoInk Inc.®, Skokie, IL, USA.

101. G. Meyer and N. M. Amer, *Appl. Phys. Lett.*, 1990, **57**, 2089-2091.

102. Z. L Wang, Z. Zhang and Y. Liu, *Handbook of Nanophase and Nanostructured Materials: Volume 2*, 4th Edition 2003, Tsinghua University Press.

CHAPTER 7

APPENDICES

7. Appendices

7.1. Chemical Structure of Dye Labels on Oligonucleotides

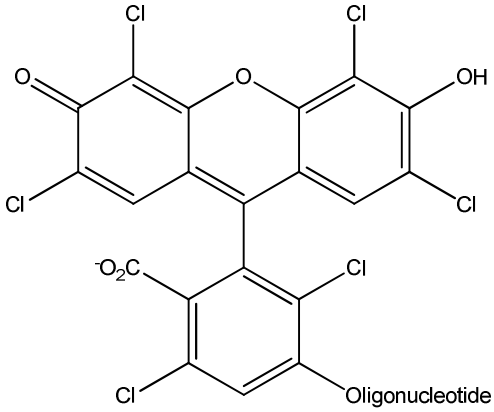

Figure 7.1: Hexachlorocarboxyfluorescein (HEX)

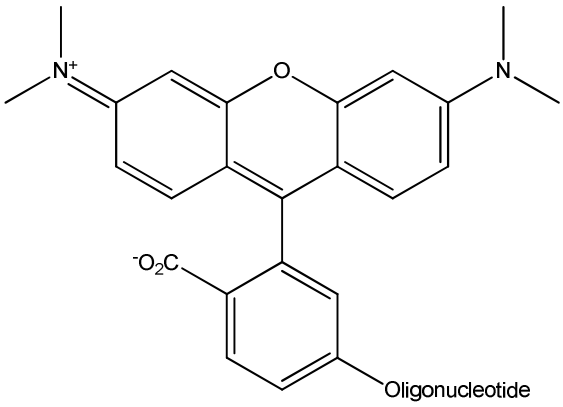

Figure 7.2: Carboxytetramethylrhodamine (TAMRA)

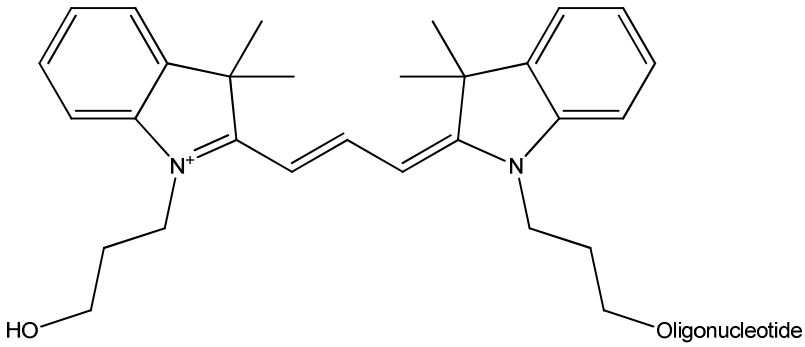

Figure 7.3: Cyanine 3 (Cy3)

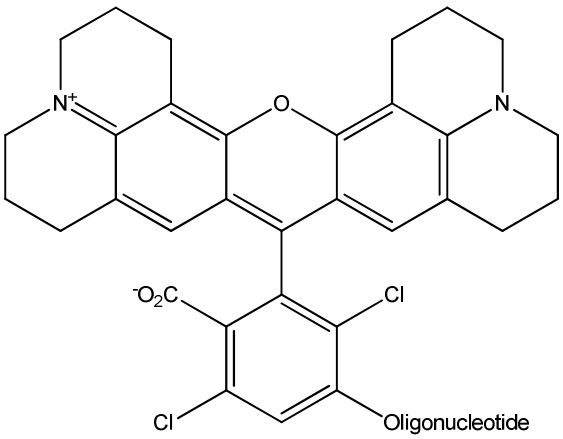

Figure 7.4: Carboxy-X-rhodamine (ROX)

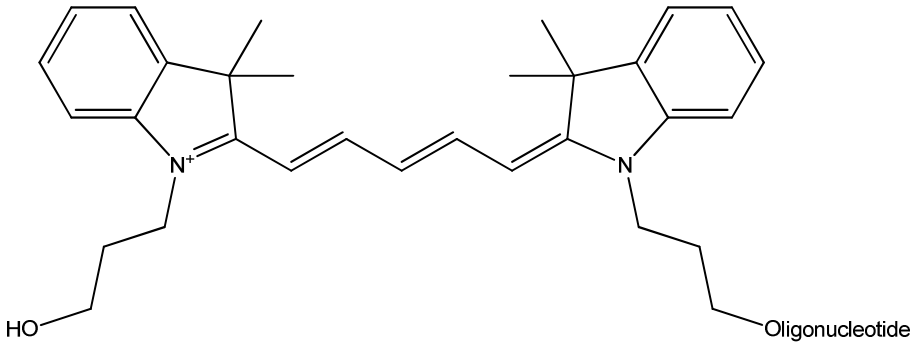

Figure 7.5: Cyanine 5 (Cy5)

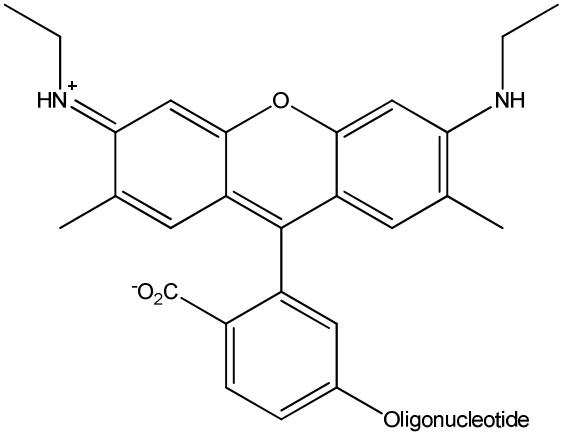

Figure 7.6: Rhodamine 6G (R6G)

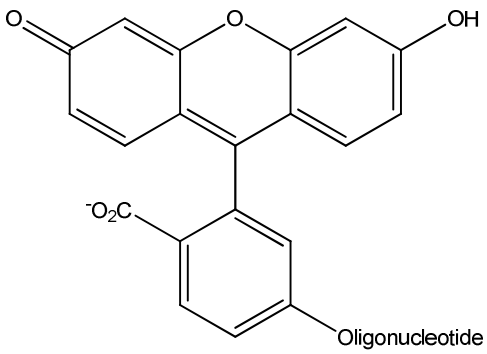

Figure 7.7: Carboxyfluorescein (FAM)

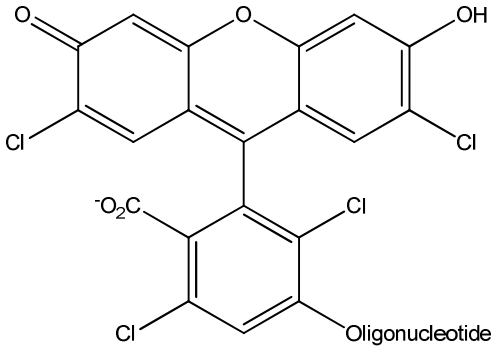

Figure 7.8: Tetrachlorocarboxyfluorescein (TET)

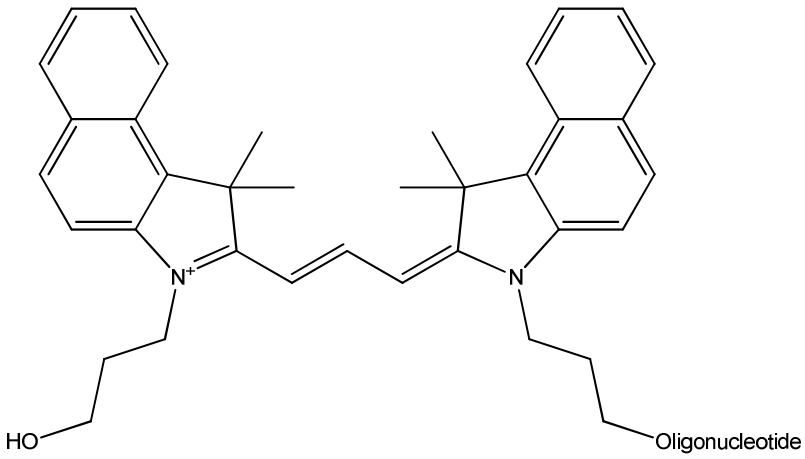

Figure 7.9: Cyanine 3.5 (Cy3.5)

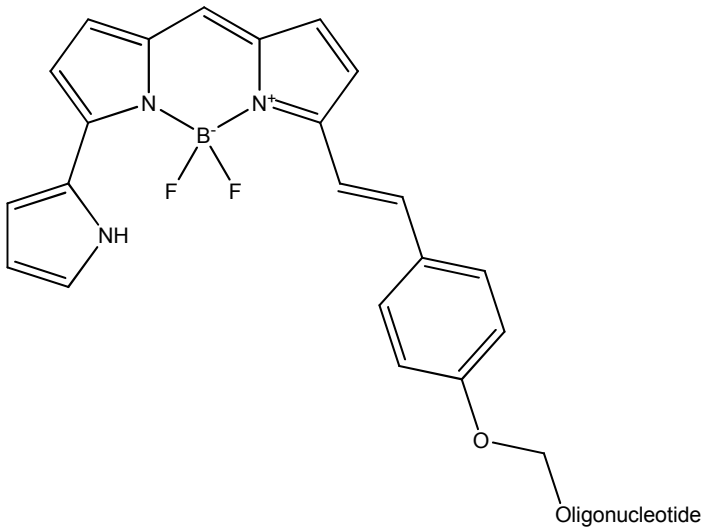

Figure 7.10: Bodipy 650/665 (BD650)

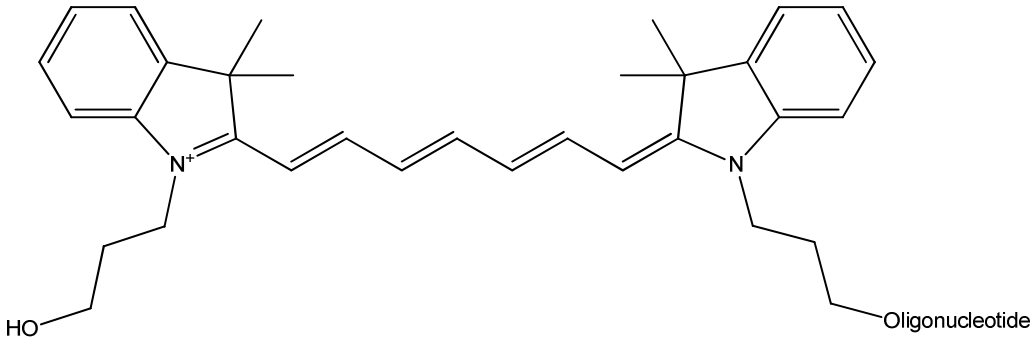

Figure 7.11: Cyanine 7 (Cy7)

7.2. Crystallographic Details and Refinement Parameters

7.2.1. 4-azido-2-hydroxybenzoic acid [1]

Empirical formula	$C_7H_5N_3O_3$	
Formula weight	179.14	
Temperature	123(2) K	
Wavelength	0.71073 Å	
Crystal system	Triclinic	
Space group	P-1	
Unit cell dimensions	a = 6.6203(7) Å	α = 108.208(6) °
	b = 7.0497(8) Å	β= 103.529(7) °
	c = 8.6791(10) Å	γ = 94.965(7) °
Volume	368.47(7) $Å^3$	
Z	2	
Density (calculated)	1.615 Mg/m^3	
Absorption coefficient	0.130 mm^{-1}	
F(000)	184	
Crystal size	0.25 × 0.12 × 0.12 mm^3	
Theta range for data collection	3.09 to 25.99 °	
Index ranges	-8<=h<=8, -8<=k<=8, -10<=l<=10	
Reflections collected	2832	
Independent reflections	1446 [R(int) = 0.0333]	
Completeness to theta = 25.99 °	99.7 %	
Absorption correction	None	
Refinement method	Full-matrix least-squares on F^2	
Data / restraints / parameters	1446 / 0 / 138	
Goodness-of-fit on F^2	1.038	
Final R indices [I>2sigma(I)]	R1 = 0.0458, wR2 = 0.1108	
R indices (all data)	R1 = 0.0773, wR2 = 0.1270	
Largest diff. peak and hole	0.279 and -0.229 $e.Å^{-3}$	

7.2.2. 2-(4-azidophenyl)acetic acid [3]

Empirical formula	$C_8H_7N_3O_2$	
Formula weight	177.17	
Temperature	123(2) K	
Wavelength	0.71073 Å	
Crystal system	Triclinic	
Space group	P-1	
Unit cell dimensions	a = 4.6250(3) Å	α = 104.972(4) °
	b = 7.2382(5) Å	β = 92.214(4) °
	c = 12.9424(10) Å	γ = 98.941(4) °
Volume	412.06(5) $Å^3$	
Z	2	
Density (calculated)	1.428 Mg/m^3	
Absorption coefficient	0.107 mm^{-1}	
F(000)	184	
Crystal size	0.24 × 0.15 × 0.04 mm^3	
Theta range for data collection	1.63 to 26.99 °	
Index ranges	-5<=h<=5, -9<=k<=9, -16<=l<=16	
Reflections collected	8740	
Independent reflections	1787 [R(int) = 0.064]	
Completeness to theta = 26.99 °	99.8 %	
Absorption correction	None	
Refinement method	Full-matrix least-squares on F^2	
Data / restraints / parameters	1787 / 0 / 146	
Goodness-of-fit on F^2	1.037	
Final R indices [I>2sigma(I)]	R1 = 0.0456, wR2 = 0.0834	
R indices (all data)	R1 = 0.1027, wR2 = 0.1025	
Largest diff. peak and hole	0.183 and -0.209 $e.Å^{-3}$	

7.2.3. 2-(((9H-fluoren-9-yl)methoxy)carbonylamino)ethyl 2-(4-azido phenyl) acetate [6]

Empirical formula	$C_{25}H_{22}N_4O_4$	
Formula weight	442.47	
Temperature	123(2) K	
Wavelength	1.54180 Å	
Crystal system	Monoclinic	
Space group	P21	
Unit cell dimensions	a = 13.7275(7) Å	α = 90 °
	b = 5.0061(4) Å	β = 99.418(4) °
	c = 15.5027(6) Å	γ = 90 °
Volume	1051.00(11) $Å^3$	
Z	2	
Density (calculated)	1.398 Mg/m^3	
Absorption coefficient	0.794 mm^{-1}	
F(000)	464	
Crystal size	0.25 × 0.04 × 0.02 mm^3	
Theta range for data collection	2.89 to 67.80 °	
Index ranges	-16<=h<=16, -5<=k<=4, -17<=l<=18	
Reflections collected	4694	
Independent reflections	2745 [R(int) = 0.0480]	
Completeness to theta = 60.00 °	99.5 %	
Absorption correction	Semi-empirical from equivalents	
Max. and min. transmission	1.00000 and 0.56625	
Refinement method	Full-matrix least-squares on F^2	
Data / restraints / parameters	2745 / 1 / 298	
Goodness-of-fit on F^2	1.059	
Final R indices [I>2sigma(I)]	R1 = 0.0507, wR2 = 0.1212	
R indices (all data)	R1 = 0.0691, wR2 = 0.1265	
Absolute structure parameter	0.4(4)	
Largest diff. peak and hole	0.256 and -0.269 $e.Å^{-3}$	

7.2.4. tert-butyl 2-(2-(4-azidophenyl)acetamido) ethyl carbamate [7]

Empirical formula	$C_{15}H_{21}N_5O_3$	
Formula weight	319.37	
Temperature	153(2) K	
Wavelength	0.71073 Å	
Crystal system	Triclinic	
Space group	P-1	
Unit cell dimensions	a = 5.0822(2) Å	α = 76.091(4) °
	b = 9.9314(4) Å	β = 89.247(4) °
	c = 17.3231(7) Å	γ = 77.953(4) °
Volume	829.39(6) $Å^3$	
Z	2	
Density (calculated)	1.279 Mg/m^3	
Absorption coefficient	0.092 mm^{-1}	
F(000)	340	
Crystal size	0.45 × 0.12 × 0.02 mm^3	
Theta range for data collection	2.72 to 29.00 °	
Index ranges	-6<=h<=6, -13<=k<=13, -23<=l<=23	
Reflections collected	20654	
Independent reflections	4328 [R(int) = 0.0309]	
Completeness to theta = 26.00 °	99.8 %	
Absorption correction	Semi-empirical from equivalents	
Max. and min. transmission	1.00000 and 0.86829	
Refinement method	Full-matrix least-squares on F^2	
Data / restraints / parameters	4328 / 0 / 219	
Goodness-of-fit on F^2	1.076	
Final R indices [I>2sigma(I)]	R1 = 0.0433, wR2 = 0.1015	
R indices (all data)	R1 = 0.0706, wR2 = 0.1088	
Largest diff. peak and hole	0.279 and -0.206 e.$Å^{-3}$	

7.2.5. 3-(tritylsulfanyl)propanoic acid [8]

Empirical formula	$C_{22}H_{20}O_2S$	
Formula weight	348.44	
Temperature	123(2) K	
Wavelength	0.71073 Å	
Crystal system	Monoclinic	
Space group	P21/n	
Unit cell dimensions	a = 8.7657(3) Å	α = 90 °
	b = 18.1770(7) Å	β = 99.218(3) °
	c = 11.3274(5) Å	γ = 90 °
Volume	1781.53(12) $Å^3$	
Z	4	
Density (calculated)	1.299 Mg/m^3	
Absorption coefficient	0.194 mm^{-1}	
F(000)	736	
Crystal size	0.35 × 0.35 × 0.30 mm^3	
Theta range for data collection	2.14 to 27.47 °	
Index ranges	-11<=h<=11, -23<=k<=20, -14<=l<=14	
Reflections collected	16201	
Independent reflections	4051 [R(int) = 0.076]	
Completeness to theta = 27.47 °	99.2 %	
Absorption correction	None	
Refinement method	Full-matrix least-squares on F^2	
Data / restraints / parameters	4051 / 0 / 230	
Goodness-of-fit on F^2	1.017	
Final R indices [I>2sigma(I)]	R1 = 0.0521, wR2 = 0.0866	
R indices (all data)	R1 = 0.1119, wR2 = 0.1029	
Largest diff. peak and hole	0.293 and -0.331 $e.Å^{-3}$	

7.2.6. *N*-(2-hydroxyethyl)-3-(tritylthio)propanamide [9]

Empirical formula	$C_{24}H_{25}NO_2S$	
Formula weight	391.51	
Temperature	123(2) K	
Wavelength	0.71073 Å	
Crystal system	Triclinic	
Space group	P-1	
Unit cell dimensions	a = 7.3283(9) Å	α = 90.154(6) °
	b = 7.9084(13) Å	β = 92.453(10) °
	c = 17.458(3) Å	γ = 100.287(9) °
Volume	994.5(3) $Å^3$	
Z	2	
Density (calculated)	1.307 Mg/m^3	
Absorption coefficient	0.183 mm^{-1}	
F(000)	416	
Crystal size	0.4 × 0.1 × 0.04 mm^3	
Theta range for data collection	3.01 to 25.00 °	
Index ranges	-8<=h<=8, -9<=k<=9, -20<=l<=20	
Reflections collected	6239	
Independent reflections	3454 [R(int) = 0.0638]	
Completeness to theta = 25.00 °	98.7 %	
Absorption correction	None	
Refinement method	Full-matrix least-squares on F^2	
Data / restraints / parameters	3454 / 0 / 258	
Goodness-of-fit on F^2	1.071	
Final R indices [I>2sigma(I)]	R1 = 0.0623, wR2 = 0.1234	
R indices (all data)	R1 = 0.1140, wR2 = 0.1458	
Largest diff. peak and hole	0.306 and -0.379 $e.Å^{-3}$	

7.2.7. 2-(3-(tritylthio)propanamido)ethyl 2-(4-azidophenyl) acetate [10]

Empirical formula	$C_{32}H_{30}N_4O_3S$	
Formula weight	550.66	
Temperature	120(2) K	
Wavelength	0.71073 Å	
Crystal system	Monoclinic	
Space group	C2/c	
Unit cell dimensions	a = 36.1103(16) Å	α = 90 °
	b = 9.1318(4) Å	β = 113.206(3) °
	c = 18.3625(9) Å	γ = 90 °
Volume	5565.2(4) $Å^3$	
Z	8	
Density (calculated)	1.314 Mg/m^3	
Absorption coefficient	0.157 mm^{-1}	
F(000)	2320	
Crystal size	0.16 × 0.03 × 0.03 mm^3	
Theta range for data collection	3.11 to 25.00 °	
Index ranges	-42<=h<=42, -10<=k<=10, -21<=l<=21	
Reflections collected	19856	
Independent reflections	4856 [R(int) = 0.0778]	
Completeness to theta = 25.00 °	99.1 %	
Absorption correction	Semi-empirical from equivalents	
Max. and min. transmission	1.000 and 0.884	
Refinement method	Full-matrix least-squares on F^2	
Data / restraints / parameters	4856 / 0 / 365	
Goodness-of-fit on F^2	1.146	
Final R indices [I>2sigma(I)]	R1 = 0.0803, wR2 = 0.1290	
R indices (all data)	R1 = 0.1309, wR2 = 0.1507	
Largest diff. peak and hole	0.307 and -0.297 e.$Å^{-3}$	